Selfdiffusiophoretic Janus Colloids

Simulations of Artificial Chemotaxis on the Long Run

Fabian Drube

München 2013

Selfdiffusiophoretic Janus Colloids

Simulations of Artificial Chemotaxis on the Long Run

Fabian Drube

Dissertation
an der Fakultät für Physik
der Ludwig–Maximilians–Universität
München

vorgelegt von
Fabian Drube
aus Immenhausen

München, den 13. Mai 2013

Erstgutachter: Prof. E. Frey
Zweitgutachter: Prof. D. Braun
Tag der mündlichen Prüfung: 17. Juli 2013

Zusammenfassung

Für die meisten Menschen ist Schwimmen eine alltägliche Erfahrung. Auch wenn man kein besonders talentierter Schwimmer ist, wird eine irgendwie geartete Paddelbewegung einen Vortrieb erzeugen. Dieser beruht auf dem Impulsübertrag vom Schwimmer auf das ihn umgebende Fluid. Es gibt jedoch Umstände, in denen eine solche Bewegung nicht möglich ist. Ein solches Regime wird durch eine kleine Reynoldszahl gekennzeichnet und ist durch kleine Längenskalen sowie relativ kleine Geschwindigkeiten charakterisiert. Für einen Schwimmer unter diesen Bedingungen fühlt sich das ihn umgebende Fluid wie Honig an. Jede Form von Bewegung wird augenblicklich gedämpft, außer sie wird durch eine permanente externe Kraft aufrecht erhalten. Für die Physik ist dieses Regime von besonderem Interesse, da es die natürlichen Bedingungen von biologischen Systemen, wie Bakterien sowie von Kolloiden beschreibt.

Der Erste, der die Bedingung für Bewegung unter solchen extremen Bedingungen formulierte, war Eric Purcell [1]. Er stellte heraus, dass ein Schwimmer bei kleinen Reynoldszahlen eine nicht zeitinvariante Folge von Zuständen durchlaufen muss, um sich voran zu bewegen, wie es z.B. bei den Schlägen des Ciliums eines Bakteriums geschieht [2]. Aufbauend auf dieser Arbeit sind viele künstliche Schwimmer entwickelt worden, die sich dieses Prinzip zu Nutze machen [3]. Diese können in mikrofluidischen Aufbauten [4] oder als Transportvehikel für Medikamente verwendet werden. Damit diese Schwimmer jedoch die verschieden Konfigurationen durchlaufen können, muss ein externer Mechanismus verwendet werden. In den meisten Anwendungen dient hierzu ein magnetisches Feld. Ob dies jedoch eine gangbare Vorgehensweise ist, um einen Schwimmer durch so komplexe Umgebungen wie den menschlichen Körper zu treiben, ist nicht klar. Eine Alternative hierzu, die in den letzten Jahren intensiv untersucht wurde, sind Schwimmer, die sich entlang externer Gradienten orientieren, insbesondere entlang von Teilchengradienten. Diese Anwendungen wurden angeregt durch die Untersuchung von Bakterien, die sich mittels Chemotaxis in komplexen Umgebungen bewegen. Für einen künstlichen Schwimmer sollten allerdings einfachere physikalische Mechanismen verwendet werden als der eher komplexe chemotaktische Apparat eines Bakteriums. Einer der vielversprechendsten Ansätze ist Diffusiophorese. Diese erklärt die Bewegung von Kolloiden in einem externen Teilchengradienten mittels eines aktiven Prozesses in der Grenzschicht zwischen dem Festkörper und dem Fluid [5]. In den letzten Jahren wurde dieser Ansatz auf sogenannte selbstdiffusiophoretische Schwimmer erweitert [6, 7]. Diese sind in der Lage selbst einen Teilchengradienten zu erzeugen und sich entlang dessen zu bewegen. Auch wenn für solche Systeme bereits erste analytische Ergebnisse bekannt sind [8, 9], sind sie auf Grund der Kopplung der Dynamik eines Teilchengradienten mit der Hydrodynamik des Fluids schwierig zu beschreiben. Ein vielversprechender Ansatz hierfür sind Simulationen des Systems.

Für Simulationen von Systemen bei kleinen Reynoldszahlen gibt es hauptsächlich zwei Ansätze. Der Erste basiert auf der effektiven Kraft, die durch das Fluid auf ein Objekt wirkt, wie z.B. in sogenannten Stokesian Dynamics Simulationen [10]. Alternativ hierzu gibt es Methoden,

die das Fluid explizit modellieren. Erstere sind z.B. geeignet, um die hydrodynamische Wechselwirkung zwischen Polymeren zu untersuchen. Sie sind allerdings schwierig auf komplexere Fluide zu erweiteren, wie sie in selbstdiffusiophoretischen Systemen notwendig sind. In dieser Arbeit wird daher der zweite Ansatz genutzt. Die meisten Fluidmodelle enthalten keine thermischen Fluktuationen. Dies ist eine vertretbare Annahme, falls die Bewegung des Systems hauptsächlich auf Konvektion beruht. Die Dynamik eines externen wie auch einen selbstproduziertes Teilchengradienten basiert allerdings auf Diffusion. Dieses Regime wird durch eine kleine Pecletzahl charakterisiert. Eine Technik, die gerade für diese Bedingungen entwickelt wurde, ist Multiparticle Collision Dynamics (MPC). Es ist ein teilchenbasierter Ansatz, der leicht auf komplexere Fluide und Objekte erweiterbar ist. Der MPC-Ansatz wurde in den letzten Jahren insbesondere angewandt um Polymere [11] und Schwimmer [12] bei kleinen Reynoldszahlen zu untersuchen. In dieser Arbeit wird die Technik ausführlich diskutiert. Es wird zwischen der kanonischen und mirkokanonischen Version der Technik unterschieden. Ferner werden ihre hydrodynamischen sowie thermischen Eigenschaften detailliert besprochen. Die Transportkoeffizienten des MPC-Fluids können als Funktionen der Modellparameter analytisch abgeleitet werden. Dadurch läßt sich das hydrodynamische Regime des simulierten Systems variieren. Hiermit kann das Verhalten des Fluids jedoch nur qualitativ beschrieben werden. Da der MPC-Ansatz auf einer Vergröberung der Freiheitsgerade des Systems beruht, wird die Zeitskalenseparation des Systems im Vergleich zum Experiment reduziert.

Janus-Kolloide sind Kugeln aus Latex oder Silica, die auf einer Hemisphäre mit Gold oder Platin beschichtet sind. In einer Wasserstoffperoxid-Lösung katalysiert die beschichtete Seite H_2O_2 in Wasser und Sauerstoff und baut so einen Gradienten auf. Dies ist der meist genutzte Ansatz um einen selbstdiffusiophoretischen Schwimmer zu untersuchen. Die zugänglichste Größe hierbei ist die mittlere quadratische Strecke, die der Schwimmer zurückgelegt hat. Besonders interessant ist dabei der Langzeitlimes. Es kann beobachtet werden, dass die Rotationsdiffusion des Schwimmers nicht vom Antriebsmechanismus beeinflußt wird, die Diffusionskonstante jedoch um mehrere Größenordnungen gegenüber der eines Brownschen Teilchens ansteigt. Mit Hilfe von Simulationen wurde dieses Regime allerdings noch nicht betrachtet. Daher wird in dieser Arbeit eben dieses mittels MPC untersucht. Es wird gezeigt, dass dieser Ansatz in der Lage ist, das im Experiment gefundene Verhalten zu erklären. Es zeigt sich kein Einfluß des Antriebs auf das Rotationsverhalten des Kolloids. Dies wird einerseits durch die Winkegeschwindigkeitskorrelation gezeigt, die den für ein Brownsches Teilchen erwarteten Abfall zeigt. Andererseits kann die Rotationsdiffusionskonstante aus dem Abfall der Orientierungskorrelationsfunktion bestimmt werden. Auch hier zeigt sich kein Einfluß des Antriebsmechanismus. Trotzdem wird ein Anstieg der Diffusionskonstante über mehrere Größenordnungen beobachtet. Dieser kann auf die erhöhte intrinsische Geschwindigkeit des Janusteilchens zurückgeführt werden. Die Geschwindigkeit ist jedoch selbst auf Grund des ihr zugrunde liegenden dynamischen Teilchengradienten eine fluktuierende Größe. Es wird gezeigt, dass im Vergleich zu einem Brownschen Teilchen die Geschwindigkeitskorrelationen auf kleinen Zeitskalen deutlich ansteigen. Auf diesen Zeitskalen kann, auf Grund der reduzierten Zeitskalenseparation des MPC-Ansatzes, die Wechselwirkung zwischen dem Januskolloid und dem Produktgradienten nur qualitativ betrachtet werden. Für die mittlere Geschwindigkeit des Schwimmers wird das aus der Literatur bekannte Skalenverhalten beobachtet. Eine quantitative Übereinstimmung kann jedoch nicht erreicht werden. Im Gegensatz hierzu wird für den Langzeitlimes der aus den Experimenten bekannte Anstieg der Diffusionskonstante in der richtigen Größenordnung beobachtet. Dies bestätigt die MPC-Technik als einen vielversprechenden Ansatz.

Abstract

Moving through a fluid is a common experience for all humans. Even if one is not a skilled swimmer any kind of paddling motion will propel you forward. The motion is based on transfer of momentum from the swimmer to the fluid. However, there are regimes, described by low Reynolds numbers, where this kind of propulsion does not work. For small length scales and sufficiently low velocities a fluid behaves similar to honey. This means, every kind of motion is immediately damped if it is not sustained by a permeant external force. For physics, this regime is of particular interest as many biological systems like bacteria or colloids are faced by these conditions.

It was first pointed out in the seminal work of Eric Purcell [1] that in order to propel at low Reynolds numbers a permanent non-time-reversal motion has to be kept up, as for example the power and recovery strokes of bacterial cilia [2]. It inspired a lot of experimental work to build up low Reynolds number swimmers based on this principle [3]. They could e.g. be used in microfluidic devices [4] or as drug carriers in the human body. However, in order to let an artificial swimmer evolve through a set of configurations in a controlled way, some kind of external mechanism has to be applied. In most applications, a magnetic field is used to derive this effect. This can be a drawback if these swimmers have to explore complex environments. In the recent years, alternative approaches based on the motion of swimmers in external gradients, especially in particle gradients, received considerable interest. The particle gradient approach has been inspired by the motion of bacteria in gradients of nutrients, called chemotaxis. This mechanism, however, relies on a rather complicated internal machinery to reorientate the bacterium. An artificial swimmer has to be based on a more simple physical principle in order to guarantee highly controllable motion. One of the most promising candidates is diffusiophoresis. It explains the motion of a colloid in an external particle gradient based on an active process at the interface between the fluid and the solid [5]. Recently, this approach has been extended to so called selfdiffusiophoretic swimmers [6, 7] which are not driven by an external gradient but produce the gradient themselves. Even though there are first analytical approaches trying to describe this phenomenom [8, 9], due to the coupling of low Reynolds number hydrodynamics to the evolution of solute particle gradients it is difficult to obtain a complete description. An alternative are simulations which are able to capture both contributions.

Classically, two approaches are used to simulate low Reynolds number hydrodynamics. The first one tries to mimic the effective force due to the fluid on the embedded objects, like for example for Stokesian Dynamic simulations [10]. The second explicitly models the fluid and its interaction with relevant boundary conditions. The former is a veritable tool to address e.g. the effect of hydrodynamics on the relaxation of polymers but it is difficult to implement more complex fluids as in the case of selfdiffusiophoretic swimmers. Therefore, the second approach is used for the simulations in this work. Most of the fluid models mimic a fluid in which thermal fluctuations can be neglected. This is a sufficient assumption if the motion of the fluid is

dominated by convection. However, the relaxation of external as well as self-produced solute gradients is based on diffusion, called the low Peclet number regime. A technique which can mimic hydrodynamic behavior and naturally contains thermal fluctuations is Multiparticle Collsion Dynamics (MPC). It is a particle based approach which can be extended straight forwardly to incorporate solute particle gradients as well as complex objects. The MPC approach gained considerable interest in the recent years especially for simulations of polymers [11] and swimmers at low Reynolds numbers [12]. In this work, the technique is described extensively. It will be distinguished between a canonical as well as a microcanocial version and their hydrodynamic as well as thermodynamic properties will be discussed in detail. As the transport coefficients of MPC can be derived analytically the fluid can be adjusted to different regimes characterized by a set of hydrodynamic numbers. In will be shown that these numbers are only recapturing the expected behavior qualitatively. In particular, the approach only leads to compressible fluids. As MPC is a coarse grained description compared to an experimental system a reduction of the time scale separation is observed.

Janus colloids are latex or silica beads which are half coated with gold or platinum. In a water peroxide solution these colloids catalyze the H_20_2 into water and oxygen and are, therefore, able to build up a solute gradient. These objects have mainly been used in experiments to investigate the behavior of selfdiffusiophoretic swimmers. Mostly, the mean square displacement of these swimmers has been evaluated as it is experimentally easy accessible, especially in the long time limit. It is observed that while the rotation diffusion of the swimmer is not effected by the propulsion mechanism, the diffusion constant is increased by several orders of magnitude. This regime has not yet been addressed with simulations. Therefore, in this work a Janus colloid is implemented into a MPC algorithm, which has not been done so far. It is shown that the interaction between the swimmer and the gradient it produces does not affect the rotation of the swimmer. This can on one hand be shown by the decay of the angular velocity correlation function which shows the typical behavior of a Brownian colloid. On the other hand, the diffusion rotation can be measured by the decay of the orientation correlation function and it is shown that it is not affected by the propulsion mechanism. Nevertheless, the diffusion constant increases by several orders of magnitude. It will be shown that this arises from the increased velocity of the Janus colloid. The velocity is a fluctuating quantity coupled to the fluctuations of the product particle gradient. It will, however, be shown that on small time scales the velocity correlations increase significantly compared to a Brownian colloid. In the short time limit, due to the shrinked time scale separation, the interaction between the swimmer and the gradient can only be considered qualitatively. The mean propulsion shows the scaling behavior as has been previously reported in literature, but the exact values do not match. In contrast, for the long time limit the increase of the diffusion constant in the simulations is of the same order of magnitude as the experimentally observed results, confirming the MPC approach.

Contents

1 Introduction

The classical theory of hydrodynamics is based on the famous Navier-Stokes equation. Together with the relevant boundary conditions, it describes the motion of fluids ranging from the turbulent flows necessary to understand the flight characteristics of an airplane to the laminar flow of lava erupting out of a vulcano. It is given by

$$\rho \frac{\partial \mathbf{v}}{\partial t} + \rho(\mathbf{v} \cdot \nabla)\mathbf{v} = \eta \Delta \mathbf{v} - \nabla p + \mathbf{f}, \tag{1.1}$$

which is a field equation for the mean velocity $\mathbf{v}$ of the fluid field. Sources of the motion are the pressure gradient p and the external force density $\mathbf{f}$ [13]. The material constant η is the viscosity which describes the amount of internal friction in the fluid. However, there are some major problems solving the Navier-Stokes equation naively. As it is a non-linear equation it is not trivial to show that the solutions obtained are stable and, therefore, of general practical use. In fact, the prove of existence and regularity of the 3D solutions of the Navier-Stokes equation is one of the millennium problems. The skilled scientist who will be able to solve it receives 1 million dollars from the Clay Institute.

1.1 Low Reynolds Number Hydrodynamics

Very early in the consideration of the Navier-Stokes equation, simplifications have been introduced to make it analytically more tractable. By far the most relevant one is the Stokes equation

$$\eta \Delta \mathbf{v} = \nabla p - \mathbf{f}. \tag{1.2}$$

If the Navier-Stokes equation (1.1) is considered as a continuous Newton equation, on the left-hand side all contributions can be treated as inertial forces while the right-hand side contains the viscous forces arising due to internal friction. The Reynolds number is defined as the ratio between these forces

$$\mathrm{Re} = \frac{\text{Inertial forces}}{\text{Viscous forces}} = \frac{\rho U L}{\eta}. \tag{1.3}$$

Here U and L are the typical velocity respectively length scales in the system considered. In systems with a low Reynolds number the viscous forces are much stronger than the inertial ones. Therefore, the left-hand side of the Navier-Stokes equation can be neglected leading to the Stokes equation (1.2). Phenomenologically, a low Reynolds number means that every motion is immediately damped if it is not sustained by a permanent force. This could be called an Aristotalian world, as Aristoteles assumed that the world can be described by a first order differential equation meaning that the force is equivalent to a velocity and not to an acceleration. Further, the Stokes equation is not time dependent and, hence, any kind of

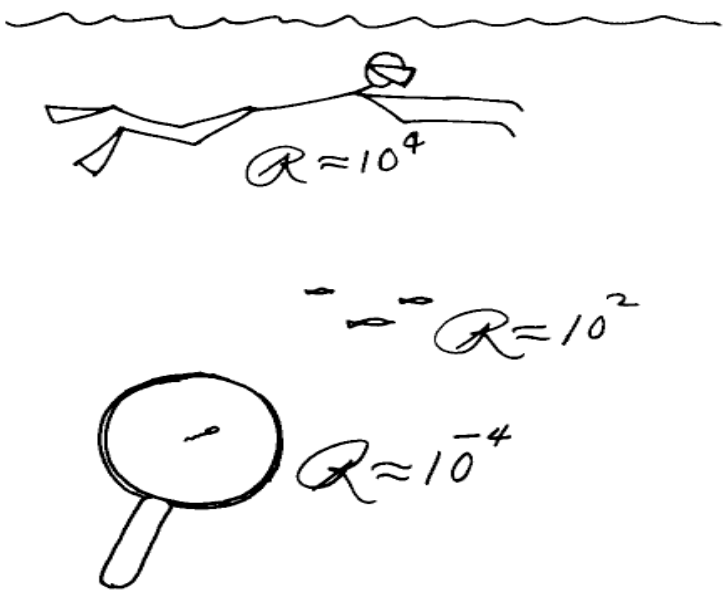

Figure 1.1: Comparison of the Reynolds numbers of humans, fish and bacteria. They cover a range of over 10^8. From the seminal paper of E. Purcell [1].

motion affecting the flow field must be incorporated via boundary conditions or time dependent forces. It has implicitly been assumed that also the "frequency Reynolds number" $\rho L\, w^2/\eta$ is small which means that the typical frequency of a motion is small.

1.2 Swimmers at low Reynolds Numbers

Due to their size and the typical length scales involved, the Stokes equation can be applied to many biological systems. The typical example here is a bacterium as can be seen in figure 1.1. It has a size of about $10\,\mu$m and swims with a velocity of around $10\,\frac{\mu\mathrm{m}}{\mathrm{s}}$ resulting in a Reynolds number of approximately $Re \approx 10^{-4}$ [14]. Hence, such an organism cannot propel itself based on inertia as fish or human beings do. It has to rely on a non-time-reversal stroke pattern, as has first been pointed out by Eric Purcell in his famous Scallop Theorem [1].

Scallop Theorem

At low Reynolds numbers it can be assumed that a swimmer propels itself through the fluid due to local interactions with the medium and, hence, no external force is applied. For further simplifications rotation of the swimmer will be neglected. As the Stokes equation is linear and time independent, the solutions have the following property sometimes called kinematic reversibility [15]. The velocity U of a swimmer can be used as a boundary condition for the Stokes equation. A rescaling of this velocity by an arbitrary factor α leads to a change of the flow field $\alpha\mathbf{v}$ as well as the pressure $\alpha\, p$ by the same factor, due to the linearity of the Stokes equation. The form of the flow lines is thus not altered by this factor, only the magnitude of the flow. This is especially true if $\alpha = -1$ which just inverts the flow field. Bearing this

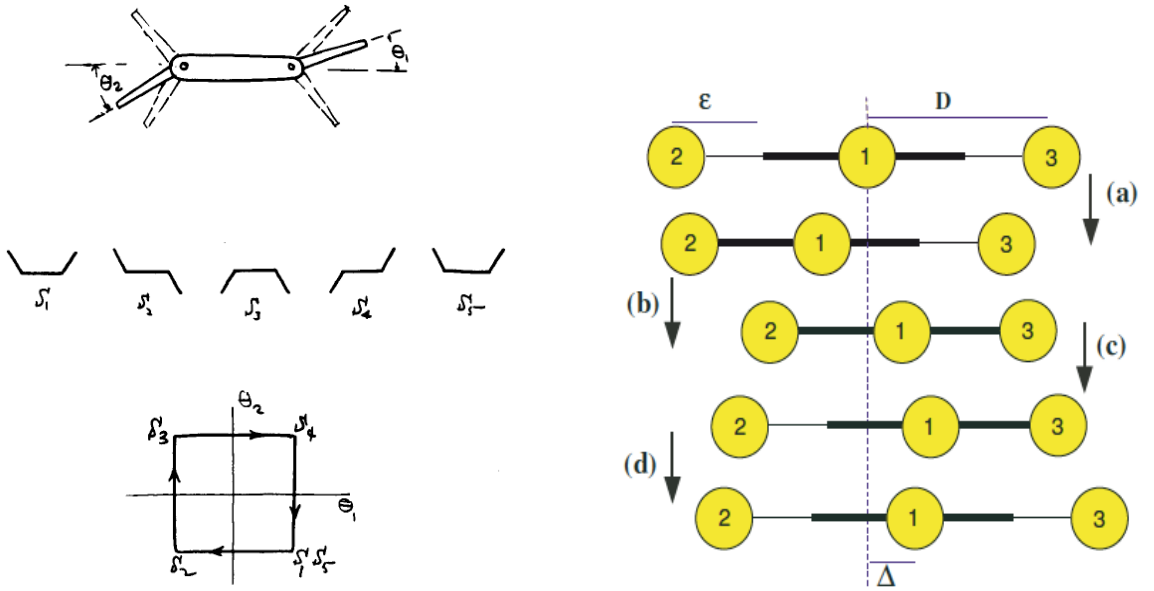

(a) (b)

Figure 1.2: (a) The simplest version of a low Reynolds number swimmer, called Purcell swimmer, is based on a non-time-reversal sequence of configurations. The swimmer consists of three rods connected by two hinges. From [1].
(b) A three spheres version of the Purcell swimmer, which is analytically tractable due to the simple structure. From [16].

in mind, it is obvious that a swimmer whose motion is based on reversible movements, like a scallop or a fish, cannot swim under these conditions. Instead, after reversing the direction of its propulsion, the swimmer will return to its starting point.

The Purcell Swimmer

The first minimal model of a low Reynolds number swimmer which is able to perform non-time-reversal motion and, hence, propel itself under these conditions, was also proposed by Eric Purcell [1]. It consists of three rods connected through two hinges as shown in figure 1.2 (a). Such a swimmer can move its two outer rods in a sequence of configurations which returns to the initial condition without passing a configuration twice. Even though this swimmer seems to be rather simple, it took more than 30 years to analyze its basic properties like efficiency or the optimal stroke pattern [17, 18]. The difficulties arise as rods are difficult to analyze with the methods developed for low Reynolds number hydrodynamics.

An alternative model which is easier to investigate was proposed by Najafi and Golestanian [16]. It consists of three spheres connected through two rods which can vary in length as shown in figure 1.2 (b). Due to its simple geometry it is possible to derive the flow field [12] and its behavior in various complex situations [19, 20]. Even though there seems to be no realization of this kind of swimmer in nature, it was possible to build an artificial version [21] which used latex beads in an optical trap.

This inspired a lot of experimental [3, 22–24] as well as theoretical work in the field [21, 25–27], all considering swimmers performing some kind of non-reversal motion. However, one of the drawbacks of such an approach is that the non-time-reversal motion has to be kept up by mechanically driven movements of parts of the body. While this is not a problem for a bacterium due to its internal machinery driven by molecular motors [2], it is difficult to maintain for an artificial swimmer. In most of the experiments, this is done by an external magnetic field which drives some kind of rotating motion [28]. However, this makes such an approach impractical for motion in an arbitrary 3D environment, e.g. as a cargo for drug delivery.

Gradient Driven Motion

An alternative approach for motion at low Reynolds numbers would be to use a swimmer which is capable of orientating itself due to external or self-produced stimuli, like bacteria do in chemotaxis [29] or phototaxis [30]. In contrast to a bacterium, the propulsion of an artificial swimmer has to be based on rather simple physical mechanisms to yield highly controllable motion. Maybe the oldest approach to move an object at low Reynolds numbers is electrophoresis where the object is driven by an external electrical field [31]. This has also been proposed on the level of a single swimmer creating the electrical field by itself [32]. In a similar manner, thermal gradients have been used to propel so called Janus colloids through a fluid [33]. These are spheres with two hemispheres of different materials. In the experiments with thermal gradients silica beads half coated with gold have been used. They moved in the spot of a defocused laser making them little radiators in the fluid. As gold conducts heat better than silica, the thermal gradients around the colloid became asymmetric leading to a net motion.

Even though a lot of progress has been achieved in controlling electrical fields as well as thermal gradients at small length scales, it is still an experimentally challenging task [34]. Alternatively, particle gradients can be imposed which are simpler to control and can be produced globally [35] by external gradients, as well as locally by a swimmer itself [6, 36–38]. Intuitively it seems to be clear that an object should move down such a gradient. However, the detailed physical mechanism behind this motion is not as clear as expected and often is confused with the motion in gaseous environment. Different approaches have been suggested [8, 39] trying to understand especially the motion in self-produced gradients. Using the old concept of diffusiophoresis pioneered by Derjaguin and later by Anderson [5] it has been proposed that a colloid can move in a self-produced particle gradient by selfdiffusiophoresis. The classical theory of phoresis assumes that an external gradient, may it be a thermal gradient, an electrical field or a particle gradient, propels an immersed object due to an interfacial process at the boundary between the fluid and the swimming object. Even though the interfacial zone is narrow it can have a profound effect on the system. It has been shown in experiments by Howse and coworkers [40] that it might also be the physical mechanism behind the propulsion of a swimmer producing the gradient itself. For a Janus colloid the mean velocity has been derived analytically. However, for a detailed comparison with experiments, further properties should be considered which can only be obtained by alternative approaches like simulations. In a closely related system of dimer swimmers producing a solute gradient, it has been shown that simulations can be used and compared to experiments of a single swimmer [41] or more

complex situations [42, 43].

For Janus colloids no such simulations have been performed so far. This work aims to close this gap, especially the long time limit of such a swimmer will be addressed. This makes it possible to compare the results with experiments where generally the long time limit is easier accessible.

1.3 Simulating low Reynolds Number Hydrodynamics

In many soft matter systems like polymers, it is sufficient to consider that the conformations and interactions of the objects are dominated by Brownian forces [44–49]. It can be assumed that the hydrodynamic forces are screened by the surrounding solution on the relevant length scales. Nevertheless, for dense systems [50] and short length scales [51] the relevance of hydrodynamics increases significantly. Further, if swimmers are investigated, their motion depends explicitly on the interaction with the fluid. In classical approaches towards hydrodynamic effects at low Reynolds numbers, approximation schemes are used to incorporate the effect of the medium rather than simulating it explicitly. However, in order to simulate swimmers at low Reynolds numbers their flow field is relevant. This holds especially true if the swimmer is driven by a particle gradient as the disturbance of the particles decays on the same length scale as the velocity field produced by the swimmer. In order to understand the significance of the explicit modeling one has to understand the basic problems of classical low Reynolds number simulation approaches.

Brownian Dynamics

The classical simulation technique to study soft matter systems is Brownian Dynamics (BD). It solves the Newton equations with a stochastic force $\mathbf{F}^{\mathrm{B}}$ which is based on a white noise random variable

$$m\frac{\partial \mathbf{v}}{\partial t} = \mathbf{F}^{\mathrm{B}} + \mathbf{F}^{\mathrm{H}} + \mathbf{F}^{\mathrm{Ext}}, \tag{1.4}$$

and can be extended to incorporate the effect of hydrodynamics with the force $\mathbf{F}^{\mathrm{H}}$ [52]. The form of the hydrodynamic force can be deduced from the Oseen tensor $\mathbf{G}(\mathbf{r})$ given by

$$\mathbf{v}(\mathbf{x}) = \mathbf{G}(\mathbf{x}-\mathbf{x}')\cdot\mathbf{F}, \text{with } \mathbf{G}(\mathbf{r}) = \frac{1}{8\,\pi\,\eta}\left(\frac{\mathbf{1}}{r}+\frac{\mathbf{rr}}{r^3}\right), r = |\mathbf{r}|, \tag{1.5}$$

$$p(\mathbf{x}) = \mathbf{H}(\mathbf{x}-\mathbf{x}')\cdot\mathbf{F}, \text{with } \mathbf{H}(\mathbf{r}) = \frac{\mathbf{1}}{4\,\pi\,r^3}. \tag{1.6}$$

The Oseen tensor is the fundamental solution of a point force $\delta(\mathbf{x}-\mathbf{x}')\,\mathbf{F}$, also called Stokeslet [15]. Such approaches have for example been used to study the synchronization behavior of semi-flexible polymers [53, 54]. In order to incorporate higher order hydrodynamics, the extended scheme of Stokesian Dynamics [10] can be used.

These approaches are constructed to solve the Stokes equation. If, however, the fluid consists of more than one particle type, a more complex set of equations describes its hydrodynamic

behavior as in the case of a binary fluid

$$\eta\Delta\mathbf{v} + \left(\bar{\eta} - \frac{\eta}{3}\right)\nabla(\nabla\cdot\mathbf{v}) = -\nabla p + \mathbf{f}, \tag{1.7}$$

$$\nabla\cdot\mathbf{v} = -\frac{\Delta\rho}{\rho}\left(\frac{\partial}{\partial t} + \mathbf{v}\cdot\nabla\right)\phi. \tag{1.8}$$

Even at low Reynolds numbers it resembles the steady-state Navier-Stokes equation. It still describes an incompressible fluid, even though the divergence of the flow field is not zero. This makes the solution more difficult than in the case of the linear Stokes equation.

Direct Numeric Solutions

One of the obvious approaches would be to directly integrate the Stokes equation as well as the corresponding equation of the density gradients. Such approaches have been used to derive the velocity of Janus particles driven by self-produced gradients. However, for more complex situations like collective effects such equations are complex and analytical solutions are difficult to find. This has been shown in the case of Janus colloids interacting with a thermal field [55].

Fluid Models

An alternative approach is to explicitly model the fluid. Here, the complete hydrodynamics are incorporated and it is possible to extend such approaches to different particle type. Classical fluid models are based on Lattice Boltzmann or Dissipative Particle Dynamics. For both it is, however, difficult to incorporate thermal fluctuations. Therefore, in this work, the fluid is modeled with the MPC approach which can simulate hydrodynamics at low Reynolds numbers straight forwardly and naturally contains thermal fluctuations. It is a particle based combination of an off-lattice solution of the Newton equations combined with a collision scheme on a lattice.

The behavior of a low Reynolds number swimmer driven by diffusiophoresis is a very interesting question, as it couples the motion of a particle gradient to a hydrodynamic problem. For this system only limited analytical results are available. Therefore, such a problem has to be addressed by simulations which are able to incorporate the basic properties of the swimmer as well as the particle gradient. This works aims to investigate this problem in the long time limit, a problem so far considered neither with analytical nor with simulation approaches.

2 Gradient Driven Motion

In biology it is well known that bacteria can orient their motion along external stimuli like light [30] or a particle gradient [56]. A bacterium needs a rather complicated internal information processing to adapt its motion [57] which itself is still under debate. However, for the macroscopic dynamic of a bacterium the details of the internal machinery are not relevant. Therefore, different artificial chemotactic swimmers have been build experimentally in the recent years [58–60] which alter their motion due to an external gradient. The motion of an object and its interaction with the gradient is only based on well defined physical mechanisms such that the motion is highly controllable. Further, experiments have been designed in which the object is not driven by an external gradient but produces the gradient itself [6, 33, 36–38, 41, 61]. Where the first is analyzed in the classical theory of phoresis, the second kind of motion may be termed selfphoresis.

In this chapter, after a short introduction to phoretic effects in general, the experimental as well as theoretical investigations of diffusiophoresis and selfdiffusiophoresis will be summarized. Thereby, the discussion will focus on the motion of a Janus colloid. Thermodynamic arguments will be given to show that such motion can be considered as an interfacial effect at the boundary between colloid and fluid relying on the existence of a slip velocity. The latter will be derived depending on the relevant parameters of the model for diffusiophoresis as well as selfdiffusiophoresis. Finally, the necessary conditions for the application of the theory will be critically discussed. This chapter will give the main aspects to understand the necessary considerations behind the simulations done in chapter 4 and distinguishes phenomena often not clearly distinct from diffusiophoresis.

2.1 Phenomenological Description of Phoretic Effects

The classical review of phoresis was given by Anderson [5] already in 1989. The four major forms of motion driven by a gradient are identified as

- Thermophoresis $\widehat{=}$ Temperature gradient [62]
- Electrophoresis $\widehat{=}$ Electrical field [63]
- Diffusiophoresis $\widehat{=}$ Particle gradient without pressure gradient [5]
- Osmosiophoresis $\widehat{=}$ Particle gradient with pressure gradient [35].

It is assumed that the first three kinds of phoretic motion can be captured by an unified theory based on the arising of a slip velocity at the boundary between the fluid and the solid body which leads to a relative motion of both and will be discussed later in this chapter.

As diffusiophoresis as well as osmosiophoresis are both based on an external particle gradient, some confusion arised about their relation [64, 65] and the physical origin of diffusiophoretic motion.

In order to understand the physical principles of the motion, it has to be stressed that the motion of an object in a particle gradient differs significantly from a gaseous to a liquid environment. If an object propels itself through the output of gas particles, like a rocket, this can be explained by the momentum transport from the object to the gas. Similarly, if a particle gradient along the x-axis exists which increases linearly with x and a sphere is placed at the coordinate x_0, its left hemisphere undergoes less collisions with the gradient particles than its right. Hence, this pressure gradient moves the sphere towards smaller x. In a fluid this cannot be the origin of motion, as becomes clear by an example given by Jülicher and Prost [66]. As the simplest model of liquid with a gradient of one solute, a binary fluid has to be considered consisting of two types of particles A and B. Let ϕ be the volume fraction of particle type A and $(1-\phi)$ respectively the one of B. One of the simplest geometries which can be considered is a pipe of length L along the x-direction which is connected to two reservoirs with mixtures of the binary fluid described by the volume fractions $\phi_{1/2}$ and the heights $h_{1/2}$. The pressure gradient along the pipe is given by

$$\partial_x P \approx g\frac{\rho_2\, h_2 - \rho_1\, h_1}{L}, \tag{2.1}$$

with the densities of the reservoirs given by $\rho_{1/2} = \phi_{1/2}\rho_A + (1-\phi_{1/2})\rho_B$. If the densities and heights of the reservoir are adjusted such that $\rho_2\, h_2 = \rho_1\, h_1$, there is no pressure gradient along the channel. However, there is a density gradient of particle type A given by

$$\partial_x \phi = \frac{\phi_2 - \phi_1}{L}, \tag{2.2}$$

which is stable on the time scale given by the diffusion of the particles. In an experiment by Nardi and coworkers [35], a latex bead was brought in a setup similar to the one described above. They used two dialysis tubes between which they were able to build up a sucrose gradient. There, no motion of the bead was observed even so a particle gradient exists. If, however, a vesicle composed of a lipid membrane was used instead of the latex bead, it moved along the gradient. The difference comes from the fact that a lipid membrane is transient for the water molecules while it is impenetrable for the sucrose. As is known from osmosis, if a semipermeable membrane separates two solutions of different solute concentration, a gradient of the chemical potential of the solute as well as the solvent exists. By diffusion through the membrane, the gradient of the chemical potential of the solvent vanishes while the gradient in the chemical potential of the solute sustains. This gives rise to a pressure gradient across the membrane. In the case of a spherical vesicle, it would be expected that it starts shrinking as solvent is moving out of it. However, this is not happening. The osmotic effect leads to a hydrodynamic flow through the vesicle from the low to the high concentration. Due to momentum conservation, the hydrodynamic flow must be compensated by a momentum flow in the opposite direction which leads to a motion of the vesicle down the sucrose gradient. Such an object might be termed an osmosiophoretic swimmer as it is propelled by an osmotic pressure produced across the membranes.

In the case of diffusiophoretic driven objects this cannot be the physical mechanism behind motion. It describes the motion of solid objects in a particle gradient without pressure.

Therefore, an alternative approach, like the one based on slip velocity discussed in this work, has to be used. Even though both phenomena seem to be similar in nature, their large scale behavior is completely different. A pressure gradient leads to the decay of the flow field according to a Stokeslet as $\mathcal{O}(r^{-1})$ while a diffusiophoretic swimmer has a flow field decaying as $\mathcal{O}(r^{-3})$ [9] which will be described in detail later on.

Even though thermophoresis, electrophoresis and diffusiophoresis have much in common, in the course of this work only the latter one will be discussed.

2.2 Experimental Studies of Diffusiophoretic Motion

In the recent years, different experimental set-ups have been brought up for swimmers at low Reynolds numbers which rely on gradient based motion [36, 59, 60, 67–69]. Various physical mechanisms have been proposed to understand the origin of the experimentally observed propulsion. There is, however, still a debate about many of the observed phenomena. This section aims to present major experimental results of objects propelled by diffusio- as well as selfdiffusiophoresis in non-electrolyte gradients. As most fluids naturally contain salt, they have to be considered as electrolytes. This makes the non-electrolyte literature substantially sparse compared to electrolyte one.

2.2.1 Diffusiophoretic Motion

The first discussion of colloids moving in gradients has already been given by Derjaguin starting in the 1940s [70, 71]. In most experiments done later, salt has been used to impose a gradient leading the motion of colloids, mostly latex beads [72–75] as well as DNA [76–78]. Hence, the fluid has to be considered as an electrolyte. It has been demonstrated that the velocity of the immersed objects is proportional to the solute gradient. Further, it has been shown that the direction of the motion is related to the diffusion constants of the anions and cations in the solution.

In contrast to the electrolyte version of diffusiophoresis, less is known about the non-electrolyte one. Even though there is a lot of theoretical work about diffusiophoresis in various situations [79–81], there is only one experiment considering the non-electrolyte version done by Staffeld and Quinn [82]. They used a Stop-Flow Chamber, shown in figure 2.1 (a), which is able to produce a solute gradient with the shape of a step function. This quasi 2D set-up has one inflow at each end. It is possible to flow in solutions with different solute as well as solvent concentrations $\{c_1, n_1\}$ and $\{c_2, n_2\}$. At the middle line, there are outflows which lead to two compartments with distinct concentrations due to a flow junction method. The horizontal set-up assures that the results are not masked by convection. In their experiment, Staffeld and Quinn used latex beads with a diameter of 1.01μm which were solved either in Dextran or Percoll. The former is a slightly branched polymer of D-glucopyranose while the latter is a polydisperse colloid solution of silica spheres coated with PVP (polyvinyl pyrrolidone) and an average diameter of 22 nm. The basic difference between both solutes is that they interact differently with the colloid. Phenomenologically this leads, however, to the same observations. Due to the step function gradient in the Dextran or Pecoll, a band of latex beads forms at

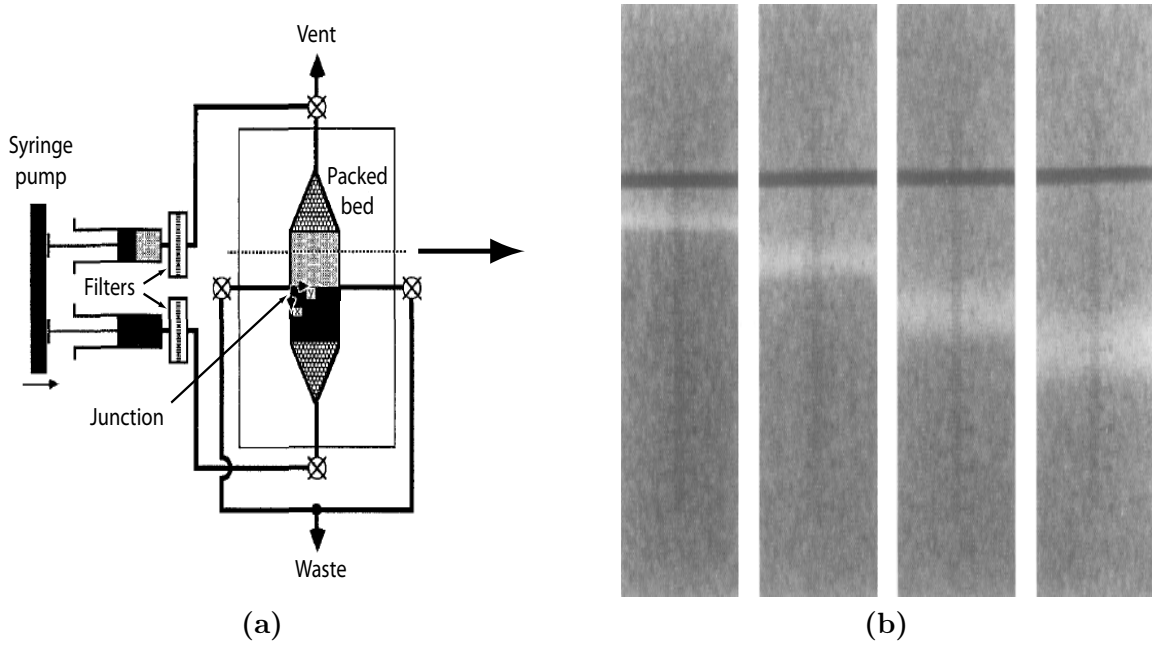

Figure 2.1: **(a)** Vertical scheme of Stop-Flow Chamber used by Staffeld and Quinn to produce a sharp gradient of Dextran as well as of Percoll. At the beginning of the experiment the latex beads are collected at the junction. The dashed line gives the position of the band of latex beads, shown in figure (b)
(b) Time series of the band of latex beads (white line) due to the influence of the solute gradient. While moving along the gradient the band starts to widen due to diffusion.
Adapted from: [74]

the middle of the chamber crossing the whole width of it. In this experiment, the band had a width of 15μm making it clearly visible to the naked eye. After the flow stopped, the band started to move due to the solute gradient, as is predicted by the theory of diffusiophoresis. It also extended due to diffusion but stayed remarkably narrow making it easy to follow its motion 2.1 (b). The velocity of the latex spheres can now be obtained from the motion of the approximated middle line of the band. Assuming that the interaction between the solvent and the latex spheres is based on a hardcore potential, Staffeld and Quinn were able to obtain the Gibbs absorption length, which is a fundamental quantity of the theory of diffusiophorsis and will be explained in detail in section 2.3.1. For Dextran 38 nm and for Percoll, depending on the exact concentration, between 13 - 31 nm were obtained. This is in the same order as the Deybe length κ^{-1} of a latex sphere, which is of the order of 10 nm. The Debye length is the screening length of a colloid. For length scales above it the colloid appears to be electrically neutral. This shows that diffusiophoresis takes place on similar length scales as surface electrical effects.

As there is a lot of theoretical work done on classical diffusiophoresis even extending it to high Peclet numbers [83], defined later in this section, or long range surface interactions [84], it would be of great interest to see new experiments on this classical topic. Interesting questions could be the behavior of gradient driven motion in complex geometries or the controlled influence of a hydrodynamic flow.

2.2.2 Selfdiffusiophoretic Motion

In contrast to classical diffusiophoresis, there are a lot of experiments addressing selfdiffusiophoresis where an object produces its gradient by itself rather than following an external one. However, care has to be taken as there are experiments where it seems as if the motion arises due to diffusiophoresis but other mechanisms are the origin of the observed propulsion. This section distinguishes between experiments of swimmers with selfdiffusiophoretic motion and closely related mechanisms and explains the differences between both. All of the experiments discussed in this section are considering the motion of rods or Janus particles which are both half coated with two different materials.

A first Hint towards Selfdiffuisophoretic Motion

The first experiment were a selfdiffusiophoretic motion was proposed have been nano rods whose one half consists of gold while the other was composed of platinum [85], respectively nickel [86]. These objects start swimming if they are put in a solution of water peroxide H_20_2. The platinum or nickel side catalyzes the H_2O_2 into water and oxygen and builds up a gradient of oxygen. If the motion would be driven by diffusiophoresis, the rods should move towards its gold end and away from the particles produced at the platinum end. However, exactly the opposite is observed [87]. The rods move towards the platinum end. Therefore, it is assumed that the rods act more like a battery and their motion is based on self-electrophoresis. While the water peroxide is catalyzed at the platinum end, an electric current occurs across the rod towards the gold end. In order to keep the water electrically neutral, H^+ ions move through the fluid from the platinum to the gold end. As is well known from electrophoresis, a free charge moving though the fluid drags water with it and leads to a fluid flow along its way. As the fluid can be assumed to be incompressible, this must lead to a motion of the rod in the opposite direction [88].

Even though it has been shown theoretically that this mechanism leads to a similar scaling behavior of the mean velocity of the swimmer as in diffusiophoresis [89], it is not clear that it will lead to the same collective as well as long time behavior. In order to model such a swimmer, the charges of the solvent and its structure have to be considered carefully and may lead to effects not expected from diffusiophoresis of non-electrolyte solutions. Nevertheless, experiments with conducting particles have been performed and show interesting new behaviors [90].

Selfdiffusiophoretic Motion in a H_2O_2 Gradient

The first experiment showing that even non-conducting spheres can produce motion if coated with platinum was done by Howse and coworkers [6]. They used latex beads of a diameter of $1.62 \pm 0.13\,\mu m$ half coated with platinum, so called Janus colloids, in a H_20_2 solution. Tracking the mean square displacement of the spheres, they showed that an increase in the water peroxide concentration can lead to a significant growth in the diffusion of the objects. Using the model of a Brownian particle with intrinsic speed V, they were able to extract the

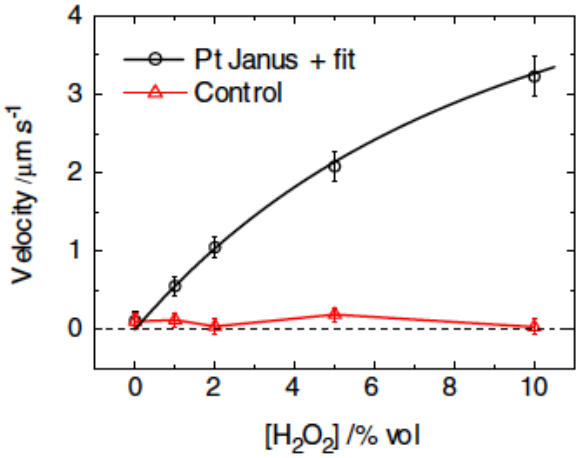

Figure 2.2: In the experiment of Howse and coworkers it was demonstrated that a latex/platinum Janus sphere can propel itself through a waterperoxide solution. The velocity clearly depends on the solute concentration (black line). In contrast, a non-coated latex bead diffuses unaffected (red line). From: [6]

mean velocity as well as the rotation diffusion time τ_r from their data with the formula for the mean square displacement

$$\Delta L^2 = 4\,D_0 \Delta t + \frac{V^2 \tau_R^2}{2}\left[\frac{2\,\Delta t}{\tau_R} + e^{-2\,\Delta t/\tau_r} - 1\right], \tag{2.3}$$

here D_0 is the bare diffusion coefficient of the spheres without propulsion. The results of the experiments are shown in figure 2.2. It can be clearly seen that the velocity of the spheres increases with the concentration of water peroxide as would be expected from the theory of selfdiffusiophoresis, even though it seems to be saturated for too high concentrations. It was proven that the colloids do not show increased Brownian motion in water. Hence, the propulsion can be attributed to the water peroxide catalysis. It is reported that with the highest concentration of H_2O_2 an increase in the diffusion constant of a factor of 30 can be observed, see figure 2.3(a), which is nearly as high as would be expected from simulations shown in chapter 4.

The effect would be even stronger, as shown in the simulations, if there would not be a significant increase of the rotation diffusion time occurring with an increase of the H_2O_2 concentration, shown in figure 2.3(b). It was assumed that due to a non-homogenous platinum coating, a net angular moment could be acting on the sphere. As the effective diffusion constant is given by

$$D_{eff} = 2\,D_0 + V^2\,\tau_r, \tag{2.4}$$

this can lead to a reduction of the effective diffusion. In simulation it can be shown that the rotation diffusion time is not effected by the details of the propulsion mechanism. This makes it difficult to compare the simulation results quantitatively with experiments. The long time limit has, however, been reproduced by the simulations shown in chapter 4.

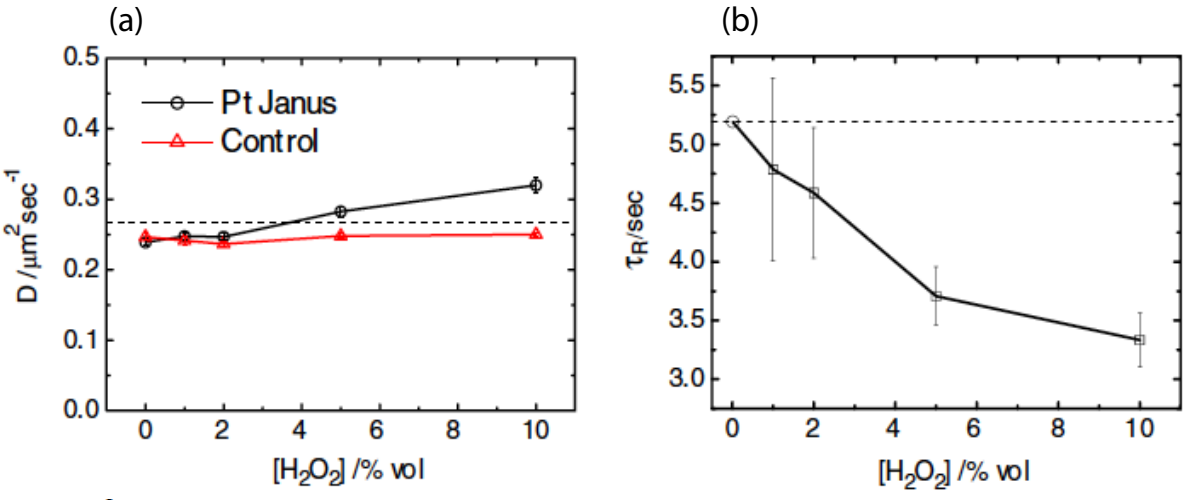

Figure 2.3: **(a)** The diffusion constant of a latex/platinum bead increases with the water peroxide concentration (black line). The diffusion constant of a control colloid is not affected at all (red line).
(b) In contrast to the prediction of the theory, the rotational diffusion time depends on the waterperoxide concentration. This can depend on details of the coating process. From: [6]

Selfdiffusiophoretic Motion in a Lutidine Gradient

The decrease of the rotation diffusion time has been avoided in experiments done in the Bechinger Group using silica beads half coated with gold [61]. The beads had diameters of $2.13\,\mu$m, $1.0\,\mu$m and $0.5\,\mu$m. Those Janus spheres were immersed in a critical mixture of water and 2,6-lutidine, which is a miscible organic fluid. In this binary fluid the spheres show unperturbed Brownian motion. This, however, changes drastically if the spheres are illuminated with non a focused laser of wave length $\lambda = 532$ nm. The diffusion of the spheres increases significantly and can be regulated via the laser intensity. As it is kept below $I < 0.2\,\mu\text{W}\,\mu\text{m}^{-2}$ it can be assured that no optical forces contribute to the motion.

The mechanism behind this motion of a bead is different to the one described so far. As the gold cap is a better heat conducter than the silica bead, the laser produces a local heating of the solution. As is well known from spinodal decomposition [91], if a binary mixture is heated above a critical temperature, spontaneous demixing occurs. Here, the fluid was initially kept below $T_C = 307\,K$ but the local heating overcomes this barrier. This leads to a lutidine gradient which drives the motion of the spheres.

Similar to previous experiments, the mean velocity and the rotation diffusion time can be extracted from equation (2.3). It has been shown that the velocity increases strongly with the laser intensity. However, the rotation diffusion time is not affected by the propulsion mechanism as can be seen in figure 2.5. As would be expected from classical Brownian theory, it only depends on the radius of the colloid. The rotation diffusion time is a measure of the time an object needs to reorientate itself and, hence, to lose the information of a prescribed direction. For times longer than this time scale, it can be assumed that the particle shows a classical Brownian motion. This means that due to the propulsion, the time scales of the Brownian motion is not altered. Nevertheless, the effective diffusion constant is significantly

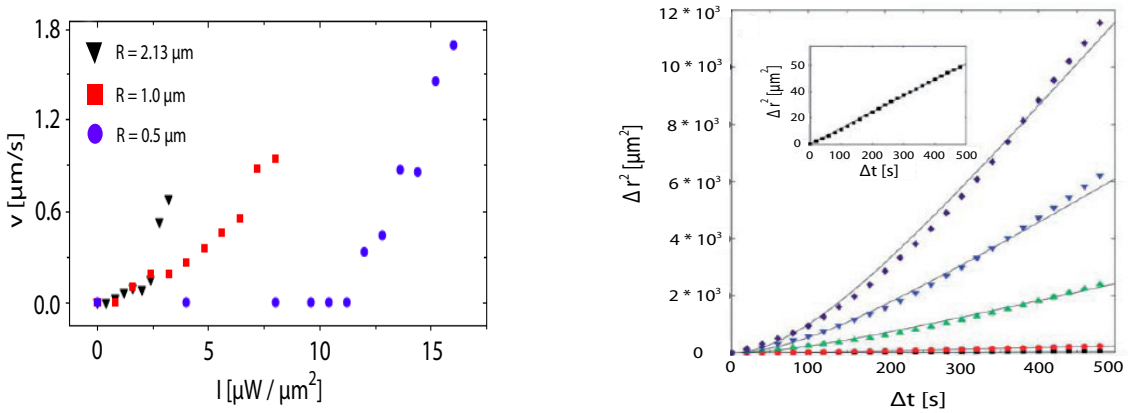

(a) (b)

Figure 2.4: **(a)** The mean velocity of a latex/gold Janus colloid clearly depends on the laser intensity and the radius of the bead. Adapted from: [61]
(b) The mean square displacement significantly increases with the laser intensity. The inset shows the mean square displacement of a non-coated colloid for comparison. Adapted from: [7]

increased as would be expected from equation (2.4). In the experiments discussed here, an increase of a factor 200 has been reported depending on the laser intensity, as shown in figure 2.4(b).

In contrast to what would naively be expected from theory, a significant effect resulting from the radius of the colloids has been observed. The smaller colloids have a much higher mean velocity than that the bigger ones, see 2.4(a). In the classical theory of selfdiffusiophoresis, described in section 2.4, this dependence is not observed. However, the velocity should depend linearly on the reaction constant of the catalytic reaction. It can be speculated that the smaller spheres have a higher reaction constant due to the better volume to surface ratio.

Both experiments discussed so far show significant effects which are attributed to a motion produced by selfdiffusiophoresis. They both show aspects which ask for further clarification and may lead to further interesting insights. In contrast to diffusiophoresis, in the case of selfdiffusiophoresis experiment is ahead of the theoretical investigation. Already, experiments have been conducted investigating selfphoretic swimmers in complex geometries [7] as well as their collective motion [77, 90].

2.3 The Classical Theory of Diffusiophoresis

As has been discussed above, it is not obvious that an object starts to move along an external particle gradient. Here, it will be shown by thermodynamic arguments that first of all, such motion can be expected if a lowering of the surface excess free energy is reached. Second, this can be related to a slip velocity at the boundary between the solution and a solid body, as a result of an interfacial process based on interfacial tension. The detailed form of the slip velocity depends on microscopic parameters which give the concrete type of interaction between

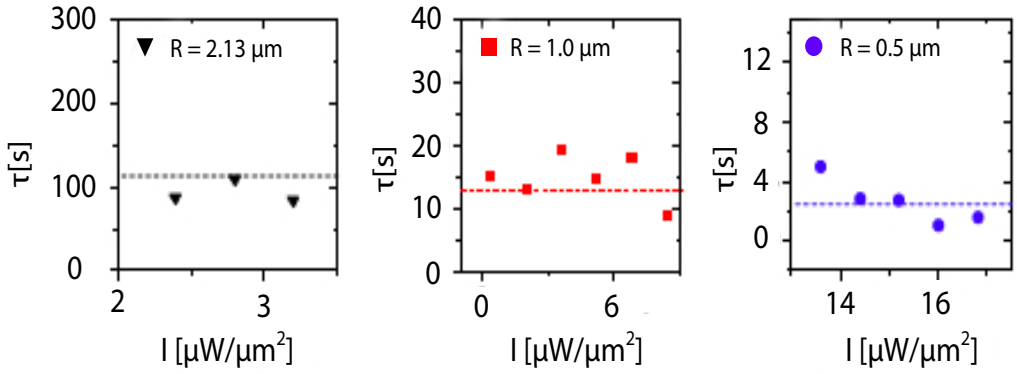

Figure 2.5: The rotation diffusion time for colloids of diameter 2.13 μm, 1.0 μm and 0.5 μm depends on their diameter as is expected from Stokes-Einstein relation. However, the laser intensity does not affect it. Adapted from: [61]

the solid surface and the solution. The microscopic derivation of the slip velocity, based on thermodynamic and hydrodynamic considerations, was given in the review of Anderson [5] and will be explained at the end of this section.

2.3.1 Thermodynamic Argument

As the experiments show that diffusiophoresis is a mechanism for motion at low Reynolds numbers, it has to be clarified which are the basic physical mechanisms behind this kind of motion. As has been discussed previously, it can be assumed that there is no pressure gradient in the system and hence no convective transport occurs. However, by thermodynamic considerations, it can be shown that a transport of a particle from a high solute concentration to a low one can decrease the free energy in the system. This makes the motion of the colloid thermodynamically favorable. This line of argumentation was originally given by Anderson and Prieve [92].

Consider a surface which can absorb or repel solute particles. A thermodynamic measure to evaluate the strength of interaction of the surface with the solute is the so called Gibbs surface excess concentration

$$\Gamma = \frac{c^{\text{surface}} - c^{\text{bulk}}}{A}. \tag{2.5}$$

It relates the concentration of the solute at the surface to the concentration in the bulk. Here, A is the size of the surface making it an intensive variable. The Gibbs surface excess concentration is positive if the surface absorbs solute particles and negative if it repels them. It can be related to the surface excess free energy or interfacial tension γ via the thermodynamic relation

$$d\gamma = s^{\text{surface}} dT - \sum_i \Gamma_i d\mu_i, \tag{2.6}$$

called Gibbs absorption equation [93]. Here, s^{surface} is the surface entropy and μ_i is the chemical potential. This equation shows that in the case of an isothermal system, the change

of the interfacial tension is proportional to the change in the chemical potential. In a dilute suspension it can be assumed that the Gibbs excess concentration is approximately constant. If for the chemical potential an ideal binary mixture is assumed, meaning an ideal gas equation of state can be expected, it can be given by

$$\mu_i = \mu_{i,0}(T) + k_B\,T \ln\left(\frac{c_i}{k_B\,T}\right). \tag{2.7}$$

Hence, in an isothermal system the change of the interfacial tension is related to the change of the bulk concentration. If a colloid is taken from a solute concentration c_1 and put into a concentration c_2, the free energy F changes according to

$$\Delta F = 4\pi R^2(\gamma_2 - \gamma_1), \tag{2.8}$$

which is just the integration of the interfacial tension along the colloidal surface. In order to observe a spontaneous motion of the object, the following condition has to hold for adsorption

$$c_2 > c_1 \quad \Rightarrow \quad \gamma_2 < \gamma_1 \quad \Rightarrow \quad \Delta F < 0,$$

as the Gibbs surface excess concentration is negative $\Gamma < 0$. Respectively, if the surface repels the solute particles $\Gamma > 0$ is positive and

$$c_2 < c_1 \quad \Rightarrow \quad \gamma_2 < \gamma_1 \quad \Rightarrow \quad \Delta F < 0.$$

For a continuously changing solute gradient the continuous version of equation (2.8) is given by

$$\begin{aligned} \nabla F &= 4\pi R^2 \nabla\gamma, && (2.9)\\ &= 4\pi R^2 \frac{\partial\gamma}{\partial c_\infty}\nabla c, && (2.10)\\ &= \frac{k_B T\Gamma}{c}, && (2.11)\\ &= k_B T K. && (2.12) \end{aligned}$$

In the last line, the Gibbs excess concentration has been substituted by the adsorption length $K = \Gamma/c_{\text{bulk}}$. It can be considered as the thickness necessary for a surface layer to end up with the same concentration as in the bulk [84]. The adsorption length can be negative if the surface is repulsive. As the Gibbs excess concentration can be obtained in experiments [94] the adsorption length can also be calculated. The adsorption length is a fundamental quantity of the system and one of the main results of a more detailed theory is to relate it to microscopic quantities of the system like the interaction potential between solute and surface.

So far, it has been shown that a surface process can lead to the motion of a colloid along a gradient. If this thermodynamic approach is used to deduce the mean velocity, wrong results arise. This stems from the fact that such an approach would use the Stokes friction to find the velocity which is no longer applicable for a surface active motion.

2.3.2 Relation between Interfacial Tension and Slip Velocity

In the previous section, it was shown by thermodynamical arguments that a colloid can move in an external gradient due to surface interaction. In order to estimate the mean velocity of such

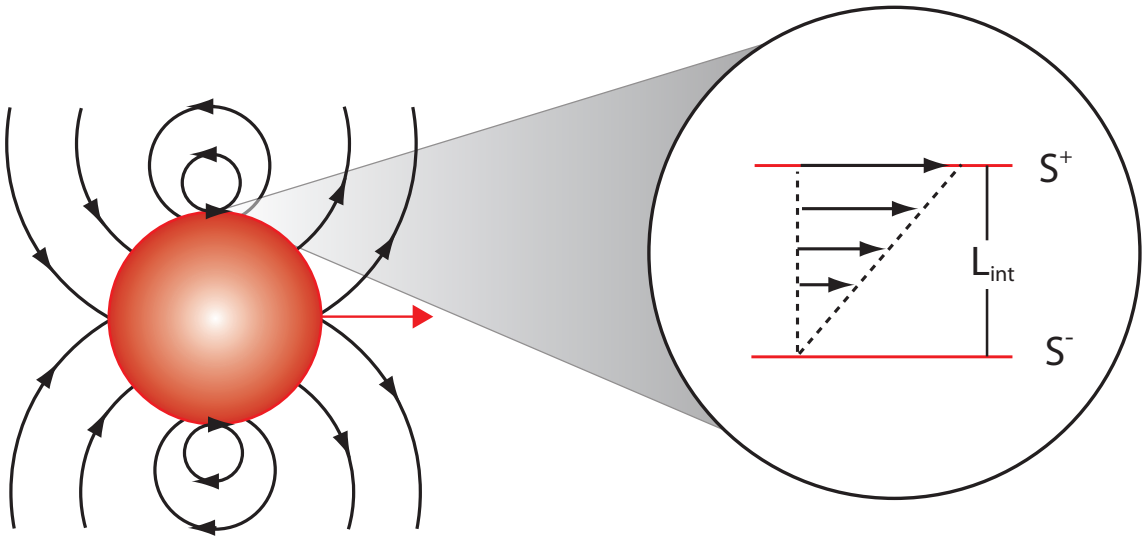

Figure 2.6: The velocity field around a diffusiophoretic sphere (red) depends on the boundary conditions on its surface. At length scales of the size of the sphere a slip velocity is proposed by theory which can be used as a boundary condition of the Stokes equation. However, a closer look reveals that on length scales $L_{\text{int}} \ll R$ much smaller than the radius of the sphere, the velocity of the fluid decays to the velocity of the sphere. The finite velocity difference between the sphere and the fluid at S^+ arises due to surface active processes.

an object, the thermodynamic description given above has to be coupled to the hydrodynamic one of the solution. Here it will be shown, that this can be done through a slip velocity at the boundary between the colloid and the fluid which serves as a boundary condition for the Stokes equation. The relation between surface tension and the slip velocity will be clarified.

A hydrodynamic flow produced by surface tension has been widely reported in literature. As the interfacial tension can be considered as a force per length, the tension along the interface between two phases results in a net force. If this force is not balanced by an external force this leads, according to the Stokes equation, to a hydrodynamic flow. This effect is called Maragoni effect and has been observed in droplets moving along surfaces with predescribed surface tension gradients [95, 96] or a flow produced by the surface tension of two immiscible fluids at equilibrium [97]. It has also been suggested as a origin of the motion of self-propelled swimmers [98, 99] and it has been stated that the slip velocity of diffusiophoresis arises due to a similar phenomenon [5]. However, as will be seen from the general treatment given here, a slip velocity can also arise without surface tension. Therefore, a general non-equilibrium thermodynamic approach will be described which captures very different situations such that a comparison between diffusiophorertic and other surface driven motions is possible. The approach shown here summarizes work previously done by Jülicher and Prost [66].

Consider an intermediate zone of height L_{int} between a fluid and a solid with a normal vector orientated along the z-axis. It can be assumed that the interfacial zone is small compared to length scales of the Stokes equation, as shown in figure 2.6. Therefore, it can be assumed that this zone can be incorporated in a hydrodynamic theory in a coarse grained way which only considers averaged quantities. In the ongoing, the top of the zone will be marked by a "+" and the bottom with a "−". If there is a finite slip velocity between the upper and lower

boundary, this is given by

$$v_i^{\text{slip}} = v_i^+ - v_i^-. \tag{2.13}$$

Further, if there is a shear stress throughout the zone, this can be defined as

$$\sigma_i^S = \epsilon\sigma_i^+ + (1-\epsilon)\sigma_i^-, \tag{2.14}$$

here $0 < \epsilon < 1$ is a weight of the contribution of the upper and lower boundary. From non-equilibrium thermodynamics it is known that the interfacial dissipation or entropy production is given by

$$T\dot{S} = \int dA \left(\sigma_{iz}^S v_i^S + j_i^S \nabla_i \mu^S\right), \tag{2.15}$$

where j_i^S is the particle flux from the surface and μ^S is the chemical potential at the surface. As is well known from linear Onsager theory, thermodynamic fluxes and forces can be obtained from this equation as

$$v_i^S = \nu\sigma_{iz}^S - \alpha\nabla_i\mu^S, \tag{2.16}$$

$$j_i^S = \alpha\sigma_{iz}^S - \xi\nabla_i\mu^S. \tag{2.17}$$

The Onsager coefficients $\{\nu, \alpha, \xi\}$ are material properties and do not depend on the boundary conditions, which in this case means the applied gradient. In the case of a diffusiophoretic object, no propulsion can be found if the particle gradient vanishes. Hence, the only cause of a slip velocity is the gradient, even though there might be a surface shear due to other effects. Therefore, the material parameter $\nu = 0$ has to be zero and the slip velocity is given as

$$v_i^S = -\kappa\nabla_i c^S + \kappa'\nabla_i P^S. \tag{2.18}$$

In an isothermal situation the chemical potential at local equilibrium is given as $\mu(c(\mathbf{r}), P(\mathbf{r}))$. The coefficients above are given as $\kappa = (\alpha/m)\,(\partial\mu^S/\partial C)$ and $\kappa' = (\alpha/m)\,(\partial\mu^S/\partial P)$. Both parameters are merely phenomenological. In order to apply them to a concrete situation they have to be related to microscopic parameters of the model as for example the interaction potential between fluid and solid. This will be given in the next section. One of the most important aspects of diffusiophoretic motion is that it is force free if the object is considered as a whole. Therefore, as the pressure is a force per surface at the outer boundary of the interaction zone, the pressure has to match the external pressure which in this case means that $\nabla P = 0$ outside the surface layer even though this is not true inside.

An important point which sometimes causes confusion is that the equation relating the thermodynamic flux to the thermodynamic forces given in equation (2.18) only describes the coupling of both. It should be stressed that the cause of the slip velocity is the gradient in the chemical potential and not the shear stress. As has been shown in the previous section, the interaction between the solute and the surface leads to a surface tension, which by force balance in the surface can be related to the shear stress at the top and bottom of the surface as

$$\sigma_{iz}^+ - \sigma_{iz}^- = -\partial_i\gamma(x,y). \tag{2.19}$$

The scheme above can also be applied to situations where there is no difference in the shear stress across the interfacial zone and, hence, no surface tension gradient. Nevertheless, there can be a slip velocity as from equation (2.16) it follows that $v_i^S = \nu\sigma_i^+$. This could be for example the situation in active gels like the cytoskeleton driven by ATP hydrolysis.

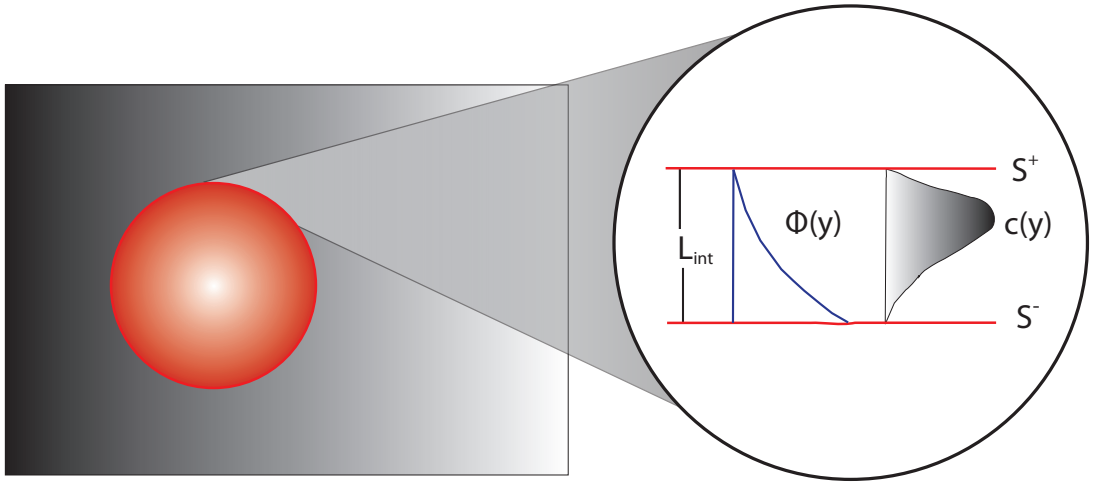

Figure 2.7: The diffusiophoretic sphere (red) moves along a solute gradient (grey shaded) and is propelled due to a slip velocity at its surface. This arises due to the local interaction of the gradient $c(y)$ with the short range potential of mean force Φ at the surface.

In the derivation so far, a few silent assumptions have been made. First of all, it was assumed that the viscosity is constant across the interface. This is justified as a decrease in the viscosity would only increase the surface slip [100]. Further, it was assumed that the particle density rearranges on a time scale much faster than the hydrodynamic flow. This corresponds to a small Peclet number, described in section 3.2. The small Peclet number condition also holds in experiment.

So far, it has been shown that a particle gradient can lead to a slip velocity due to interfacial tension. However, the description in terms of an interfacial region cannot not be directly proven by experiments as the interface has a length L_{int} which is the range of nm. Therefore, the phenomenological constant κ introduced above has to be related to a microscopic model of the interfacial zone. This will be done in the next section for diffussio- as well as selfdiffusiophoresis.

2.3.3 Microscopic Derivation of the Slip Velocity

As has been shown by the general thermodynamic arguments given in the previous section, it is possible to relate the propulsion of an object in a particle gradient to an effect at the interface between the solution and the solid body. Here, a general microscopic theory is described which relates the mean velocity of the imbedded object to an effective slip velocity at the surface which arises due to a microscopic potential instead of relating it to thermodynamic quantities like the surface tension. This mainly means to find a microscopic expression for the Onsager coefficient κ introduced in the previous section.

In most applications of the Navier-Stokes as well as the Stokes equation it is assumed that at an interface between a fluid and a solid the no slip boundary condition can be applied. For no slip boundary conditions it is assumed that the velocity of the fluid decays to the

velocity of a imbedded surface on a length scale which is not resolvable within the field theory. However, situations have been proposed like e.g. a system with a reduced viscosity close to a surface in which a slip velocity can arise [100]. In the general theory of diffusiophoresis it is assumed that the slip velocity arises due to the interaction of the immersed object with the externally imposed gradient [5]. Therefore, the system is divided into two regions. In the first one, close to the surface and characterized by a length scale L_{int}, already introduced in the previous section, the Stokes equation has to be solved taking into account the interaction between the solute and the colloid. The second one is much larger and given by L_{St}. Here, the Stokes equation is force free and the effect of the solute is only incorporated via the boundary condition at the colloid surface. Hence, it is assumed that the interaction between the external gradient and the object only takes place in the small interfacial area L_{int}, see figure 2.7. The interaction is mediated through a potential of mean force $\Phi(\mathbf{r})$, which can be considered as an effective potential acting on the solute radial to the interface. The only condition onto this potential is that it is short range meaning that it decays faster or equal to $\mathcal{O}(R^{-1})$. It is assumed that the Peclet number in the interfacial region is much smaller than one $Pe \ll 1$. The Peclet number $Pe = U\,L/D$ compares the convective transport in a system, given by the typical velocity U and length scale L, with the diffusive, measured by the diffusion constant D. As this quantity is small here, the solute transport in this interfacial region is dominated by diffusion and, hence, it can be assumed that the solute concentration is given by a Boltzmann distribution

$$c = c^S \exp(-\Phi/k_B\,T). \tag{2.20}$$

Here, c^S is the concentration at the outer edge of the surface interfacial layer L_{int}. Hence, the Stokes equation in the interfacial region can be solved with an external force resulting from the potential of mean force between the colloid and the solute particles

$$\frac{\partial p}{\partial y} + c\frac{d\Phi}{dy} = 0, \tag{2.21}$$

$$\eta\frac{\partial^2 v_x}{\partial y^2} - \frac{\partial p}{\partial x} = 0. \tag{2.22}$$

At the outer boundary of L_{int} an effective slip velocity $\mathbf{v}^s$ is obtained as

$$\mathbf{v}^S = -\frac{k_B T}{\eta}\int_0^\infty y\,[\exp(-\Phi/k_B T) - 1]dy\frac{dc}{dx}, \tag{2.23}$$

which depends on the strength of the tangential solute gradient. Here, two length scales can be introduced

$$K = L_{int}\int_0^\infty [\exp(-\Phi/k_B T) - 1]dy, \tag{2.24}$$

$$L = \frac{L_{int}}{K}\int_0^\infty y\,[\exp(-\Phi/k_B T) - 1]dy, \tag{2.25}$$

where K is the Gibbs adsorption length introduced in the previous section and L is the expectation value of the solute distribution. The integration variable is rescaled as $y = (r - R)/L_{int}$ where r is the distance from the surface and R the radius of the colloid. The resulting slip velocity is given by

$$\mathbf{v}^S = \frac{k_B\,T}{\eta}K\,L\frac{dc^S}{dx}. \tag{2.26}$$

As has been described previously, the adsorption length can be obtained in the different experiments. The length scale L, however, is not accessible experimentally. Mostly, it is assumed that it is similar to the interfacial height L_{int}.

Using the slip velocity derived above, it is now possible to solve the Stokes equation in the outer region with the boundary conditions

$$\text{at } \mathrm{L_{int}}: \ \mathbf{v} = \mathbf{U} + \mathbf{\Omega} \times \mathbf{r} + \mathbf{v}^S, \tag{2.27}$$

$$\mathbf{r} \to \infty : \mathbf{v} \to 0. \tag{2.28}$$

Here $\mathbf{U}$ and $\mathbf{\Omega}$ are the velocity as well as angular velocity of the object. It can be shown that the mean velocity of a passive driven sphere is

$$\mathbf{U} = \frac{k_B\,T}{\eta} K\,L \frac{dc}{dx}\bigg|_{\infty}. \tag{2.29}$$

Here $\frac{dc}{dx}\Big|_{\infty}$ is the unperturbed gradient of the solute which drives the motion. Remembering the definition on L and K one can rewrite this result as [101]

$$\mathbf{U} = \frac{k_B\,T}{\eta} L_{int}^2 \kappa_1 \frac{dc}{dx}\bigg|_{\infty}, \tag{2.30}$$

with the first order integral of the form

$$\kappa_n = \int_0^{\infty} y^n \left[\exp(-\Phi/k_BT) - 1\right] dy. \tag{2.31}$$

From equation (2.30) it can be seen that the mean velocity of a diffusiophoretic driven sphere does not depend on its size. This is a typical property of surface driven objects. The propulsion depends only on the square of the heights of the interaction zone. For selfdiffusiophoretic motion size dependence has been reported but can be attributed to a more complex reaction at the surface [102].

From the form of the velocity it is not clear how the diffusiophoretic swimmer interacts with its environment. As the external gradient, in contrast to an external force, does not lead to a net force acting on the object, the body is torque and force free

$$\int_S \mathbf{n} \cdot \sigma dS = 0, \tag{2.32}$$

$$\int_S \mathbf{r} \times (\sigma \cdot \mathbf{n}) dS = 0. \tag{2.33}$$

This has significant effects on the flow field produced by the swimmer. In contrast to a sphere driven by a Stokeslet, which decays as $\mathcal{O}(\mathbf{r}^{-1})$, it decreases as $\mathcal{O}(\mathbf{r}^{-3})$. As the disturbance in the concentration filed decays like a dipole field, hence as $\mathcal{O}(\mathbf{r}^{-2})$ [89], and the velocity depends on the gradient of this field, effects due to hydrodynamics and to concentration disturbance are on the same length scale. Therefore, to investigate collective effects of diffusiophoretic swimmers it is necessary to use an approach that is able to resolve hydrodynamic as well as concentration effects, like the MPC technique that will be described in chapter 3.

2.3.4 Extensions to Electrolytes

The diffusiophoretic motion discussed so far has only been considering non-electrolyte solutions as otherwise the electrical charge of the solute has to be included in the analysis. Here, a short remark on electrolytes will be given, even though they are not relevant for this work. A slip velocity for electrolytes has been given by Prieve [83]

$$\mathbf{v}^S = \frac{\epsilon}{2\,\pi\eta}\left(\frac{k_B\,T}{Ze}\right)^2 \ln(1-\zeta^2)\frac{d\ln(c^S)}{dx} + \frac{\epsilon\zeta}{4\,\pi\,\eta}\mathbf{E}^S, \tag{2.34}$$

here ζ is the zeta potential describing the electric interaction between the colloid and the electrolyte. The rest is well known material properties. The significant difference between the mechanism described here and the non-charged version is the arising of second contribution. The first term in the slip velocity is called chemiphoretic as it is related to the motion due to the gradient of electrolytic concentration just as it is the case in diffusiophoreis. The second term is the electrophoretic contribution and leads to a motion in the opposite direction. It arises because the cations and anions in the solution do not have the same diffusion constant, which leads to a microscopic electric field. As most aqueous solutions are electrolytes they are much more amenable to experimental investigations and have been studied extensively [72–78]. From a simulations perspective it is the other way around, as capturing the long rang electrostatic interactions is rather difficult. However, there have been attempts to simulate electrolytes [103] in the context of thermophoresis [104].

2.4 The Theory of Selfdiffusiophoresis

In contrast to diffusiophoresis, in selfdiffusiophoresis it is assumed that the object considered, here mostly a sphere, is not driven by an external gradient but produces a gradient itself. In the former case, the symmetry in the system is broken by the external gradient while the colloid itself has a homogenous surface structure. If in the latter case the sphere would produce the gradient homogeneously around its surface, e.g. through a catalytic reaction, this would only lead to an increase in the diffusion constant but no directed motion would be observed. Therefore, the simplest model which can produce an asymmetric particle gradient around a spherical object is a Janus particle which has only one active hemisphere producing particles while the other one does not. This model will be used throughout this section as well as in the simulations done in chapter 4.

2.4.1 Fundamental Equations of the Theory

In diffusiophoresis it is assumed that the external particle gradient is only slightly affected by the motion of the embedded object and can hence be considered as constant during the relevant timescales. In the selfdiffusiophoretic version the gradient concentration itself becomes a dynamic quantity as it is permanently altered by the production at the active surface. Following Sabass and Seifert [89], here a Janus colloid is considered which converts a solute

particle of a type A into type B particles through a catalytic reaction at the active hemisphere. This can be done straight forwardly by using a simple field approach

$$\partial_t c_A(\mathbf{r},t) = -\nabla c_A \mathbf{v} + D_A \nabla^2 c_A(\mathbf{r},t), \tag{2.35}$$

$$\partial_t c_B(\mathbf{r},t) = -\nabla c_B \mathbf{v} + D_B \left(\nabla^2 c_B(\mathbf{r},t) + \nabla\big(\frac{c_B}{k_B T}\nabla\Phi\big)\right), \tag{2.36}$$

$$\eta\nabla^2\mathbf{v} - \nabla p = c_B\,\nabla\Phi. \tag{2.37}$$

The first term on the right side of the first two equations describes the motion of the educt respectively product particles through a convective flow, while the second describes their motion due to diffusion. It is assumed that the conversion takes place while the educt particles of type A hit the surface. The particles of type B interact with the surface via an effective potential Φ which is considered repulsive in the rest of this work but could also be attractive. It is similar to the potential of mean force used in the microscopic derivation of the diffusiophoretic model. The interaction with the potential is the only difference between the two particle types as it is assumed that their relevant physical properties, here their mass $m_{A/B} = m$ and diffusion constant $D_{A/B} = D$, are equal. This is justified e.g. for 0_2 and H_20_2. Finally, the hydrodynamic velocity described by the Stokes equation is the mean velocity of a fluid element composed of both particle types.

To solve this set of equations, boundary conditions have to be given by

$$\mathbf{e}_r \mathbf{J}_{(A,B)}(R,\theta) = \alpha_{(A,B)}(R,\theta), \tag{2.38}$$

$$\nabla c_{(A,B)}(\infty,\theta) = 0. \tag{2.39}$$

Here, the first condition describes the conversion of the particles at the surface of the sphere given by its conversion rate $\alpha_{(A,B)}$, whose detailed form will be discussed later. The second states that the concentrations of both particle types are constant far away form the sphere. For the Stokes equation no slip boundary conditions can be assumed as an explicit potential is given and no assumptions of a slip velocity have been used so far.

This set of equations is the most general possibility of describing the motion of the two particle species. They are non-linear and in general difficult to solve. Therefore, they are solved in a regime where the non-linearities can be neglected. This is the case if the Peclet number of the fluid $Pe \ll 1$ is small. Hence, in a steady-state, equation (2.35) and following can be rewritten in a non-dimensional form where the effect of the Peclet number can explicitly be seen

$$\nabla^2 c_B + \nabla\cdot(c_B\nabla\Phi) - \frac{Pe}{\delta}\mathbf{v}\cdot\nabla e^{-\Phi} = Pe\,\mathbf{v}\cdot\nabla c_B, \tag{2.40}$$

$$\nabla^2 c_A = Pe\,\mathbf{v}\cdot\nabla c_A. \tag{2.41}$$

Here $\delta = c_B/c_{B,\infty}$ is the relative deviation from the equilibrium distribution. If it can be assumed that the gradients in the system are small and the deviation from the equilibrium distribution are not of the same order as the Peclet number, the final set of equations to solve is given by

$$\nabla^2 c_B + \nabla\cdot(c_B\nabla\Phi) = 0, \tag{2.42}$$

$$\nabla^2 c_A = 0, \tag{2.43}$$

$$\nabla^2\mathbf{v} - \nabla p - \frac{1}{\lambda^2}\,C_B\nabla\Phi = 0, \tag{2.44}$$

with $\lambda = L_{int}/R$. Here L_{int} is the typical decay length of the potential, described previously in section 2.3.2. In order to solve this set of equations, two different approaches have been used. The first one assumes that on the length scale of the Stokes equation the potential Φ decays to zero and its effect can be introduced via a slip velocity at the boundary of the Janus particle analog to the diffusiophoretic case in 2.3.3. The second approach explicitly solves the set of equations derived above in a zone close to the surface and in one far from the surface and uses a matching procedure to obtain the mean velocity of the swimmer. Even though both approaches lead to similar results, the necessary conditions for the applicability differ fairly.

2.4.2 Explicit Slip Velocity

In the approach pioneered by Golestanian [105], the surface activity of the sphere is captured in a slip velocity which is similar to the one obtained for diffusiophoresis in section 2.3.3 and can be written as

$$\mathbf{v}_S = \kappa(\mathbf{r}_S)\nabla_{||}c_B. \tag{2.45}$$

This gives the boundary condition for the Stokes equation on a length scale where the potential has decayed to zero. Here, κ is a phenomenological function which captures the specific interaction of the solute particles with the sphere. It depends on the detailed surface structure of the sphere as well as the microscopic potential. For a Janus colloid with particle conversion only on one half-sphere but an isotropic surface potential, the conversion rate α and the surface activity κ are given by

$$\{\alpha(\theta), \kappa(\theta)\} = \begin{cases} \{\alpha_0, \kappa_0\}, & \text{if} \quad 0 < \theta < \frac{\pi}{2}, \\ \{0, \kappa_0\}, & \text{if} \quad \frac{\pi}{2} < \theta < \pi, \end{cases} \tag{2.46}$$

where θ is the azimuthal angle. The functions $\{\alpha(\theta), \kappa(\theta)\}$ contain the catalytic activity and the interaction of the sphere with the product particles and specify the boundary problem completely. However, in this approach it is assumed that the concentration of the educts is much higher than the concentration of the products $c_A \gg c_B$ and, hence, can be assumed to be constant throughout the system.

For equation (2.45) it is, like in the diffusiophoretic version, assumed that the Peclet number is small, such that the process in the boundary layer as well as the relaxation of the product concentration is controlled by diffusion.

Using the slip velocity (2.45) it is possible to solve the Stokes equation via an expansion in the eigenfunctions of the Laplace operator [9]. With the further assumption that the Janus particle is force and torque free it is possible to obtain the hydrodynamic flow field around the sphere. In most experimental investigations the flow field is difficult to measure. Therefore, it is of more general interest to determine the mean velocity of the Janus particle, which is easier accessible in experiments. It can be obtained straight forwardly by using the so called reciprocal theorem [105] whose detailed form will be given later in this section.

For a Janus type colloid this approach leads to the mean propulsion velocity [6]

$$\mathbf{U}_{Golestanian} = \frac{k_B T L_{int}^2}{4\,\eta}\frac{\alpha_0}{D}. \tag{2.47}$$

Here, the surface activity is defined as $\kappa_0 = k_B T L_{int}^2/\eta$, similar to the form of a diffusiophoretic sphere in section 2.3.2. It shows the same dependence on the interaction length as the diffusiophoresis in an external gradient. However, in contrast thereto, instead of depending linearly on the external gradient it depends on the ratio of the production rate at the surface divided by the diffusion constant of the products.

In this approach it is assumed that the interaction zone described by L_{int} is small compared to the length scale relevant for the solution of the Stokes equation. In simulations, like the ones described in chapter 4, it is not possible to keep this constraint as the boundary layer has to be modeled explicitly. Otherwise, the simulation has to capture two distinct length scales which makes it computationally inappropriate. As will be shown in the next section this is, however, still a good first order approach.

Reciprocal Theorem

In order to derive equation (2.47), the so called reciprocal theorem [106] has been used. As this is of general interest for objects with surface driven motion, its basic principles will be described here. The reciprocal theorem is a straight forward approach to obtain the mean velocity of a propelled object at low Reynolds numbers. However, if further informations about the object are needed, like its hydrodynamic flow field, alternative approaches like the streaming function have to be used [66]. The reciprocal theorem has previously been used in low Reynolds number hydrodynamics [107] but has first been applied to surface driven swimmers by Stone and Samuel [108]. The basic idea is to consider two solutions of the Stokes equation with the same boundary condition at infinity. The solutions are given in terms of the velocity fields $\mathbf{u}$ and $\mathbf{u}'$ as well as the shear tensors σ and σ'. The first solution gives a flow field which is produced by the boundary conditions at the surface $S(t)$ of an immersed object. The second is produced by a Stokeslet force acting on the object. Due to the principle of virtual work and the linearity of the Stokes equation it can be shown that

$$\int_{S(t)} \mathbf{n}\,\sigma' \cdot \mathbf{u}\,dS = \int_{S(t)} \mathbf{n}\,\sigma \cdot \mathbf{u}'\,dS, \tag{2.48}$$

with $\mathbf{n}$ the outwards normal of the surface. As the for the solution with an external force the surface velocity is equal to the propulsion velocity $\mathbf{u}' = \mathbf{U}'$, it does not contribute to the integral on the right-hand side of equation (2.48), which now becomes the total force of the first situation and is, hence, zero. If on the left-hand side the surface velocity is decomposed into the propulsion velocity $\mathbf{U}$ and the surface velocity $\mathbf{u}_s$ it yields

$$\mathbf{F}'(t) \cdot \mathbf{U}(t) = -\int_{S(t)} \mathbf{n}\,\sigma' \cdot \mathbf{u}_s\,dS. \tag{2.49}$$

If it is further used that the force of a Stokeslet is given by $\mathbf{F}' = -6\,\pi\eta R\,\mathbf{U}'$ and the shear tensor by $\sigma' = (-3\eta/2R)\,\mathbf{U}'$, it follows that the mean propulsion of a surface driven swimmer is

$$\mathbf{U}(t) = -\frac{1}{4\pi R^2}\int_S \mathbf{u}_s\,dS. \tag{2.50}$$

In the case of a selfdiffusiophoretic Janus particle the velocity at the surface is given by the slip velocity described in equation (2.45),$\mathbf{u}_s = \mathbf{v}_s$, yielding

$$\mathbf{U}(t) = -\frac{1}{4\pi}\int \kappa(\mathbf{r}_S)\nabla_{||}C(R,\theta,\phi,t)d\Omega. \tag{2.51}$$

This makes it quite easy to obtain the mean propulsion with this approach. However, if convection disturbs the product concentration considerably, a more general approach should be applied as described in the next section. Similar to the mean velocity of an object, its angular velocity can be obtained by the same approach

$$\mathbf{\Omega}(t) = -\frac{3}{8\pi R^2}\int_S \mathbf{n}\times\mathbf{u}_s\, dS. \tag{2.52}$$

In the recent years, the reciprocal theorem has been applied to many different kinds of swimmers at low Reynolds numbers [105, 109, 110].

2.4.3 Matching Procedure

In order to obtain results behind the assumption of a small surface layer, Sabass and Seifert explicitly solved the Stokes equation in the interaction zone as well as outside and used a matching procedure and the Pade approximation to find the mean velocity of a selfdiffusiophoretic Janus particle. This approach has previously been used by Anderson and coworkers to derive the propulsion velocity of a diffusiophoretic particle in an external gradient [101]. For the Stokes equation the boundary conditions here recast the classical ones of a colloid in a fluid, which are no slip at the surface and zero at infinity

$$\mathbf{v}(\mathbf{r} = \mathbf{r}_S) = U, \tag{2.53}$$
$$\mathbf{v}(\mathbf{r} \to \infty) = 0. \tag{2.54}$$

For practical reasons, most calculations are done in the rest frame of the colloid, leading to a mean velocity of the sphere as [89]

$$\mathbf{U}_{Sabass} = \frac{k_B\, T L_{int}^2}{3\,\eta}\frac{\alpha}{D}. \tag{2.55}$$

It can easily be extended to larger interaction zones

$$\mathbf{U}(\lambda) \approx \mathbf{U}_{Sabass}/\big[1 + \lambda\left(\kappa_0 + \frac{7\,\kappa_2}{2\,\kappa_1} + \frac{Pe}{\delta}\frac{M}{2} + \frac{N}{\kappa_1}\right)\big]. \tag{2.56}$$

It still has to be assumed that the interaction between the colloid and the products has to take place in an area in which diffusion dominates. However, the condition is not as strict as in the approach used by Golestanian but has to be $\lambda\, Pe \ll 1$. This states that if the Peclet number becomes larger due to convection, the ratio of the interaction zone height and the radius of the Janus particle has to decrease.

The results of Golestanian and Sabss only deviate from each other by a prefactor. The factor κ_n is defined as in equation (2.31) and M as well as N are similar defined integrals not relevant

for the result. Finally, $\delta = c_B/c_{B,\infty}$ is the deviation of the local product concentration from its concentration at infinity.

With this approach and numerical solutions it is possible to show that for lager interaction zones the velocity scales less than linearly with its length L_{int}. Further, the interaction potential has only a quantitative effect on the propulsion velocity.

2.4.4 Assumptions of the Theory

The general applicability of the theory described in section 2.4.1 is still under debate [111, 112] as the proposed slip velocity has only been observed experimentally under very strong thermal gradients [113]. This asks for further experiments, also investigating the other phoretic effects as for example diffusiophoresis.

The main assumption for the motion of a selfdiffusiophoretic Janus particle is that the Peclet number is small. It is a necessary condition to ensure that the process in the surface layer, mainly the equilibration of the product concentration, is dominated by diffusion and not by convection. Care has to be taken as in the literature [26] the Peclet number has sometimes been defined using the diffusion constant of the propelled object rather than the of the solutes. This quantity can be larger than one, as this diffusion constant is significantly smaller than the one of the solute particles.

In general, a dilute concentration of the solute particles, whether the educts or products, is assumed, often stated as $c_{A/B}\, a^3 \ll 1$, where a is the size of the the solute molecules. Therefore, it is a valid assumption that the solute molecules only interact via elastic collision and hence an ideal gas equation of state can be expected. This is justified as in most experiments using water peroxide, the concentration is below 10%. If H_2O_2 is used for the propulsion of the swimmer it can be assumed that from a physical point of view it has the same properties as H_2O. It might be that in a more detailed theory of diffusiophoresis the weakly acid nature of water peroxide has to be considered. For the effect on the surface tension it has been shown that there is no significant difference between both constituents [114].

Further, it has to be ensured that the time scale separation necessary for the theory can also be obtained in the respective experiments. For the problem considered here, the two relevant time scales are the diffusion time of the solvent molecules $\tau_D = R^2/D_{A/B}$ and the rotational diffusion time $\tau_{rot} = 1/(2\, D_{rot})$. For the theory to be applicable it has to be assured that $\tau_D \ll \tau_{rot}$. Using the Stokes-Einstein relation this can be recaptured to be $a \ll R$. Here a is the radius of the solvent molecules and R is the colloid radius. In experiments with water peroxide the solvent size is in the range of $\sim$ Å and the colloid has a diameter $\sim \mu$m. As the propulsion mechanism does not affect the time scale separation, it stays a valid approximation. Otherwise, the rotation of the colloid has to be incorporated in the field equation via an extra term $e_\theta r D_{rot} \partial_\theta c_{A/B}$.

Finally, for the field theoretical approach given by the Stokes equation to hold, it has to be ensured that the local equilibrium condition is valid in the fluid as well as in the surface layer. For the latter it is necessary that the solute molecules are much smaller than the typical height of the interaction zone $a \ll L_{int}$. The relaxation of the hydrodynamic flow field is much faster

than the time scale of the particle conversion. Therefore, it can be assumed that in the surface layer the particle gradient is balanced by a local pressure gradient even though outside the layer the pressure gradient vanishes.

All the conditions above naturally apply to the experiments done so far. However, to go a step further, there is an urgent need to develop the standard theory of diffusiophoresis beyond these approximations. Especially, it would be interesting to extend it further to bigger solvent molecules where the hydrodynamic description might not be sufficient. Then, such ambitious approaches as to apply diffusiophoresis to other phenomena like cell division [46] could be studied in detail.

2.4.5 Motion in Confinement

So far, mainly the mean velocity of a freely moving selfdiffusiophoretic Janus particle has been considered. In order to use such an artificial swimmer for practical applications, its behavior in more complex situations has to be analyzed. Using the explicit description of the slip velocity given in equation (2.45) it was possible to derive expressions for the Janus particle confined in a spherical environment. For the mean velocity two correction terms have been found due to the confinement [9]

$$\mathbf{U}_{bound} = \mathbf{U}_{free}\chi_1(\epsilon)\chi_2(\epsilon), \tag{2.57}$$

here $\epsilon = R_{bound}/R$ is the ratio of the radii of the confinement and the colloid. The hydrodynamic contribution $\chi_1(\epsilon) < 1$ is smaller than one, as vortices can arise due to the confinement, resulting from the reflection of the hydrodynamic field at the boundaries. This reduces the hydrodynamic back flow responsible for the propulsion of the swimmer. The diffusive contribution is always greater than one $\chi_2(\epsilon) > 1$, as the boundaries lead to an increase of the particle concentration around the swimmer. For small ϵ the diffusive contribution dominates, which can lead to a sustainable increase of the velocity, in contrast to a decrease proposed in [22]. The effect of the diffusive contribution is only correct for a sufficiently small particle concentration produced by the swimmer. If the concentration becomes to high, the ideal gas equation of state of the product particles breaks down as the higher order correlation becomes significant. In the limit of large ϵ, both contributions cancel each other out. This can be understood qualitatively as follows: The hydrodynamic flow field of a phoretic swimmer decays as $\mathcal{O}(r^{-3})$ and the concentration gradient decays as $\mathcal{O}(r^{-2})$. For the motion of the swimmer, however, the gradient of the concentration is relevant and hence, both effects decay equally. The effect of the confinement becomes relevant for both contributions on the same length scale. Even though there have been experiments on the effect of confinement and complex geometries on the behavior of the swimmer [7], a detailed experimental study of the velocity of a Janus particle in confinement is still lacking.

Another interesting question is the effect of a cargo on the swimmer. Using again equation (2.45) for the slip velocity, this has already been addressed [115]. It was shown that the connection between the cargo and the colloid is highly relevant for the propulsion speed. Experimentally, it has been proven that the cargo leads to a decrease of the swimmer velocity [116]. In a further set of experiments, it has been shown that the cargo leads to a stabilization of the motion of the swimmer. This can be seen by highly straight trajectories leading to an increase of the rotation diffusion time [40]. Simulations of a dimer swimmer lead to results confirming that this kind of motion could be expected [39, 117].

ΔL^2_{sym}	$\simeq \frac{8\,\alpha_0 (k_B T\, L)^2}{3\pi^{3/2} D^{3/2} \eta^2 R^3}\, t^{3/2}$	$t \ll \tau_D$
ΔL^2_{sym}	$\simeq \frac{2 c_1 \alpha_0 (k_B T\, L)^2}{(\pi D \eta R)^2}\, t$	$t \gg \tau_D$
ΔL^2_{asym}	$\simeq v_0^2\, t^2 \left[1 - \frac{4 c_2}{\pi}\left(\frac{\tau_D}{\tau_r ot}\right)\right]$	$t \ll \tau_D$
ΔL^2_{asym}	$\simeq v_0^2\, t^2 \; - \left(\frac{8 v_0^2 \tau_D^{3/2}}{3\sqrt{(\pi)}\tau_{rot}}\right) t^{3/2}$	$\tau_D \ll t \ll \tau_{rot}$
ΔL^2_{asym}	$\simeq 2 v_0^2\, \tau_{rot} t^2$	$\tau_{rot} \ll t$

Figure 2.8: Considering the symmetric and antisymmetric surface pattering separately, different scalings arise on various time scales which cannot be observed for a classical Brownian colloid. They arise due to the altered particle distributions around the colloid.

2.4.6 Longtime Limit of the Swimmer

In an experiment, it is rather difficult to extract the short time behavior of a swimmer while the long time behavior can be obtained more easily [6, 7]. In simulation it is vice versa as the long time limit is much more time consuming than the short time limit and computational time is always a bottleneck in simulations [117, 118]. From a simulation point of view this work is the first one which tackles the long time limit of a selfdiffusiophoretic swimmer in detail.

In most experiments the mean velocity of the swimmer can only be derived through the mean square displacement of a Brownian particle with an internal velocity v_0 [119]. However, Golestanian [120] was able to derive an expression for the diffusion constant of a surface active swimmer with an arbitrary surface structure

$$D_{eff} = \underbrace{\frac{k_B T}{6\pi\eta R}}_{\text{hydrodynamic}} + \underbrace{\frac{v_0^2 \tau_R}{3}}_{\text{asymmetric}} + \underbrace{\frac{c_1 \alpha_0 k_B T \kappa_0^2}{3\eta(\pi D R)^2}}_{\text{symmetric}}. \tag{2.58}$$

Here, $c_1 = 1.1781$ is a numerical constant coming from the derivation and α_0 the conversion rate at the surface. The diffusion constant was obtained using the velocity derived with the reciprocal theorem. This was used to determine the autocorrelation function of such a swimmer. With this result, it is straight forward to find the mean square displacement via

$$\Delta L^2(t) = \langle [\mathbf{r}(t) - \mathbf{r}(0)]^2 \rangle = \int_0^t dt_1 \int_0^t dt_2 \langle \mathbf{v}(t_1) \cdot \mathbf{v}(t_2) \rangle. \tag{2.59}$$

The hydrodynamic contribution recaptures the Stokes-Einstein relation. While the symmetric contribution depends on the structure of the surface described by the surface activity κ_0 as well as the conversion rate α_0, the asymmetric contribution only depends on the internal velocity v_0. Even though the diffusive regime has been recaptured in the long time limit for

time scales smaller than the rotation diffusion time $t \ll \tau_{rot}$, various other regimes have been found, as shown in figure 2.8. This shows that the propulsion cannot only be described by a colloid driven with an intrinsic velocity as is described in many active systems [121, 122], but the coupling of the swimmer to the solvent leads to a profound set of new behaviors.

Recently, it has been shown that for a colloid producing particles symmetrically, hydrodynamic effects have to be incorporated to observe the expected $t^{3/2}$ regime in the mean square displacement [123]. With a SRD/MPC simulation this regime should in principle be addressable. It is, however, quite difficult to match all the necessary time scales in this regime. In experiments [6, 7, 118] as well as in simulations with SRD/MPC, see chapter 4, the asymmetric contribution to the diffusion coefficient has been clearly visible.

2.5 Conclusion

In this chapter, the motion of a diffusiophoretic as well as a selfdiffusiophoretic colloid has been discussed. It has been shown that for both kinds of motion there are experimental evidences and theoretical approaches explaining their basic properties. However, there are open questions for both phenomena which have not been consistently explained in literature.

Diffusiophoresis

The classical theory of diffusiophoresis describes the motion of a colloid in an electrolyte as well as a non-electrolyte particle gradient at low Reynolds numbers. In contrast to a gaseous environment the propulsion mechanism in such a regime cannot be based on momentum propagation. Therefore, it is proposed that the colloid is driven by a surface active process which leads to a relative slip velocity between the fluid and the colloid surface. The slip velocity as well as the net propulsion velocity of the colloid are proportional to the local particle gradient. It is assumed that the interaction between the colloid and the particle gradient takes place at a very narrow region L_{int} around the colloid which is significantly smaller than the scale of the flow field around the swimmer. However, the slip velocity scales with the square of this interaction length. Even though this seems to be a basic approach to propel objects at low Reynolds numbers only very few experiments have been performed to study this mechanism in detail. Especially for non-electrolyte gradients, only one experiment has been conducted by Staffeld and Quinn which confirms that the velocity of the colloids can be correctly derived from the theory.

The theory of diffusiophoresis, however, has been extended in various directions as e.g. different environments like channels or different kinds of surface structures. However, beside the experiments of Staffeld and Quinn, there is no systematic study of the motion of particles in external gradients which try to understand the influence of the environment or other boundary conditions. As a particle gradient is an ideal guiding line for the motion of an object at low Reynolds numbers, avoiding the drawbacks of mechanically driven swimmers, this experimental gap should be closed. Further, the theory as well as the experiments so far have only addressed a colloid in a solute gradient with solute molecules significantly smaller than the colloid itself. However, if the solute particles have a similar size as the colloid, the classical

theory based on field descriptions should not hold any longer. This could be a possibility to study the transition from a discrete description to a field equation.

Selfdiffusiophoresis

Inspired by the classical approach of diffusiophoresis, selfdiffusiophoresis has been proposed as an alternative to propel a swimmer at low Reynolds numbers. Experimentally, Janus colloids have been used that are able to produce asymmetric particles gradients themselves. These are mainly latex beads which are half-coated with gold respectively platinum. The coated hemisphere catalyzes e.g. H_2O_2 into water and oxygen. It has been observed that this leads to a significant increase of the diffusion constant which increases with the square of the intrinsic velocity of the sphere. This has previously been predicted by the theory of selfdiffusiophoresis [120].

For colloids driven by a self-produced gradient, experiments have been set up which consider the effect of the environment [7] and their collective behavior [77, 90]. Theoretically, less is known about such situations as the coupling of the hydrodynamics to the evolution of the motion driving field is analytically difficult to address. So far, such situations have only been investigated for colloids coupled to self-produced thermal gradients [55]. However, in models for chemotaxic bacteria [124], mimicked as brownian spheres with a constant velocity, interesting new phenomena and collective behavior have been found due to the interaction of the object with a chemoattractant as well as a repellent [125, 126]. For selfdiffusiophoretic swimmers, similar behavior can be expected, especially as not only the direction depends on the particle gradient but also the magnitude of the velocity.

3 Multiparticle Collision Dynamics

The Navier-Stokes as well as the Stokes equation describe the hydrodynamics of systems in terms of field variables like the mean velocity $\mathbf{v}(\mathbf{r}, t)$ or the density $n(\mathbf{r}, t)$. Considering smaller and smaller objects, the discrete nature of the system becomes apparent. The smooth field variables show small scale thermal fluctuations, paradigmatically shown in the Brownian motion [127], ubiquitous at length scales in the μm range. The classical simulation techniques to address hydrodynamic behavior are Lattice Boltzmann Simulations (LB) and Dissipative Particle Dynamics (DPD). The former is a lattice based method to solve the discrete Boltzmann equation while the latter is an off-lattice technique using soft potentials. In both techniques it is rather difficult to incorporate thermal fluctuations. An alternative approach towards hydrodynamics, used in this work, is Multiparticle Collision Dynamics (MPC) which naturally contains thermal fluctuations. It combines the advantage of a lattice with the one of an off-lattice approach. It consists of the integration of Newton's equation of motion in free space and local collisions of the fluid elements on a lattice. For the local collisions, different approaches have been introduced. In this chapter, between the two most common ones will be distinguished. The first one, based on a microcanonical ensemble, is termed Stochastic Rotation Dynamics (SRD) while the second one, based on a canonical ensemble, is just called Multiparticle Collision Dynamics (MPC). The simulations performed for chapter 4 are based on a canonical ensemble and therefore the MPC version is used.

This chapter introduces the MPC as well as the SRD algorithm, describes their basic properties and discusses the differences. It will be shown that both algorithms lead to thermodynamically consistent results and exhibit hydrodynamic behavior in the long time limit. The details of the implementation will be explained, with a focus on the necessary parameter to obtain the correct hydrodynamic behavior. It will be described how the results of a simulation can be mapped to the "real world" which requires an understanding of the meaning of units in simulations. Finally, the advantages of the MPC approach towards alternative techniques, especially LB and DPD, will be discussed. There is an increasing literature of applications of the MPC algorithm to many soft matter systems, making it a field of intensive research. In order to appreciate the results of these applications a profound understanding of the underlining technique is necessary.

3.1 The Basic Principles

The MPC approach is a particle based simulation technique consisting of N point particles. Their velocity and space coordinates are updated through a streaming and a collision step. In the streaming step, the particles can move freely in space according to Newton's equation of

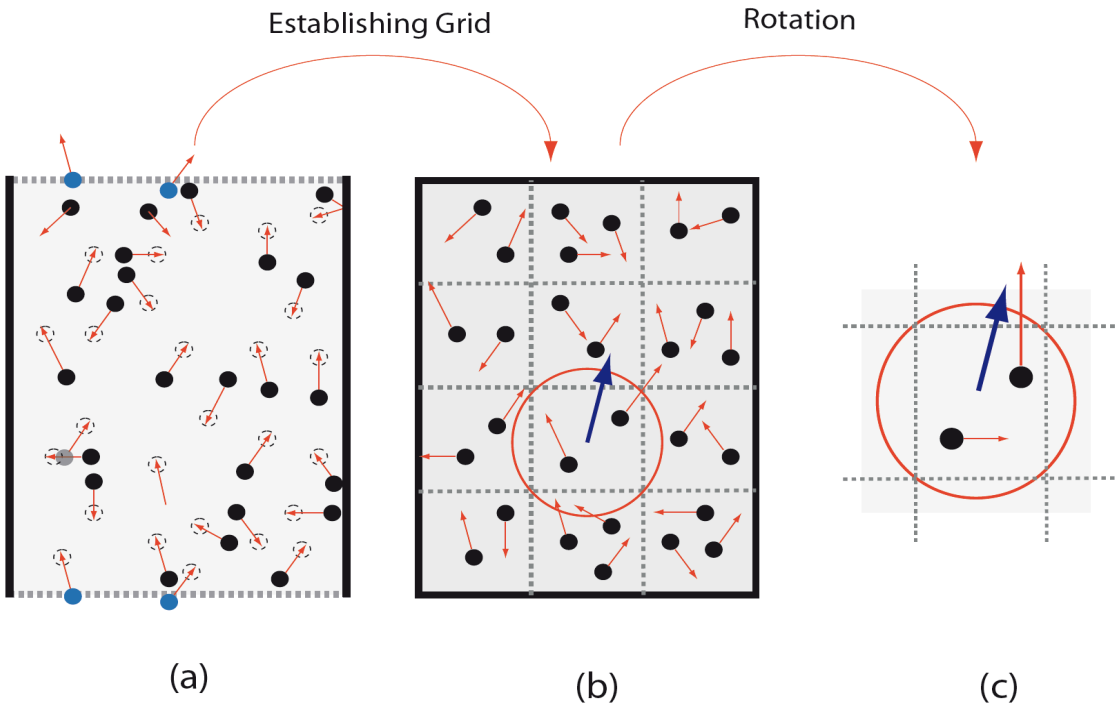

Figure 3.1: Basic scheme of a MPC/SRD algorithm. (a) Updating of the particles according to Newton's equation. (b) Imposing a grid for the collision step. (c) Local rotation of the particle velocities conserving total momentum.

motion

$$\mathbf{r}_i(t+\Delta t) = \mathbf{r}_i(t) + v_i(t)\Delta t + \frac{\mathbf{f}_{ext}}{2\,m}\Delta t^2, \tag{3.1}$$

$$\mathbf{v}_i(t+\Delta t) = \mathbf{v}_i(t) + \frac{\mathbf{f}_{ext}}{2\,m}\Delta t, \tag{3.2}$$

where $\mathbf{f}_{ext}$ can be an arbitrary external force like gravity. In most situations treated in this work, $\mathbf{f}_{ext}$ will simply be zero. During the streaming step the particles do not feel each other and can cross the path of other particles without interactions. In order to mimic the collisions between particles, relevant for the behavior of a real fluid, a multi-particle collision step has to be applied. Therefore, the particles are sorted into a cubic lattice with a lattice constant a_0. For a simulation to show hydrodynamic behavior the total momentum of a system has to be conserved if no external force is applied. As in the MPC approach all particles have the same mass this is equivalent to conserve the mean velocity. This is naturally received as the collision operator is only applied to the velocity of each particle relative to the mean velocity $\mathbf{v}_{i,c} = \mathbf{v}_i - \mathbf{v}_\xi^C$ in the respective cell. Therefore, the new velocity of a particle is given as

$$\mathbf{v}_i(t+\delta t_c) = \mathbf{v}_\xi^C + \mathbf{\Omega}[\mathbf{v_{i,c}}]. \tag{3.3}$$

Here ξ is the cell coordinate to which a particle is assigned. The detailed form of the collision operator $\mathbf{\Omega}$ depends on the approach used and will be discussed in the next section. The collision operator stochastically changes the particle velocity as a coarse grained description of their various interactions while it preserves the total momentum. The MPC approach is

a generalization of the Direct Simulation Monte Carlo Method (DSMC) pioneered by Bird [128], which instead uses only two particle collisions.

The particles of this approach should not be considered as fluid atoms like in a Molecular Dynamic Simulation (MD). They should, similar to the DPD approach, be considered as the collective effect of many fluid molecules, like the "Blobs" introduced in polymer theory by de Gennes as a coarse grained level of description [129]. In de Gennes argument, large segments of a polymer are treated due to their resulting effect onto the macroscopic behavior of it. Here, the fluid particles are mainly carrying the momentum of the fluid.

3.1.1 Microcanonical Collision Step (SRD)

A first microcanonical collision operator $\mathbf{\Omega}$ was introduced by Malevanets and Kapral around 2000 [130, 131]. This approach will be termed Stochastical Rotation Dynamics (SRD) in this work as has become common in literature. They suggested the use of a set of rotation matrices ω_i^α as these naturally conserve momentum and energy. The precise form of the rotation and the rotation axis can be chosen arbitrary as long as semi-detailed balance is satisfied, which will be explained in the context of the thermodynamic properties of the algorithm in section 3.3. In practice, two implementations have been widely used. In one, it is randomly chosen between rotations around the three coordinate axes with an angle $\pm\alpha$. In the second, the rotation axis is drawn completely random. Both models lead practically to the same results [132]. Non of these algorithms conserve angular momentum. The consequence thereof will also be discussed together with the hydrodynamic properties of the algorithm in section 3.3. Nevertheless, it is possible to modify the approach towards angular momentum conservation.

In SRD, the rotation angle α is a free parameter which defines the transport coefficients of the fluid like its diffusion constant or viscosity. The global behavior of a fluid depends on a set of transport coefficient e.g. to distinguish between a laminar and a turbulent flow. Therefore, the parameter can be used to tune the simulation. However, as all transport coefficients depend on this parameter, certain restrictions in the chosen regime occur as will be discussed in detail in section 3.2. As the SRD approach also conserves energy if an external field is applied, the fluid temperature increases due to viscous heating. In order to overcome this, isothermal (canonical) approaches have been suggested like the ones described in the next section. Most of these are, however, significantly slower than the classical SRD approach.

3.1.2 Canonical Collision Step (MPC)

There are two distinct approaches towards an isothermal algorithm. The first one consists of a simple rescaling of the particle with respect to a certain temperature or energy distribution. The other one applies the Anderson thermostat to the relative velocities.

Rescaled SRD - Collision

The rescaling approach conserves the temperature in a system by multiplying the relative velocities of the particles after the collision step with a constant α as follows

$$\mathbf{v}_{i,c}^{new} = \alpha\, \mathbf{v}_{i,c}. \tag{3.4}$$

This rescaling factor can be determined locally or globally. As the rescaling factor is applied to the relative velocities the profile of the flow field is not alter. Such a schemes is termed profile-unbiased. In general, the rescaling factor is determined with respect to a given temperature T

$$\alpha = \sqrt{\frac{3(N_c-1)k_B\,T}{m\sum_{i=1}^{N_c}\mathbf{v}_{i,c}^2}}, \tag{3.5}$$

where N_c is the number of rescaled particles. This leads to a local Maxwell-Boltzmann distribution of the relative velocity but neglects particle fluctuations. Further, the energy as well as the particle density are not reproduced correctly [133]. Nevertheless, it gives the viscosity within a sufficient error and flow profiles can be reproduced correctly. As the approach is additionally relatively fast, it might be applied in situations where the local distributions are not crucial.

A further rescaling possibility is the so called Maxwell-Boltzmann-scaling thermostat (MBS). Here, the velocities are rescaled with respect to a fluctuating local kinetic energy

$$\alpha_{MBS} = \sqrt{\frac{2E_k'}{m\sum_{i=1}^{N_c}\mathbf{v}_{i,c}^2}}, \tag{3.6}$$

where E_k is drawn from the energy distribution obtained from the local Maxwell-Boltzmann distribution for the relative velocities

$$P(E_k) = \frac{1}{E_k\,\Gamma((3(N_C-1)/2))}\left(\frac{E_k}{k_B\,T}\right)^{\frac{3(N_c-1)}{2}}\exp\left(-\frac{E_k}{k_B\,T}\right), \tag{3.7}$$

with Γ being the Gamma function. This approach reproduces the correct local distribution of the relative velocities including the particle fluctuations. Further, the distribution of energy and particle density are obtained correctly. However, drawning the fluctuating energy from the corresponding probability distribution is computationally extremely costly. The effect on the correlation functions and transport coefficients of the system will be discussed in section 3.4.

MPC Collsion

Instead of a rescaling procedure, a thermostat can directly be applied to the fluid during the collision step. Therefore, the so called Anderson thermostat is used, which randomly draws the new relative velocities $\mathbf{v}_j^{\mathrm{ran}}$ directly from a Maxwell-Boltzmann distribution characterized by the desired velocity

$$\mathbf{v}_i(t+\delta t_c) = \mathbf{v}_\xi^C + \mathbf{v}_i^{\mathrm{ran}} - \sum_{j\in cell}\frac{\mathbf{v}_j^{\mathrm{ran}}}{N_C}. \tag{3.8}$$

with N_C being the number of particles in a cell [134]. The last term on the right side ensures that the momentum is conserved. Due to historical reasons, this approach will be called Multiparticle Collision Step (MPC) in this work. In literature, the terms SRD and MPC are not distinguished as strictly as will be done here.

The Anderson thermostat approach is related to the Langevin thermostat given by the classical Langevin equation which samples the velocity fluctuations around a steady state arising due to white noise. It can be shown that these two thermostats are equal in certain regimes if momentum conservation is imposed on the Langevin approach. Actually, there has been an MPC algorithm introduced based on a Langevin thermostat. It has, however, not gained significantly attention as it has similar properties as the Anderson thermostated version [135].

As in the MPC algorithm a random number for each velocity component has to be drawn per particle, the approach is up to a factor of two slower than the SRD version, where only one random number per cell has to be obtained. However, the loss of speed can be compensated as the relaxation time of the MPC fluid decays with the number of particles as $\ln(N)^{-1}$ where in SRD the relaxation times increases. For the SRD, the particle number per cell should be between $3-20$ to ensure that the internal relaxation can be neglected [136] for MPC no such limitation exists. The differences in the transport coefficients between the SRD and MPC approach will be discussed in section 3.4.

3.1.3 Anguar Momentum Conservation

In contrast to Dissipative Particle Dynamics the MPC and SRD algorithms do not conserve angular momentum. The procedures can, however, be extend to an angular conserving version straight forwardly [137] by introducing an additional term

$$\mathbf{v}_i(t+\delta t_c) = \mathbf{v}_\xi^C + \boldsymbol{\Omega}[\mathbf{v}_{i,c}] + m\,\boldsymbol{\Pi}^{-1} \sum_{j\in cell} \{\mathbf{r}_{j,c} \times (\mathbf{v}_{j,c} - \boldsymbol{\Omega}[\mathbf{v}_{j,c}])\} \times \mathbf{r}_{i,c}. \tag{3.9}$$

Here, $\boldsymbol{\Pi}$ is the moment of inertia tensor of the particles in the cell and $\mathbf{r}_{i,c} = \mathbf{r}_i - \mathbf{r}_\xi^C$ and $\mathbf{v}_{i,c} = \mathbf{v}_i - \mathbf{v}_\xi^C$ are again the coordinate as well as the velocity with respect to the center of mass of the particular box. In the case of the SRD collision, this extension does not preserve energy anymore. This can only be adjusted by a further rescaling step as discussed above [133]. In the following, the angular and non angular momentum conserving versions of the algorithms are distinguished by adding $\pm a$, as has become conventional in literature.

The momentum propagation in a classical fluid is described by a symmetrical stress tensor. If angular momentum is not conserved a further asymmetric contribution arises. The Navier-Stokes equation can be derived from the stress tensor but is only indirectly affected. The asymmetric contribution leads to a further contribution to the viscosity but does not change the general form of the equation. Hence, the resulting flow field does qualitatively show the correct behavior even though there might be small quantitative deviations. Also, the transport coefficients of the fluid are affected by the angular momentum conservation as can be seen in figure 3.2 (a).

The shape of the flow field is not effected if the boundary conditions are given by velocities, but in the case of force boundary conditions spurious effects can occur. If the system of a

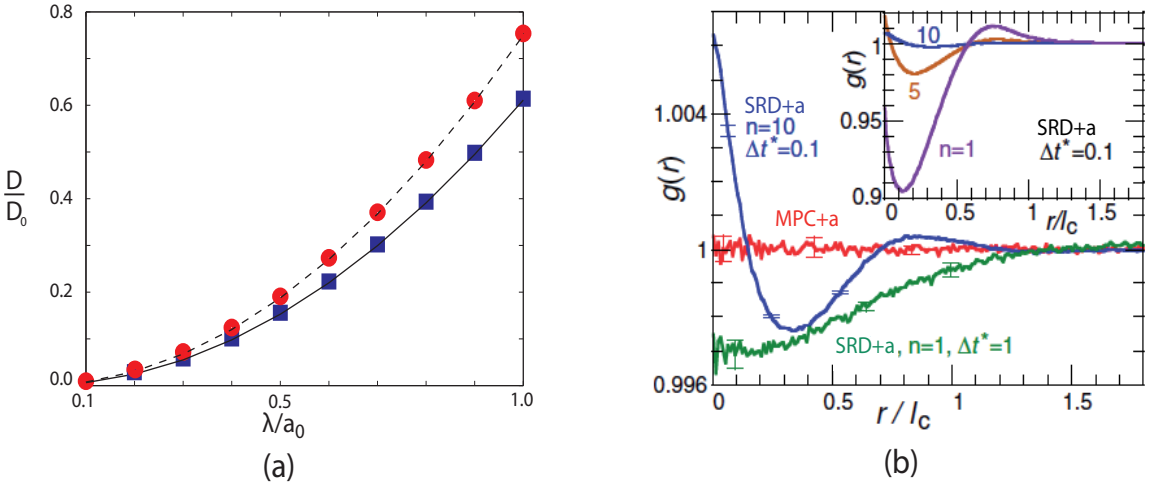

Figure 3.2: **(a)** The diffusion constant D depending on the mean free path λ, measured in units of the grid size a_0. The red circles are MPC+a simulations and the blue squares are MPC−a simulations performed for this work. Both are in excellent agreement with the analytical results. The angular momentum conservation leads to an increase of the diffusion constant. **(b)** The radial distribution function $g(r)$ of a SRD+a and a MPC+a fluid, as was given previously in the literature, figure adapted from Nouguchi et al. [137]. Only the MPC approach, depicted by the red curve, shows the flat behavior expected from analytical results. All other techniques lead to deviations for small distances. Here, l_c is the mesh size of the grid.

Couette flow is investigated where an inner and an outer cylinder rotate with the same angular velocity Σ, no torque should act on the cylinders. However, for simulations without angular momentum conservation significant torques have been observed at the inner and out boundary [138]. The inner and outer torque do not match which is attributed to a finite-size effect.

It has further been shown by Noguchi [137], that the radial distribution $g(r)$ significantly differs between SRD+a and MPC+a as can be seen in figure 3.2 (b). The radial distribution measures the density modulation of a system. For a system with an ideal gas equation of state like the SRD and MPC approaches it should be flat. For SRD+a this is clearly not the case. For a small mean free path significant deviations from the flat curves appear. These decrease with the particle number per cell but still persist. These small time steps are necessary to observe the correct fluid like behavior as is described in section 3.4.2. This effect has previously been observed in DPD simulations [139]. It arises due to the lack of time reversibility of the SRD+a algorithm in contrast to all versions of MPC±a. Therefore, the SRD+a algorithm should not be applied for small collision times.

In most simulations of soft matter systems like vesicles [140] or bacteria [141] a low Reynolds number is needed which only can be obtained with small collision times. Therefore, in this work the MPC+a algorithm is used.

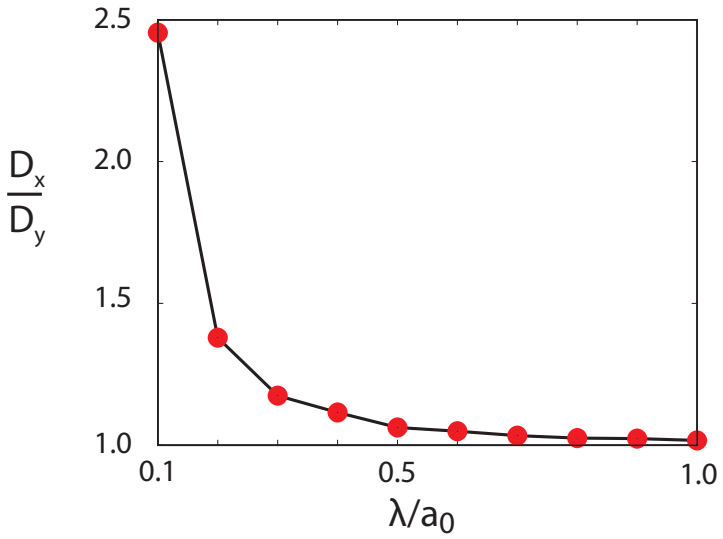

Figure 3.3: **(a)** If a flow in x direction is imposed on the system without grid shifting the diffusion constant depends on the direction. This effect vanishes with increasing mean free path λ, measured in units of the grid constant a_0. The simulations shown here use a MPC−a algorithm with a particle density $n = 10$.

3.1.4 Grid Shifting

As the MPC algorithm is a mixture of a lattice and an off-lattice algorithm, it suffers from similar drawbacks as the Lattice Boltzmann (LB) approach, namely a lack of Galilean invariance imposed by the grid. If the mean free path λ of the particles is smaller than the cell size a_0 certain particles are in the same collision cell for consecutive steps, which leads to a break down of the molecular chaos assumption. As the mean square path is given by $\lambda = \delta t_c \sqrt{k_B T/m}$, this effect is especially significant for small collision times. The particles are pre-correlated before a collision step. Their correlation depends on the imposed flow field. This can be seen by the self diffusion coefficient of a system with homogenous flow along one direction, as shown in figure 3.3 (a).

In order to overcome this artificial behavior, Ihle and Kroll suggested a grid shifting procedure [142]. Before each collision step, the grid is shifted by a random value between $(-a_0/2, a_0/2)$, such that each fluid particle is rotated in a new environment. They could show that this procedure significantly reduces spurious lattice effects for systems with and without flow [143].

So far, the basic constituents of the MPC as well as SRD algorithm have been described. It has been shown that it is based on simple principles which make it an efficient approach towards hydrodynamics. In section 3.3.2, it will be shown that based on these principles it can be proven that the algorithm reproduces the correct hydrodynamic as well as thermodynamic behavior. This is important, as it ensures that the proposed algorithm gives reliable results even for problems where a comparison with analytical results is no longer possible.

3.2 Hydrodynamic Numbers in SRD/MPC

In order to describe the behavior of a fluid, hydrodynamic numbers have been introduced to distinguish different regimes. For an SRD fluid the significance of these numbers has first been discussed by Padding and Louis [144]. Here, a brief review will be given discussing the properties of the most important ones as well as their constraints in the MPC algorithm.

Mach Number

The Mach number compares the velocity of a flow of the fluid or of an immersed object with the sound propagation in the medium

$$\mathrm{Ma} = \frac{v_S}{c_S}. \tag{3.10}$$

Hence, it is not an intrinsic property of the fluid but depends on the situation investigated. The sound propagation in a classical fluid is extremely fast, in the order of 10^3 m/s. However, as will be discussed in section 3.3.3, particle based simulation techniques are much more compressible than Navier-Stokes fluids and, therefore, have a reduced speed of sound propagation. This leads also to an increase of the Mach number. Effects of the Mach number, however, scale only with Ma^2. Hence these effects can be neglected if the square of the Mach number is smaller or equal to the Reynolds number [145]. The Mach number does not have to be as small as for a real fluid, but in order to keep it sufficiently short, the following constraint of the flow velocity in a MPC fluid $v_S \leq 0.1\, c_S$ has been proposed in literature [144] and holds for most applications [146, 147]. Here, the sound velocity can be derived form the equipartition theorem as the MPC fluid only contains kinetic energy. If applications with higher velocities should be considered, the MPC extensions described in section 3.3.3 should be used.

Knudsen Number

The Knudsen number compares the typical mean free path λ of the fluid components with the typical length scales in a system L_{typ}, e.g. the radius of an colloid

$$\mathrm{Kn} = \frac{\lambda}{L_{typ}}. \tag{3.11}$$

It is the relevant parameter for the Chapman-Enskog expansion discussed in section 3.3.2. From literature it is known that for $\mathrm{Kn} \geq 10$, the continuum description of the Navier-Stokes equation breaks down. However, even for $\mathrm{Kn} \geq 0.1$, significant effects of the discrete nature of the fluid can be observed [144]. In water at room temperature, the mean free path is of the order of $3 \cdot 10^{-10}$ m. If a colloid of micrometer size is considered in the fluid, the Knudsen number is $Kn \approx 10^{-4}$. In the SRD/MPC algorithm, this can only be achieved with a very small mean free path or large colloids. Such a simulation would be extremely time consuming. In the simulations considered in this work, the Knudsen number is between $Kn \approx 0.1 - 0.01$, which means that the discrete nature of the fluid should become apparent by fluctuation of the relevant variables.

Reynolds Number

The most famous hydrodynamic number is the Reynolds number, which compares the inertial to the viscous effects in a fluid. It is classically given by

$$\mathrm{Re} = \frac{v_{typ}\, L_{typ}}{\nu}. \tag{3.12}$$

Here, v_{typ} and L_{typ} are the typical velocity respectively length scale in a system and ν the kinematic viscosity. It should be recaptured, that the kinematic viscosity has the unit of a diffusion constant and measures the diffusion of velocity fluctuations. For small Reynolds numbers, the system is dominated by viscous effects which damp all kind of motion immediately and reduce the Navier-Stokes equation to the much simpler Stokes equation as time and convective derivative vanish

$$\underbrace{\left(\frac{\partial \mathbf{v}}{\partial t} + (\mathbf{v}\cdot\nabla)\mathbf{v}\right)}_{\sim Re} = \nu\Delta\mathbf{v} + \frac{\nabla p}{\rho} + \frac{\mathbf{f}}{\rho}. \tag{3.13}$$

For biological or nanotechnological applications, the Reynolds number is of the order of $Re \sim 10^{-6}$, which is not feasible in particle based simulation techniques like the SRD/MPC approach. In most applications of the algorithm the Reynolds number is between $Re \sim 0.1 - 10$. This means, deviations in the stream lines of hydrodynamic flows can be observed due to inertial effects [144].

Peclet Number

The Peclet number is closely related to the Reynolds number as it measures the significance of directed motion over diffusion

$$\mathrm{Pe} = \frac{v_{typ}\, L_{typ}}{D}. \tag{3.14}$$

Here again v_{typ} and L_{typ} are the typical velocity and length scale in a system. However, in the literature some confusion can be found discussing the nature of the diffusion constant. Considering swimmers or bacteria, the diffusion constant is the one of the object embedded in the fluid, which typically leads to a Peclect number in the order of $Pe_{swim} \sim 10^2$ [29, 40, 141]. This means, the direct transport is considerably stronger than the diffusion. On the other hand, if surface effects are of interest like for a selfdiffusiophoretic swimmer, considered later in this work, the diffusion constant considered is the one of the components of the fluid. This leads to a Peclet number in the order $Pe \sim 10^{-2}$ [89, 105]. In a SRD/MPC fluid, the Peclect number ranges for a swimmer or a Colloid from $Pe \approx 10^2 - 10^3$ and for the fluid itself from $Pe \approx 10^{-1} - 10^2$.

Schmidt Number

The Schmidt number will be discussed in detail in section 3.4.2 to distinguish between the collective and the Brownian regime of the velocity autocorrelation function. It is given by

$$\mathrm{Sc} = \frac{\nu}{D}, \tag{3.15}$$

comparing the diffusive velocity transport given by the kinetic viscosity to the mass transport due to diffusion. As will be described in section 3.4.2 for $Sc \approx 1$ the system behaves gas like, while for $Sc \gg 1$ fluid like behavior is observed. The Schmidt number is inversely proportional to the square of the mean free path of the SRD/MPC approach $Sc \sim 1/\lambda^2$. For classical simulation parameters of $\lambda \approx 0.1 - 0.01$, Schmidt numbers between $Sc \approx 10^1 - 10^2$ can be obtained. This is sufficient to simulate hydrodynamic behavior with the algorithm and of the same order as other approaches like Lattice Boltzmann and Dissipative Particle Dynamics.

Relations between the Hydrodynamic Numbers

So far five, hydrodynamic numbers have been discussed, describing a plethora of different hydrodynamic regimes. However, these numbers cannot be varied independently from each other. It can be shown that they are related by the following relations [144]

$$Sc \sim \lambda^{-2}, \tag{3.16}$$

$$Re \sim Ma \cdot R \cdot \lambda, \tag{3.17}$$

$$Pe^{max} \sim \lambda^{-2} \cdot Re \sim \lambda^{-1} \cdot Ma, \tag{3.18}$$

here again, R is the radius of an embedded colloid and λ the mean free path of the fluid. As has been discussed previously, the Mach number should be kept small by considering only systems with sufficiently slow hydrodynamic flows. Further, in order to guarantee sufficient small Schmidt and Reynold numbers, a small mean free path should be used. This also leads to an increase in the Peclet number. As the mean free path is given by the collision time of the algorithm, it could be decreased arbitrarily. However, for reasons of computational efficiency, collision times between $\tau \approx 0.1 - 0.01$ are used.

3.3 Thermodynamic and Hydrodynamic Properties

In order to prove that the SRD/MPC fluid recaptures the static and dynamic properties of a classical Navier-Stokes fluid, the following points have to be clarified

(i) Does the simulation show the expected equilibration behavior?

(ii) Does the algorithm show Navior-Stokes-like behavior on large length scales?

(iii) Does the approach obey an ideal gas equation of state?

The first two issues will be addressed naturally while investigating the dynamics of the algorithm. The last point is a first step towards an interpretation of the fluid, extensively done in section 3.4.

3.3.1 Equilibration of the SRD/MPC Fluid

Different approaches have been used to investigate the theoretical foundations of the SRD/MPC fluid. Here, kinetic theory is used to discuss the equilibration of the fluid model [148]. The basic principles of the theory will be outlined briefly and applied to the SRD/MPC algorithm.

The starting point of the investigation is the Liouville equation, first introduced by Malevanets and Kapral [130] and later refined by Ihle [149]

$$P(\mathbf{V}^{(N)}, \mathbf{X}^{(N)} + \mathbf{V}^{(N)}\delta t_c, t + \delta t_c) = \mathcal{C}P(\mathbf{V}^{(N)}, \mathbf{X}^{(N)}, t). \tag{3.19}$$

This equation describes the evolution of the complete probability distribution of the system during the streaming and collision step where $\mathbf{X}^{(N)} = \{\mathbf{x}_1, \ldots, \mathbf{v}_N\}$ and $\mathbf{V}^{(N)} = \{\mathbf{v}_1, \ldots, \mathbf{v}_N\}$ are the positions and velocities of the constituents of the fluid. The collision operator on the right-hand side is given by

$$\begin{aligned}\mathcal{C}P(\mathbf{V}^{(N)}, \mathbf{X}^{(N)}, t) = \frac{1}{\|\Omega\|^L} \sum_{\Omega^L} \frac{1}{a^d} \int_0^a d\mathbf{b}^{(d)} \int d\mathbf{V}^{(N)}(t + \delta t_c)\, P(\mathbf{V}^{(N)}(t + \delta t_c), \mathbf{X}^{(N)}, t) \\ \times \prod_{i=1}^{N} \delta(\mathbf{v}_i - V_\zeta - \hat{\omega}_\zeta[\hat{v}_i - \mathbf{V}_\zeta]).\end{aligned} \tag{3.20}$$

The delta function gives the selected operator for a particular collision and $\int_0^a d\mathbf{b}^{(d)}$ is the integration over the possible shifting vectors discussed in section 3.1.4. The center of mass velocity V_ζ depends explicitly on the shifting procedure as this decides which particles are in the same cell.

The central equation of the kinetic theory is the Boltzmann equation, which describes the evolution of the one particle distribution function of the system. This distribution gives the probability that there is a particle at certain point in the system. The Boltzmann equation can be derived from the Liouville equation using the assumption of molecular chaos, which states

$$P(\mathbf{V}^{(N)}, \mathbf{X}^{(N)}, t) = \prod_{i=1}^{N} P_1(\mathbf{v}_i, \mathbf{x}_i, t). \tag{3.21}$$

It is assumed that the distribution of the system can be rewritten as the product of one-particle distribution functions neglecting correlation between the particles. For the SRD/MPC fluid, this assumption is justified for mean free paths of the fluid particles being larger than the grid constant a_0. For simulations with smaller mean free paths, there is an effect on the transport coefficients which will be discussed in section 3.4. One aspect often not discussed when using the molecular chaos assumption, is that it neglects the hydrodynamic back-flow effect which leads to the long time tails in many autocorrelation functions. The contribution of the back flow to the response coefficients of the SRD/MPC fluid will also be stated in section 3.4.

The distribution above can be written in terms of the one particle distribution function $f(\mathbf{v}_i, \mathbf{x}_i, t) = N * P_1(\mathbf{v}_i, \mathbf{x}_i, t)$. Here N is the total number of particles in the system as P_1 in contrast to f distinguishes between different particles. The Boltzmann equation can now be obtained as

$$f(\mathbf{v}, \mathbf{x} + \mathbf{v}\delta t_c, t + \delta t_c) = \mathcal{C}_\mathcal{B} f(\mathbf{v}, \mathbf{x}, t). \tag{3.22}$$

The collision operator here is

$$\mathcal{C}_{\mathcal{B}} f(\mathbf{v},\mathbf{x},t) = \sum_{n=1}^{\infty} \frac{e^{-\rho_\zeta}}{n\,!} \frac{1}{a^d} \int_0^a d\mathbf{b}^{(d)} \int d\mathbf{V}^{(N)}(t+\delta t_c) \prod_{i=1}^{n} f_i(\mathbf{v}(t+\delta t_c),\mathbf{x},t) \\ \frac{1}{\|\Omega\|} \sum_{\Omega} \delta(\mathbf{v} - V_\zeta - \hat{\omega}_\zeta[\hat{v} - \mathbf{V}_\zeta]). \tag{3.23}$$

The prefactor on the right-hand side accounts for the fact that the number of particles in a cell is Poisson distributed. The density ρ_ζ is the one of a particular cell with coordinates ζ.

One of the major results of the classical kinetic theory for gases is the H-Theorem which shows that the following inequality is correct

$$H(t) \geq H(t+\delta t), \tag{3.24}$$

with the functional $H(t)$ defined as

$$H(t) = \int d\mathbf{v}(t) d\mathbf{x} f(\mathbf{v}(t),\mathbf{x},t+\delta t_c) \ln(f). \tag{3.25}$$

The functional $H(t)$ decreases continuously during the evolution of the distribution $f(t)$ of a closed system. It can be shown that this is equivalent to the statement that the entropy increases. If it can further be shown that particle density, momentum and energy are conserved quantities, a Gibbs distribution is the lower bound of the H-Function. Using the Boltzmann equation 3.22 for the SRD fluid a H-Theorem can be proven as the SRD fluid is constructed to conserve these moments. The microcanonical distribution function of this approach is given by

$$P(\mathbf{V}^{(N)},\mathbf{X}^{(N)},t) = A\,\delta\Big(\frac{\beta}{2N}\sum_{i=1}^{N}\|\mathbf{v}_i\|^2 - \frac{d}{2}\Big)\,\delta\Big(\sum_{i=1}^{N}[\mathbf{v}_i - \mathbf{u}]\Big), \tag{3.26}$$

with $\mathbf{u}$ being the mean velocity of the system, which converges to a Maxwell - Boltzmann distribution in the limit $N \to \infty$. The MPC is constructed to give this kind of distribution at equilibrium. Numerical results indicate that the algorithm is ergodic and sample this distribution homogeneously. A necessary condition for ergodicity is that the phase space measure is invariant under the flow resulting from the streaming and collision step. For the streaming step, the invariance is obvious as it only shifts the space coordinate. In order to prove the invariance for the collision step two conditions have to be fulfilled. The probability of a certain collision operator must not depend on the velocity of any particle and the semi-detailed balance condition has to hold

$$\sum_j W_{j\,i} = 1 \quad ,\forall i. \tag{3.27}$$

That means the total flux towards every microscopic state of the system is equal [150]. Both conditions are satisfied by the algorithm with the following transition probability

$$W_{j\,i} = p\left(\mathbf{V}^{(N)}(t+\delta t_c) = \hat{\omega}(\mathbf{V}^{(N)}(t)) \,|\, \mathbf{V}^{(N)}(t)\right), \tag{3.28}$$

with $\hat{\omega}$ a specific rotation matrix. For lattice gases, Henon has shown that semi-detailed balance is a sufficient condition for an H-Theorem [151]. So far, it has been shown that the

algorithm obeys an H-Theorem if the molecular chaos approximation is correct. However, as has been stated previously, that is not always the case for the algorithm. A more general prove would be to show that the simulation obeys detailed balance which is a necessary and sufficient condition for an H-Theorem

$$P_i W_{ij} = P_j W_{ji}. \tag{3.29}$$

This equation states that there is no probability flux in the system at equilibrium. If detailed balance is fulfilled, semi-detailed balance is also given but not vice versa. For other simulation techniques, like e.g. DPD, detailed balance has been proven for various circumstances [152, 153]. There exists no such general proof of detailed balance for the SRD/MPC algorithm yet.

For a 2D MPC system with rotation angle $\pm\alpha$ detailed balance can be proven [154]. Basically, it has to be shown that the inverse rotation occurs with the same probability as the forward rotation. This assumption can be made for all version of the SRD/MPC fluid as far as boundary conditions can be neglected.

So far, it has been shown that under certain conditions it can be assumed that the SRD/MPC algorithm leads to the correct equilibration behavior while no general proof exists. Therefore, in order to ensure that the results of a simulation show the correct equilibrium behavior, care has to be taken.

3.3.2 Hydrodynamic Behavior of the Algorithm

Even though the algorithm conserves momentum by construction this does not necessarily mean that on large length scales a Navier-Stokes behavior can be observed. However, here it will be shown that the SRD/MPC technique leads to the correct large scale behavior even if, as will be discussed later on, the stress tensor of the algorithm is not symmetric in every circumstance.

Basically, two approaches have been applied to deduce the Navier-Stokes equation from the algorithm, on the one hand discrete projection operator techniques [131], on the other hand a Chapman-Enskog expansion [130]. Here the approach of Ihle [149] for an Chapman-Enskog expansion [155] is outlined shortly as it also accounts the collision contribution for transport coefficients in contrast to the older approach by Malevanets and Kapral [130]. For the details of the collision contribution see section 3.4.1. A Chapmann-Enskog expansion leads to the same results as the projection method and is more straight forward to apply. Further, it can be used for a broader field of systems like for active ones as the complete gradient expansion of a set of field equations can be derived.

The starting point of the Chapman-Enskog equation is the Boltzmann equation discussed in the previous section 3.3.1. Instead of the collision term, there, a pre-averaged expression is used

$$\mathcal{C}_E(f(\mathbf{v},\mathbf{x},t)) = \frac{1}{\|\Omega\|}\langle\langle\sum_{n=1}^{\infty}\frac{e^{-M_\zeta}}{n!}\, n\, f(\hat{v}_1,x,t)\delta(\mathbf{v}-\mathbf{U}_\zeta-[\hat{v}_1-\mathbf{U}_\zeta]) \times\prod_{i=2}^{n} f(\hat{v}_i,x_i,t)\rangle_{\hat{v}}\rangle_{\mathbf{x}}\rangle_b. \tag{3.30}$$

The first average $\langle \dots \rangle_{\hat{v}}$ is over all pre-collision velocities, the second $\langle \dots \rangle_{\mathbf{x}}$ is over all positions of the $n = 2 \dots N$ other particles in a collision. Finally, the last term sums over all possible shifts of the grid.

The Chapman-Enskop expansion is based on the assumption of a small parameter ϵ, which can be related to the Knudsen number Kn. For a discussion of the Knudsen number see section 3.2. As a first step the left-hand side of the Boltzmann equation is expanded in terms of the collision time δt_c, leading to

$$f(\mathbf{v}, \mathbf{x} + \mathbf{v}\delta t_c, t + \delta t_c) = \sum_{k=0}^{\infty} \frac{\tau^k}{k!} (\partial_\tau + u_\alpha \, \partial) f(\mathbf{v}, \mathbf{x}, t). \tag{3.31}$$

From here on, it is assumed that $\partial_\tau = \partial_t$. After rescaling the spatial $\partial_\alpha \to \epsilon \, \partial_\alpha$ and temporal $\partial_t \to \epsilon \, \partial_t$ derivative in terms of the expansion factor ϵ, the latter is expanded in the same parameter

$$\partial_t = \epsilon \, \partial_{t_1} + \epsilon^2 \, \partial_{t_2}, \tag{3.32}$$

where t_1 can be treated as a convective time scale and t_2 as diffusive time scale. Finally, the collision term and the distribution function are also expanded leading to the Enskog equation

$$\begin{aligned} &\sum_{k=0}^{\infty} \frac{(\epsilon \, \tau)^k}{k \, !} (\partial_{t_0} + \epsilon \, \partial_{t_1} + \dots + v_\alpha \, \partial_\alpha)^k \underbrace{[f_0 + \epsilon \, f_1 + \epsilon^2 \, f_2 + \dots]}_{=f} \\ &\quad = \underbrace{\mathcal{C}_0 + \epsilon \, \mathcal{C}_1 + \epsilon^2 \, \mathcal{C}_2 + \dots}_{=\mathcal{C}_E} . \end{aligned} \tag{3.33}$$

Defining the operator $L = \partial_{t_0} + v_\alpha \partial_\alpha$ and collecting terms of the same power in ϵ leads to

$$\mathcal{O}(\epsilon^0) \quad f_0 = \mathcal{C}_0, \tag{3.34}$$

$$\mathcal{O}(\epsilon^1) \quad \tau \, L \, f_0 + f_1 = \mathcal{C}_1, \tag{3.35}$$

$$\mathcal{O}(\epsilon^2) \quad \tau \, \partial_{t_1} \, f_0 \tau \, L \, f_1 + \frac{\tau^2}{2} \, L^2 \, f_0 + f_2 = \mathcal{C}_2. \tag{3.36}$$

As f_0 is the equilibrium distribution equation 3.34 shows that it is a fixed point of the collision operator $\mathcal{C}_0$. The local collision invariants of the algorithm are $J_k = \{1, \mathbf{v}, \frac{\mathbf{v}^2}{2}\}$. Multiplying each of them with the equation of the order ϵ and performing a thermal average leads to the dissipativeless Euler equation. In order to get the Navier Stokes equation the first and the second order term in ϵ have to be combined,

$$\tau[\partial_{t_1} \, f_0 + \frac{1}{2} \, L \, (f_1 + \mathcal{C}_1)] + f_2 = \mathcal{C}_2. \tag{3.37}$$

Multiplying this equation again with the collision invariants and performing a thermal average gives

$$\partial_t \rho + \partial_\alpha (\rho u_\alpha) = 0, \tag{3.38}$$

$$\partial t (\rho u_\alpha) + \partial_\beta (\rho u_\alpha u_\beta) + \partial_\alpha - \partial_\beta (\sigma_{\alpha\beta}^{coll} + \sigma_{\alpha\beta}^{kin}) = 0, \tag{3.39}$$

$$\partial_t e + \partial_\beta (u_\beta [e + p] - u_\alpha)[\sigma_{\alpha\beta}^{coll} + \sigma_{\alpha\beta}^{kin}] - [\kappa^{coll} + \kappa^{kin}]) \partial_\beta T) = 0. \tag{3.40}$$

For detailed expressions of the moments $\langle J_n \mathcal{C}_m \rangle$ necessary to find these expressions see [149]. During the derivation it has been assumed that the SRD/MPC fluid obeys an ideal gas equation of state $p = \rho k_B T$. For a justification therefore see the next section 3.3.3.

Here, the kinetic contribution of the macroscopic stress tensor is symmetric and can be identified as

$$\sigma_{\alpha\beta}^{kin} = \rho(x)\nu^{kin}\left(\partial_\alpha u_\beta + \partial_\beta u_\alpha - \frac{2}{d}\delta_{\alpha\beta}\partial_\gamma u_\gamma\right). \tag{3.41}$$

This result recaptures the stress tensor of a Navier-Stokes fluid with a bulk viscosity $\gamma = 0$ and the kinematic viscosity defined as $\nu = \eta/\rho$. The collision part, however, is in contrast to its classical result asymmetric

$$\sigma_{\alpha\beta}^{coll} = \rho(x)\nu^{coll}\partial_\beta u_\alpha(x). \tag{3.42}$$

It can be shown that $\nu^{coll} = \nu_{symm}^{coll} + \nu_{asymm}^{coll}$ consists of a symmetric and an asymmetric contribution.

This is one of the fundamental differences between a Navier-Stokes and a SRD/MPC fluid and arises because the simplest version of the latter does not conserve angular momentum due to the multi-collision step. This result has been obtained previously with different approaches [156, 157]. If the angular conserving version of the SRD/MPC fluid is considered, the asymmetric contribution to the collisional stress tensor vanishes [138]. The Chapman-Enskog procedure can give an expression for the response coefficients in terms of the microscopic parameters of the simulation. Their detailed form will be discussed in section 3.4.

3.3.3 The Equation of State

One result from the Chapman-Enskog expansion, which is not obvious from the brief outline given here, is that the SRD/MPC algorithm obeys an ideal gas equation of state [158]

$$p = \rho k_B T. \tag{3.43}$$

As a consequence, the fluid is, in contrast to a classical Navier-Stokes fluid, compressible, as there are no internal forces between the fluid particles beside the collisions. One effect arising from this is that the sound velocity in this kind of approach is slower than in a real fluid. Further, this means that there is a maximum speed in the simulation after which the simulation is not applicable, since the Mach number has to be kept small, as discussed in section 3.2.

If a incompressible fluid or dense gas is investigated, an intermolecular potential has to be mimicked in the spirit of a viral expansion

$$P = \rho k_B T + \frac{1}{3V}\sum_i \langle \mathbf{r}_i \cdot \mathbf{F}_i \rangle, \tag{3.44}$$

where $\mathbf{F}_i$ is the force onto a particle exerted by all other particles in the system. In a standard SRD/MPC fluid this force is obviously zero. However, introducing a further step in the collision procedure can lead to a non-ideal contribution to the equation of state

$$P = \rho k_B T + \left(\frac{1}{2\sqrt{2}} + \frac{1}{4}\right)\frac{A M^2}{2}\frac{k_B T}{a\Delta t} + \mathcal{O}(A^3 T^2). \tag{3.45}$$

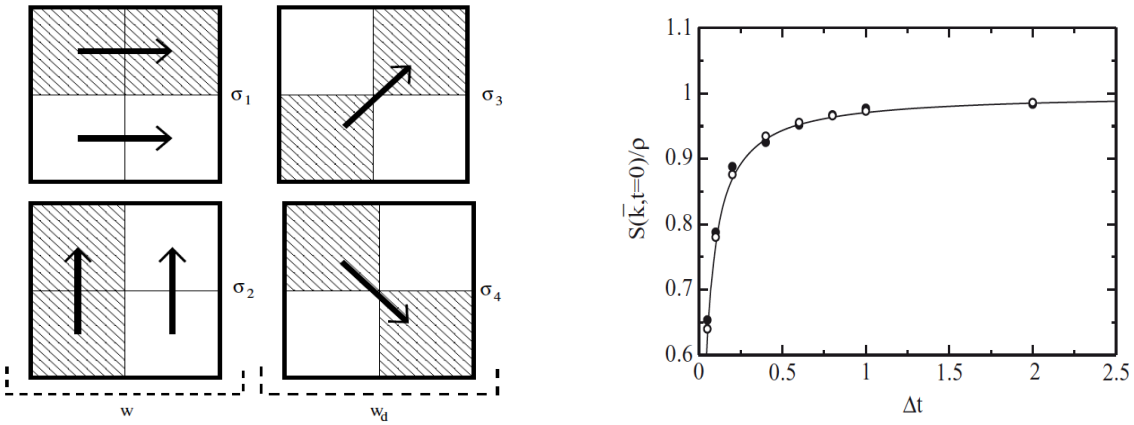

Figure 3.4: **(a)** The lattice with lattice constant $2\,a_0$ has four different collision possibilities: horizontal σ_1 and horizontal σ_2 as well as diagonal σ_3 and σ_4. From: [159]
(b) The static structure factor $S(k, t = 0)$ obtained from derivatives of the pressure (open ciricles) and directly from the density correlation function (filled circles). The solid line shows the analytic prediction. From: [160]

The non-ideal pressure term comes from the following additional procedure

- impose a second grid with box length $2\,a$
- apply a grid shifting procedure as in the classical SRD/MPC algorithm
- select two cells according to figure 3.4 (a) and determine the center of mass velocity $\mathbf{u}_n$
- project the the difference of the center of mass velocities on the vector connecting the two cell centers $\Delta u = \mathbf{d}_{12} \cdot (\mathbf{u}_1 - \mathbf{u}_2)$
- if $\Delta u < 0$, no collision is performed, otherwise the probability of a collision is drawn from the probabilty

$$p_A = \Theta(\Delta u) \tanh(\Lambda), \quad \Lambda = A\,\Delta u N_1 N_2. \tag{3.46}$$

Here, $N_{1/2}$ are the numbers of particles in the respective cells. The constant A can be tuned to alter the non-ideal contribution in the equation of state. As a collision rule, there are the same procedures possible as for a classical SRD/MPC algorithm. As the algorithm inherits the dynamic properties of the underlining MPC/SRD approach the algorithm is able to reproduce hydrodynamic behavior. In oder to prove that it leads to the correct thermodynamic results, the following equation can be used

$$S(k, t = 0) = \rho k_B T \left.\frac{\partial \rho}{\partial p}\right|_T . \tag{3.47}$$

The left-hand side is the structure factor. It is the Fourier transform of the density correlation function. On the right-hand, side thermodynamic quantities are given. Both sides can be measured with the algorithm and compared as has been done in figure 3.4 (b), which shows

an agreement of both results. Finally, it is not clear that the extended procedure conserves detailed balance. The proof used for the classical algorithm cannot be used as this approach has a velocity depended collision step and leads to a contraction of the phase space volume. Nevertheless, using projector methods the transport coefficients of the simulation have been obtained in terms of the parameters of the algorithm. They nicely agree with simulation results. Therefore, the extended algorithm can be considered as a first step towards simulations of fluids with higher speed of sound which would be necessary to investigate the effect of pressure gradients.

3.4 Response Coefficients and Correlation Functions

In the previous sections, the static and dynamic behavior of the fluid have been investigated. It has been found that the SRD/MPC fluid shows the correct long time limit and has an ideal gas equation of state. In the dynamic equations response coefficients like the viscosity have been introduced merely phenomenologically. Here, these coefficients are related to the microscopic parameters of the algorithm giving the possibility to distinguish certain regimes of the simulation. Further, it will be discussed how well these analytic expressions agree with numerical results.

The analytic expressions can be derived through various approaches like kinetic theory or Chapman-Enskog expansion. Here, they are obtained through Green-Kubo relation [161]. This shows the natural connection between the response coefficients and the corresponding autocorrelation function.

3.4.1 Viscosity

The viscosity η is determined using the Green-Kubo relation (GK) for the shear correlation function, depicted in figure 3.5(b),

$$\eta = \frac{\rho\,\tau}{N\,k_B\,T}\sum_{n=1}^{\infty}\langle\sigma_{xy}(0)\,\sigma_{xy}(n\,\tau)\rangle_{\mathrm{e}}, \tag{3.48}$$

here, σ_{xy} is the macroscopic stress tensor of the system of interest. The ensemble average is over an equilibrium distribution as it is assumed that the system is only slightly out of equilibrium. Otherwise, the GK relations are not applicable. For the SRD/MPC fluid the derivation of the viscosity uses the microscopic expression for the stress tensor known from kinetic theory. Also, this expression can be split in a kinetic and a collision part [162]

$$\sigma_{xy}^{kin} = -\sum_{j} v_{jx}(n\,\tau)\,v_{jy}(n\,\tau), \tag{3.49}$$

$$\sigma_{xy}^{coll} = -\frac{1}{\tau}\sum_{j} v_{jx}(n\,\tau)\,B_{jy}(n\,\tau). \tag{3.50}$$

This directly links the stress to momentum flux. The kinetic part describes the flux due to the streaming step. The collision contribution arises because of the grid shifting during the

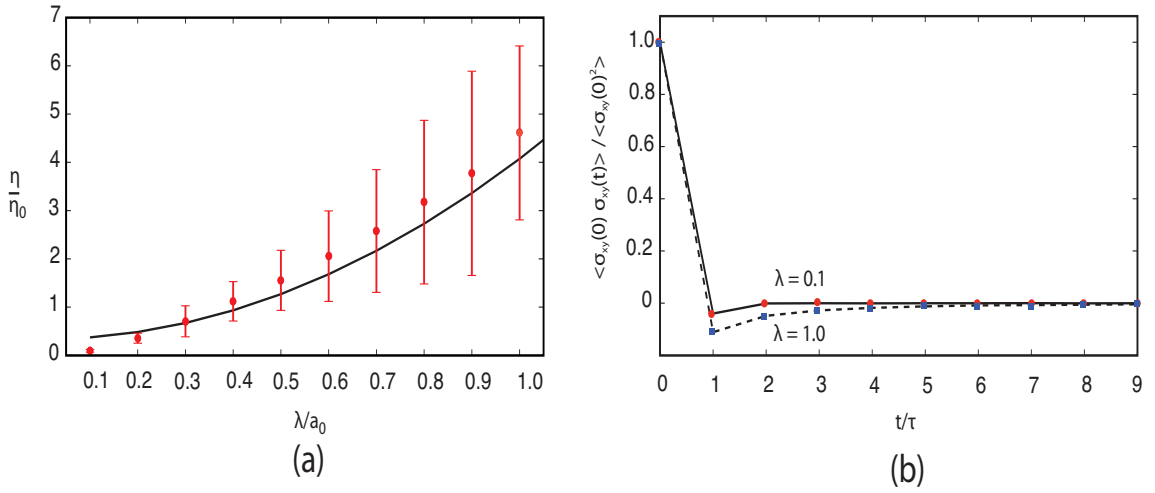

Figure 3.5: The simulations shown here are based on a MPC−a algorithm developed for this work. All simulations use a $24a_0 \times 24a_0 \times 24a_0$ grid with a particle density $n = 5$.
(a) The viscosity η increases with the mean free path λ, measured in units of the grid constant a_0. For large mean free paths there are significant error bars as the Green-Kubo relation used here does not converge sufficiently. Better results could e.g. be obtained using the mean square displacement of the colloid.
(b) The shear correlation function shows a significant decay on a short length scale for $\lambda = 0.1$ (red) and $\lambda = 1.0$ (blue). The anticorrelation, well reported in literature, is less strong for smaller mean free paths.

multicollision step. The stochastic variable [162]

$$B_{j\beta}(n\,\tau) = \zeta^s_{j\beta}((n+1)\,\tau) - \zeta^s_{j\beta}((n\,\tau) - \tau v_{j\beta}(n\,\tau), \tag{3.51}$$

takes the underlying lattice structure into account. Here ζ^s is the cell coordinate during the shifting procedure. It has the following temporal correlation

$$\langle B_{j\alpha}(n\,\tau)\, B_{j\beta}(m\,\tau)\rangle_{\mathrm{e}} = \frac{a^2}{12}\delta_{\alpha\beta}(1+\delta_{ij})(2\delta_{n,m} - \delta_{n,m+1} - \delta n, m-1). \tag{3.52}$$

Further, it was shown numerically that $\langle B_{j\beta}(n\,\tau)\rangle = 0$ [157]. The kinetic as well as the collisional contributions to the shear tensor do not depend on the cell coordinate during the streaming even though it has been reported in literature otherwise [142]. However, that was expected because if the grid shifting procedure reproduces Galilean invariance there should not be any dependence on the lattice structure. The appearance of the coordinates of the shifted lattice do not conflict with this as it only approximates for the momentum flux.

This becomes more obvious if the origin of the two contributions is considered. Therefore, instead of the viscosity the kinematic viscosity is used $\nu = \eta/\rho$, which rescales the former with the local density. It has the unit length square per time and, hence, can be considered as a diffusion constant of the momentum flux

$$\frac{\partial \delta\mathbf{v}}{\partial t} = \underbrace{(\nu^{kin} + \nu^{col})}_{\nu} \nabla^2 \delta\mathbf{v}. \tag{3.53}$$

In appendix A it is shown that the kinetic contribution scales like

$$\nu^{kin} \sim \frac{\lambda}{\delta t_c}, \tag{3.54}$$

where λ is the mean free path. This dependence indicates that the kinetic part accounts for the random walk like motion of the particles in the fluid carrying momentum with them.

The collisional contribution to viscosity scales like

$$\nu^{col} \sim \frac{a_0}{\delta t_c}, \tag{3.55}$$

where a_0 is the cell length of the grid. The momentum "jumps" from one cell to the next without mass transport. Nevertheless, both parts contribute to the momentum diffusion in system as can be seen from equation (3.49).

It should be mentioned that the temperature dependence differs between a Navier-Stokes fluid and a SRD/MPC fluid. For the former one, the kinetic part of the viscosity scales with the square root of the temperature $\nu^{kin}_{NSF} \sim \sqrt{T}$, while for the latter one, it scales linearly $\nu^{kin}_{SMF} \sim T$. This behavior results from the possibility of the latter to tune the mean free path independently from the density as in the streaming step particles do not feel each other.

From the expression above it is obvious that the kinetic contribution dominates for $\lambda \gg a_0$, while the collisional contribution dominates in the opposite regime. In general, in both regimes the analytical expressions agree very well with the numerical results [132, 135, 163]. Even the long time tail of the shear stress correlation could be reproduced [164],

$$\langle \sigma_{xy}(0)\, \sigma_{xy}(t) \rangle \sim \frac{(k_B\, T)^2}{\rho d(d+2)} \left(\frac{d^2-2}{(8\pi\nu t)^{d/2}} + \frac{1}{(4\pi\Gamma)^{d/2}} \right), \tag{3.56}$$

where d is the dimension and Γ is the sound attenuation, which will be explained in detail together with the thermal diffusion coefficient later in this section.

3.4.2 Diffusion Constant

The diffusion constant of the fluid can either be obtained from the mean square displacement $\langle (\mathbf{r}_i(t) - \mathbf{r}_i(0) \rangle$ or via a GK relation, given by the decay of the velocity correlation function in figure 3.6

$$D = \frac{\tau}{2m} \sum_{n=0}^{\infty} \langle \mathbf{v}_i(0) \cdot \mathbf{v}_i(n\,\tau) \rangle. \tag{3.57}$$

The general form of the diffusion constant of the SRD/MPC algorithm is given by

$$D = \frac{k_B T \delta t_c}{m} \left(\frac{1}{s_m} - \frac{1}{2} \right), \tag{3.58}$$

where s_m is given by the decay of velocity autocorrelation function of the particular method and depends on its parameters. As the mean free path is given by $\lambda = (\delta t_c / a_0)\sqrt{k_B T/m}$, it can be seen that the diffusion constant scales similarly to the kinetic part of the viscosity. As

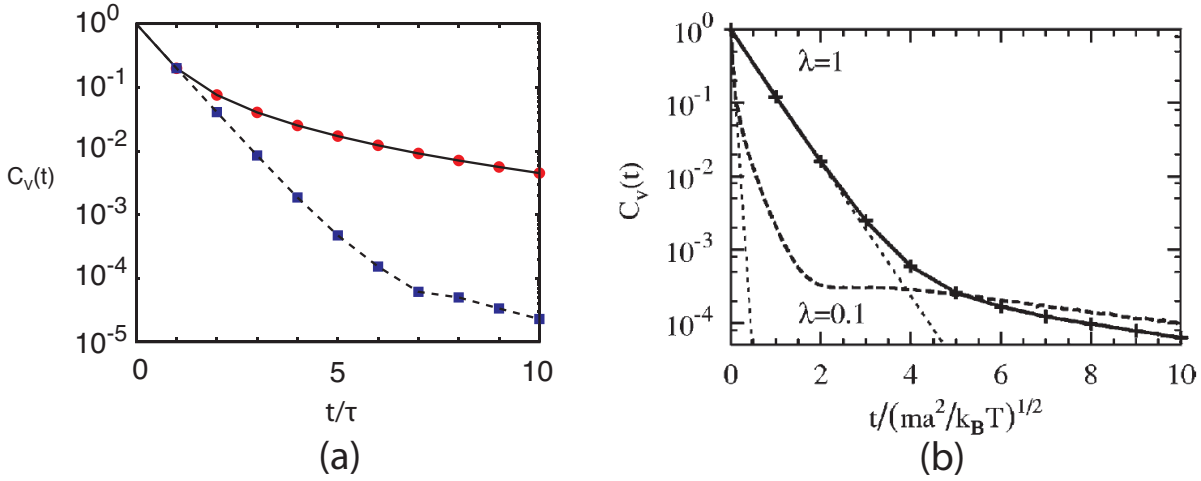

Figure 3.6: **(a)** The simulations shown here are based on a MPC−a algorithm developed for this work. They use a $24a_0 \times 24a_0 \times 24a_0$ grid with a particle density $n = 10$.
The velocity autocorrelation function $C_V(t) =< \mathbf{v}(0) \cdot \mathbf{v}(t) > / < \mathbf{v}(0)^2 >$ is obtained with the MPC algorithm for a mean free path $\lambda = 1.0\,a_0$ (red dots) and $\lambda = 0.1\,a_0$ (blue squares), where the latter decays significantly faster. The long time tail cannot be seen clearly.
(b) Simulations of the autocorrelation functions with the SRD algorithm. As for MPC, the simulation with the smaller mean free path decays faster and for it, the long time tail can be guessed, leading to a slower decay on longer time scales. From: [165].

expected, there is no collisional contribution to the diffusion as the multiparticle step does not lead to a particle motion.

Nevertheless, there are two distinguishable regimes in the velocity autocorrelation function defined by the Schmidt number $Sc = \nu/D$, see section 3.2. For a small Schmidt number the relaxation of velocity fluctuations in the fluid is dominated by diffusion as would be expected in a gas like system. For a larger Schmidt number collective effects have to be accounted and fluid like behavior arises. In SRD, the dependence of the Schmidt number from the mean free path is given by [144]

$$Sc \approx \frac{1}{3} + \frac{1}{18\,\lambda^2}. \tag{3.59}$$

That explains the decay of the velocity autocorrelation function of a SRD algorithm in figure 3.6(b). For small mean free paths, the system behaves fluid-like. This has two effects. First of all, the diffusion constant decreases which leads to a faster decay of the correlation function as $\langle \mathbf{v}(0) \cdot \mathbf{v}(t) \rangle \sim e^{-D\,t}$. Second, the hydrodynamic long time tail $\sim t^{-3/2}$ is approached early and slows down the decay. This can be seen in the break down of the molecular chaos approximation for simulations with mean free path below $\lambda < 0.5$. From the short time decay of the autocorrelation function it would be assumed that the equation (3.57) is dominated by the exponential decay. However, for small λ the long time tail significantly contributes to the time average. In the MPC algorithm this effect is not as distinct as in SRD, as shown in 3.6(a). However, as it is neglected in the derivation of the analytic expression for the diffusion coefficient in SRD as well as MPC considerable deviations can be observed as can be seen in figure 3.7 (a). If, however, the effect of correlation due to consecutive collision with the

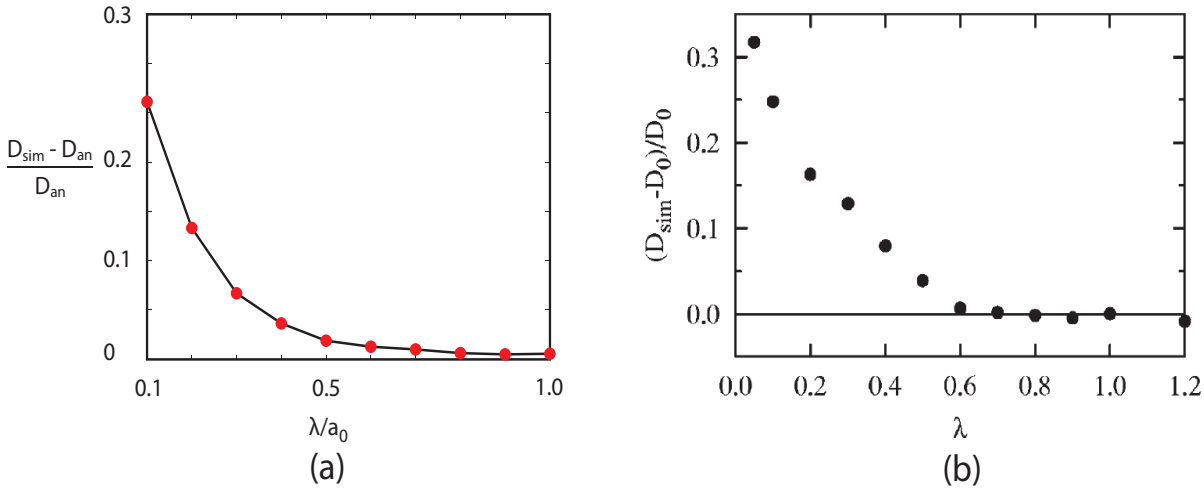

Figure 3.7: **(a)** The MPC+a algorithm, developed for this work, shows a deviation from the analytic result for small mean free paths λ. The diffusion constant is measured by the decay of the velocity autocorrelation function. Here, the relative deviation of the analytical result from the measured one is shown. For the simulation a grid of size $24a_0 \times 24a_0 \times 24a_0$ is used with a particle density $n = 10$.
(b) It was previously reported in literature that the SRD−a algorithm shows similar deviations from the analytic result. From: [165]

same particles in a collision box is incorporated this deviation decays. As both algorithms are developed to investigate hydrodynamics in soft matter systems it is important to incorporate higher order correlations in the system and hence use the approach in the collective regime with a sufficient high Schmidt number.

3.4.3 Thermal Diffusion Constant

The thermal diffusion constant, describing the energy transport in the system, is derived from the following Green Kubo relation

$$D_T = \frac{\tau}{5 * c_p V k_B T} \sum_{n=0}^{\infty} \langle \mathbf{J}_q(0) \cdot \mathbf{J}_q(n\tau) \rangle, \tag{3.60}$$

with $\mathbf{J}_q$ the energy flux of the fluid and c_p the specific heat at constant pressure. As there are, beside the multiparticle collisions, no interactions between the constituents of the fluid the energy flux $\mathbf{J}_q$ has the following form [132]

$$\mathbf{J}_q(n\tau) = \sum_i \Bigg[\underbrace{\left(c_v T - \frac{\mathbf{v}_i^2(n\tau)}{2} \right) \frac{\Delta\zeta_i(n\tau)}{\tau}}_{\text{streaming}} + \underbrace{\frac{1}{2} \Delta\mathbf{v}_i^2(n\tau) \frac{\Delta\zeta_i^S(n\tau)}{\tau}}_{\text{collisional}} \underbrace{k_B T \mathbf{v}_i(n\tau)}_{\text{mechanical}} \Bigg]. \tag{3.61}$$

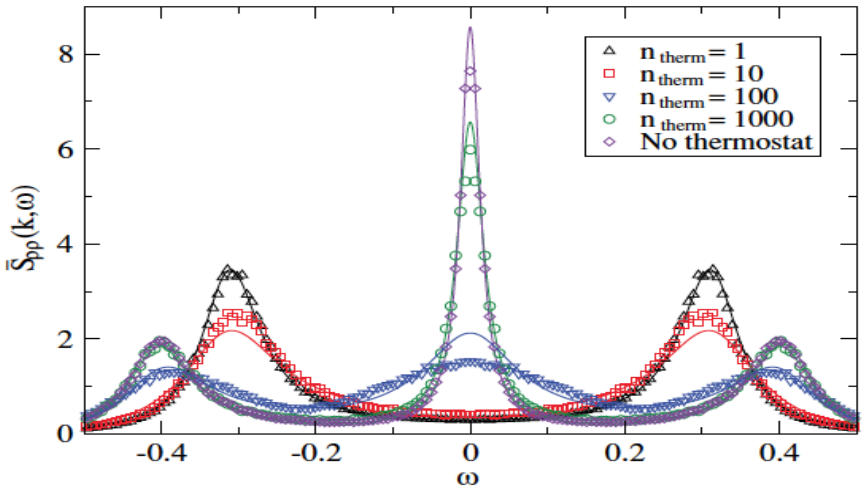

Figure 3.8: The normalized structure factor shows very good agreement between analytical results (lines) and simulations (symbols) with a thermostated SRD−a algorithm. The use of the MBS thermostat leads to decreasing sound peaks and even stronger decreasing thermal peaks. The former are also shifted to higher frequences. From: [166].

The first and second contribution are the change of the internal energy due to the streaming and collisional motion. The third part is the mechanical contribution per particles as discussed before due to the ideal gas equation of state, see 3.3.3.

In contrast to the density, the energy can be transported through the collision and the streaming step. Therefore, the thermal diffusion constant has two contributions. For a 3D SRD fluid, one obtains for the kinetic part

$$D_T^{kin} = \frac{k_B T \delta t_c}{2m} \left(\frac{3}{1-\cos(\alpha)-1} + \frac{6}{\rho} \left[\frac{4}{5} - \frac{1}{4} \csc^2(\frac{\alpha}{2}) \right] \right), \tag{3.62}$$

and for the collisional part

$$D_T^{col} = \frac{a^2}{15\,\rho\,\delta t_c} \left(1 - \frac{1}{\rho} \right) [1-\cos(\alpha)]. \tag{3.63}$$

Both contributions scale similar to the respective counterpart for the viscosity, which shows that the same physical transport phenomena contribute to them.

Classically, this transport coefficient has been measured with the Green-Kubo relation given above [157, 162] or in terms of kinetic theory [156, 167], where in the latter the thermal conductivity κ is measured and the relation $\kappa = c_V\, D_T$ is used. Here, c_V is the specific heat capacity at constant volume. Contrary to the viscosity and the diffusion constant which are not affected by a rescaling procedure, strong effects have been found on the thermal diffusion constant. In order to understand these effects an alternative approach to measure the thermal diffusion has been introduced based on the dynamic correlation function respectively the Laplace transformed

$$S_{A_i A_j}(\mathbf{k},\omega) = \int_0^\infty dt \int d(\mathbf{r}-\mathbf{r}')\, e^{i\omega t - i\mathbf{k}\cdot(\mathbf{r}-\mathbf{r}')} \left\langle [A_i(\mathbf{r},t) - \langle A_i \rangle]\, [A_j(\mathbf{r}',0) - \langle A_j \rangle] \right\rangle, \tag{3.64}$$

where A_i is a hydrodynamic variable like the density ρ or the momentum density $\mathbf{g}$. This function can be used to analyze the hydrodynamic modes contained in a system [168]. The density-density correlation function is called the dynamical structural factor and has the following well known form [91]

$$S_{\rho\rho}(k,\omega) = 2k_BT\rho\left(\frac{\partial\rho}{\partial p}\right)_T\left[\frac{(c_v/c_p)c^2k^4\Gamma}{(\omega^2-c^2k^2)^2+(\omega k^2\Gamma)^2}+\frac{(1-c_v/c_p)k^2D_t}{\omega^2+(k^2D_T)^2}-\left(1-\frac{c_v}{c_p}\right)\frac{(\omega^2-c^2k^2)k^2D_T}{(\omega^2-c^2k^2)^2+(\omega k^2\Gamma)^2}\right]. \tag{3.65}$$

Here, $c_{p/v}$ is the heat capacity at fixed pressure respectively volume, c is the speed of sound and Γ is the sound attenuation. Since the SRD/MPC fluid has an ideal gas equation of state the capacities are given by the classical result $c_p = k_B/m + c_v = (d+2)k_B/2m$. The sound attenuation of the algorithm deviates slightly from the ideal fluid

$$\Gamma = D_T\left(\frac{c_p}{c_v}-1\right)+2\left(\frac{d-1}{d}\right)\nu^{kin}+v^{col}. \tag{3.66}$$

In the ideal fluid the prefactor of the kinetic contribution would apply for the total kinematic viscosity ν. As can be seen from figure 3.8, the dynamical structure factor has three maxima which correspond to three longitudinal modes in the system

$$\omega_{\text{therm}} = -i\,D_T\,k^2 \quad \text{and} \quad \omega_{\text{sound}} = \pm c\,k - \frac{i}{2}\,\Gamma\,k^2. \tag{3.67}$$

The width of the peaks is given by $D_T\,k^2$ and $\Gamma\,k^2$ for the thermal (Rayleigh) and the sound (Brillouin) mode. In the hydrodynamic limit $k \to 0$ the thermal peak is at $\omega_{\text{therm}} = 0$ and the sound one $\omega_{\text{sound}} = \pm c\,k$. If for the thermal diffusion and the kinetic viscosity the analytically obtained results are used and the sound viscosity is given by $c = \sqrt{2k_BT/m}$ the structure factor nicely agrees with simulation results for an SRD thermostat without a fit parameter.

However, the result significantly alters if a thermostat is applied to the fluid as in the case of MPC or an SRD fluid with an MBS procedure described in section 3.1.2. For an MBS thermostat fluid it has first been shown by Huang and coworkers [133] that the central peak of the structure factor vanishes and Brillouin peaks are shifted towards a smaller frequency. This shift shows that the sound mode propagates with the isothermal sound velocity c_T instead of the adiabatic velocity c_S. Both velocities are related through the relation $c_S = \sqrt{\gamma}\,c_T$ with $\gamma = c_p/c_V$. The vanishing of the central peak was attributed to the lack of energy transport as the thermostat leads to the correct energy distribution on the cell level. However, it was shown by Hijar and Sutmann [166] that it is a bit more subtle. They applied the MBS thermostat not every time step τ but every $n_{\text{therm}} > 1$ step. Based on the fluctuating hydrodynamics formalism introduced by Landau and Lifschitz [169], they extended the linear hydrodynamic equations by a periodically applied fluctuating energy source and were able to derive an expression for the structure factor $S_{\rho\rho}$ which depends on the periodicity of the thermostat. Using this result they were able to show that none of the transport coefficients of the SRD fluid are effected by the thermostating procedure even not the thermal diffusion constant. Hence, the procedure neither influences the momentum nor the energy flux of the fluid model. The central diffusive peak disappears due to the modification of the relaxation time scale due the

thermostating procedure. In classical Navier Stokes fluid the typical relaxation rates are given by $\tau_S^{-1} = c_T k$ for the relaxation due to sound modes and $\tau_l^{-1} = D_l k^2$ and $\tau_{\text{therm}}^{-1} = \gamma D_T k^2$ for the diffusive longitudinal momentum and thermal relaxation. They satisfy the following relations

$$\tau_S^{-1} \gg \tau_l^{-1}, \tau_{\text{therm}}^{-1}, \tag{3.68}$$

which show that sound modes relax much faster than the diffusive modes. In a thermostated SRD fluid there is a further contribution to the thermal relaxation rate $\tau_{\text{therm}}^{-1} = \gamma D_T k^2 + \tau^{-1}$ which arises due to the application of the thermostat. In the limit $n_{\text{therm}} \to \infty$ the classical fluid is recaptured. However, in a strongly thermostated case $n_{\text{therm}} = 1$ the ordering of the time scales is changed

$$\tau_{\text{therm}}^{-1} \gg \tau_l^{-1}, \tau_S^{-1}, \tag{3.69}$$

which shows that the thermal relaxation is significantly reduced. With the intermediate periodicity the decrease of the central peak in figure 3.8 can be understood.

In this section the basic transport coefficients of the MPC fluid have been described and related to their corresponding autocorrelation. The physical properties of the fluid have been outlined and different regimes have been identified depending on the form of the transport coefficient. Finally, the deviations from a Navier-Stokes equation have been explained.

3.5 Imbedded Objects

In simulations, complex objects are implemented in a fluid either as an excluded volume [44] or as being composed of spheres with a central potential [170]. In contrast, in direct solutions of the Navier-Stokes equation objects can be introduced via boundary conditions. Here, it is in general assumed that at these boundaries the velocity of the fluid flow field decays to the velocity of the object on a length scale not resolvable through the Navier-Stokes equation and is practically identical to it. In simulation approaches like MPC the hydrodynamic velocity is obtained by averaging over a set of fluid particles and, hence, it it cannot be assumed that their velocity decays fast enough to the velocity of a boundary and, therefore, there could be a relative velocity between the fluid and the object called slip velocity. Even though there are application were a slip velocity is proposesd [98, 171] e.g. to ensure propulsion, this has to be introduced in a controlled way and not as a spurious effect of the simulation approach. In the following section, it will be shown how to avoid slip due to artifacts of the simulations and its impact on behavior of an object, here a spherical colloid, is explained.

3.5.1 Colloids

In this section, the three most common implementations of a colloid into an SRD/MPC fluid are described. For the sake of completeness first of all a Lenard-Jones object is described, which, however, is not relevant for the rest of this work. Afterwards, two implementations for an excluded volume object are explained and simulation results of them are compared.

Lennard-Jones Objects

In principle, colloids can be implemented in a SRD/MPC algorithm as heavy point like particles interacting with a Lennard Jones potential or a similar central potential

$$\beta\, V_{\mathrm{ci}}(\mathbf{r}) = \epsilon_{\mathrm{ci}}\left[\left(\frac{\sigma_{\mathrm{ci}}}{\mathbf{r}}\right)^{2n} - \left(\frac{\sigma_{\mathrm{ci}}}{\mathbf{r}}\right)^{n} + \frac{1}{4}\right] \quad (\mathbf{r} \leq 2^{\frac{1}{n}}\,\sigma), \tag{3.70}$$

here $\{V_{\mathrm{cc}}, \sigma_{\mathrm{cc}}, n = 24\}$ describes the interaction between the colloids and $\{V_{\mathrm{cf}}, \sigma_{\mathrm{cf}}, n = 6\}$ between colloid and fluid particles. This approach has successfully been used to investigate colloids systems [172, 173]. Further, with a modified potential between the colloids it can be used to build up more structures like rods [174], polymers [11, 175, 176] and even more complex structures like a lipid bilayer membrane [177]. As the fluid particles are only reflected by the potential this leads to an effective slip between the object and fluid [178]. In average half of the fluid particles are approaching the colloid while half are reflected, such that the normal component vanishes on average while a tangential component sustain. A further drawback of this approach is that for a single colloid there is no angular transfer, which, however, is necessary to investigate rotating objects.

Stochastic Reflection Boundary Condition

An alternative approach is to model a colloid as an excluded volume and define collision rules for a fluid particle passing the boundary between the object and the fluid. A real colloid does not have a smooth surface but a rather rough one as there can be grafted polymers or co- and counter ions. Therefore, if a fluid particle crosses the surface of the colloid its new velocity is determined by the following distributions

$$p(\mathbf{v}_n) = \frac{m\,\mathbf{v}_n}{k_B\,T}\exp\left(\frac{m\,\mathbf{v}_n^2}{2k_B\,T}\right), \tag{3.71}$$

$$p(\mathbf{v}_t) = \sqrt{\frac{m}{2\,k_B\,T}}\exp\left(\frac{m\,\mathbf{v}_t^2}{2k_B\,T}\right), \tag{3.72}$$

where n denotes the direction normal to the surface and t the perpendicular one.The normal component can be obtained by calculating $\sqrt{x_1^2 + x_2^2}$ of two independent Gaussian distributed random variables [179]. One advantage of this approach is that the colloid acts as a thermostat for the fluid.

Bounce Back Boundary Condition

In order to obtain real non-slip boundary conditions the velocity of the fluid particles has to be reverted when hitting the surface. In a homogenous fluid that means half of the particles are approaching the wall while the other half is reflected and moves away from the wall which, at the length scale of the Navier-Stokes equation, leads on average to no slip tangential to the wall. In the case of a moving object the local surface velocity has to be taken into account

$$\mathbf{v}_i^{\mathrm{new}} = \mathbf{v}_i^{\mathrm{old}} + 2\mathbf{v}_s, \tag{3.73}$$

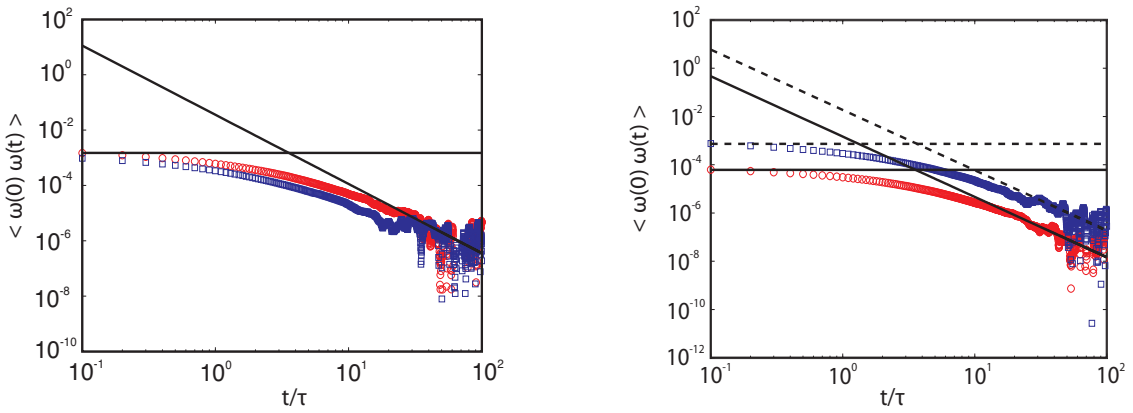

Figure 3.9: The angular correlation function $\langle \omega(0)\,\omega(t)\rangle$ of a colloid of radius $R = 3$ in a MPC+a fluid with a particle density of $n = 5$.
(a) Comparison of the Stochastic Reflection Boundary Condition (blue squares) and the Bounce Back Boundary Condition (red dots) with $\lambda = 1.0$, measured in units of the grid constant a_0. While the latter approaches the long time limit as would be expected, the former is not approaching it smoothly. This has previously been described in literature [180]. However, it was also reported that the Stochastic Reflection Boundary leads to a slower decay, which could not be confirmed here.
(b) The angular correlation function of $\lambda = 1.0$ (blue squares) and $\lambda = 0.29$ (red dots) with Bounce Back Boundary Condition both approach the long time as well as short time limit correctly.

with $\mathbf{v}_s$ being the surface velocity, defined as

$$\mathbf{v}_s(\mathbf{r}^* - \mathbf{R}_{\text{coll}}) = \mathbf{v}_{\text{coll}} + \Omega \times (\mathbf{r}^* - \mathbf{R}_{\text{coll}}). \tag{3.74}$$

Here, $\mathbf{r}^*$ is the collision point of the fluid particle at the surface. Like for the virtual particles in the collision step momentum and angular momentum are transferred to the colloid.

Comparison of the Boundary Conditions

It can be shown that both implementations of the boundary conditions lead to correct behavior of the velocity as well as the angular velocity autocorrelation function. The long time limit of the correlation functions is obtained from mode coupling theory to be

$$\lim_{t\to\infty} \langle \mathbf{v}(t)\,\mathbf{v}(0)\rangle = \frac{k_B\,T}{12\,m\,\rho(\pi(\nu + D_c)t)^{3/2}}, \tag{3.75}$$

$$\lim_{t\to\infty} \langle \omega(t)\,\omega(0)\rangle = \frac{k_B\,T}{m\,\rho(4\pi(\nu + D_c)t)^{5/2}}. \tag{3.76}$$

Here, ρ is the particle density, ν is the kinetic viscosity of the fluid and D_c is the diffusion constant of the colloid. As can be seen in figure 3.9(a) and 3.10(a), both boundary conditions lead to the correct decay. It has to be stressed that there is no fitting parameter in these results as the parameters can be calculated for SRD as well as MPC.

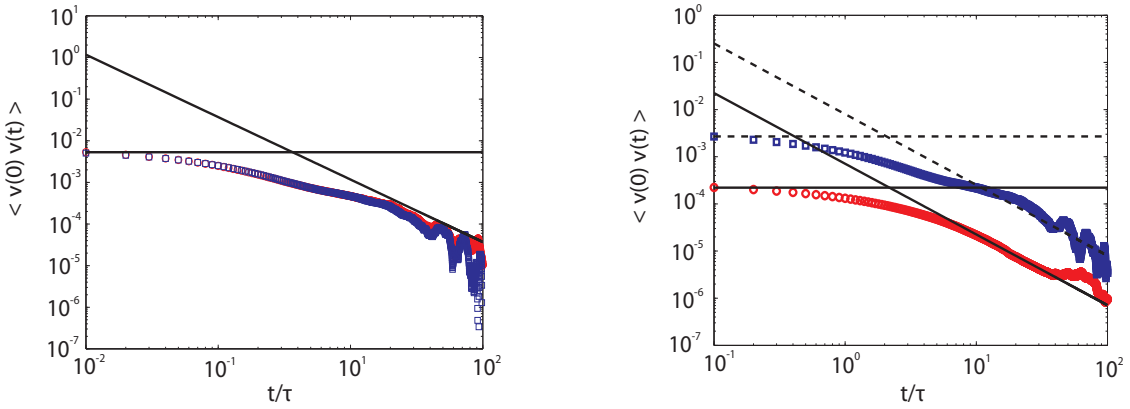

Figure 3.10: The velocity correlation function $\langle v(0)\, v(t)\rangle$ of a colloid of radius $R = 3$ in a MPC+a fluid with a particle density of $n = 5$.
(a) In contrast to what has been proposed previously in literature [180], no significant deviation is observed for the correlation function of the Stochastic Reflection Boundary Condition (blue squares) and the Bounce Back Boundary Condition (red dots) for a mean free path $\lambda = 1.0$, given in units of the grid size a_0.
(b) The simulations with Bounce Back Boundary Condition for $\lambda = 1.0$ (blue squares) and $\lambda = 0.29$ (red dots) both approach the long time as well as the short time limit.

The short time limit can be obtained from Enskog theory of dense gases which assumes that the autocorrelation function decay exponentially because of momentum transfer due to binary collision

$$\lim_{t\to 0}\langle \mathbf{v}(t)\, \mathbf{v}(0)\rangle = \langle \mathbf{V}^2\rangle \exp\big(-\zeta^V_{ENS} t\big), \tag{3.77}$$

$$\lim_{t\to \infty}\langle \omega(t)\, \omega(0)\rangle = \langle \omega^2\rangle \exp\big(-\zeta^\omega_{ENS} t\big), \tag{3.78}$$

with $\langle \mathbf{V}^2\rangle = k_B\, T/M$ as well as $\langle \omega^2\rangle = k_B\, T/I$ and the Enskog friction coefficients given by

$$\zeta^V_{ENS} = \frac{8}{3}\left(\frac{2\pi\, k_B\, T\, m\, M}{m\, +\, M}\right)^{1/2} \frac{\rho R^2}{M}\, \frac{1+2\chi}{1+\chi}, \tag{3.79}$$

$$\zeta^\omega_{ENS} = \frac{8}{3}\left(\frac{2\pi\, k_B\, T\, m\, M}{m\, +\, M}\right)^{1/2} \frac{\rho R^2}{M}\, \frac{1}{1+\chi}, \tag{3.80}$$

where $\chi = I/(MR^2) = 2/5$ being the gyration radius. It has first been stressed by Padding and coworkers [181] that, in contrast to the Brownian approach with the hydrodynamic friction coefficients $\zeta^V_h = 6\pi\eta R/M$ and $\zeta^\omega_h = 8\pi\eta R^3/I$, the velocity autocorrelation decays faster than the angular velocity correlation function. They further proved that for small diameters of the colloid the frictions coefficients cannot be added in parallel to obtain the total friction. While for colloids with a radius $\sigma > 2\, a_0$ it was shown that this is reliable

$$\frac{1}{\zeta} = \frac{1}{\zeta_{ENS}} + \frac{1}{\zeta_h}. \tag{3.81}$$

Therefore, it is recommended to use colloid with a diameter bigger than two. It has further been shown that if the virtual particles, explained in detail in the next section 3.5.2, are neglected, the Enskog contribution to the friction is significantly underestimated [182].

It has been proposed [144] that as both versions of the boundary conditions lead to the correct long time and short time decay of the correlation functions, this is a proof that both lead to non-slip boundary conditions. However, recently, it has been shown that these two correlation functions are not sufficient to distinguish slip from non slip boundary conditions and it was highly doubted that Stochastic Reflection Boundary conditions are sufficient to yield non slip boundary conditions [180]. To incorporate a defined slip velocity a modified version of the bounce back condition is used

$$\mathbf{v}_n^{\text{new}} = -\mathbf{v}_n^{\text{old}}, \tag{3.82}$$

$$\mathbf{v}_t^{\text{new}} = (2\Gamma - 1)\,\mathbf{v}_t^{\text{old}}, \tag{3.83}$$

where the subscribed t and n denotes the tangential and normal component of the velocity. The slip parameter varies between $\Gamma = 0$ for no slip and $\Gamma = 1$ for perfect slip boundary conditions. It was found that the variation of this parameter does not alter the long time tail of the correlation functions, but the Enksog friction as well as the the cross over behavior is affected. It was empirically found that the Stochastic Rotation Boundary conditions match simulations with a parameter between $\Gamma \in [0.6, 0.8]$ and hence produce spurious slip. This was further confirmed with simulations of a Poiseuille flow, which will be discussed in the next section. However, this could not fully been confirmed by our simulations, see figure 3.9(a) and 3.10(a). Only for the angular velocity autocorrelation function deviations could be observed in the crossover region.

Nevertheless, to ensure that the colloid shows no slip boundary conditions and guarantee the correct angular momentum transfer from the fluid to the colloid Bounce Back Boundary Conditions should be used. This is especially true in the simulations where rotation is significant, as is described in chapter 4.

3.5.2 Virtual Particles

In simulations of a flow in a channel driven by an external gravity field (Poiseuille flow) it was first realized by Lamura and coworker [134, 143] that even applying the Bounce Back rule at the walls of the channel leads to spurious slip in the SRD fluid. It has later been shown that this is a generic problem if boundaries are incorporated in a SRD/MPC fluid [180, 182]. The effect can be explained as follows; in the collision step the shifting of the grid leads to partially filled cells at the boundaries. In these cells, the viscosity is locally reduced, resulting in a slip velocity.

Therefore, the concept of virtual particles was introduced. If a cell overlaps with a boundary after the grid shifting procedure, this cell is filled virtually with particles whose velocity is drawn from a Maxwell-Boltzmann equation. The virtual particles, hence, only interact with fluid particles during the collision step as they contribute to the new mean velocity in the cell

$$\mathbf{v}_\zeta^C = \frac{\sum_{i=1}^{n_{\text{fluid}}} \mathbf{v}_i + \sum_{i=1}^{n_{\text{VP}}} \mathbf{v}_i^{\text{VP}}}{n_{\text{fluid}} + n_{\text{VP}}}. \tag{3.84}$$

If the angular momentum is neglected during the collision step the detailed positions of the virtual particles can be neglected. Further, as the sum over Gaussian variables is again

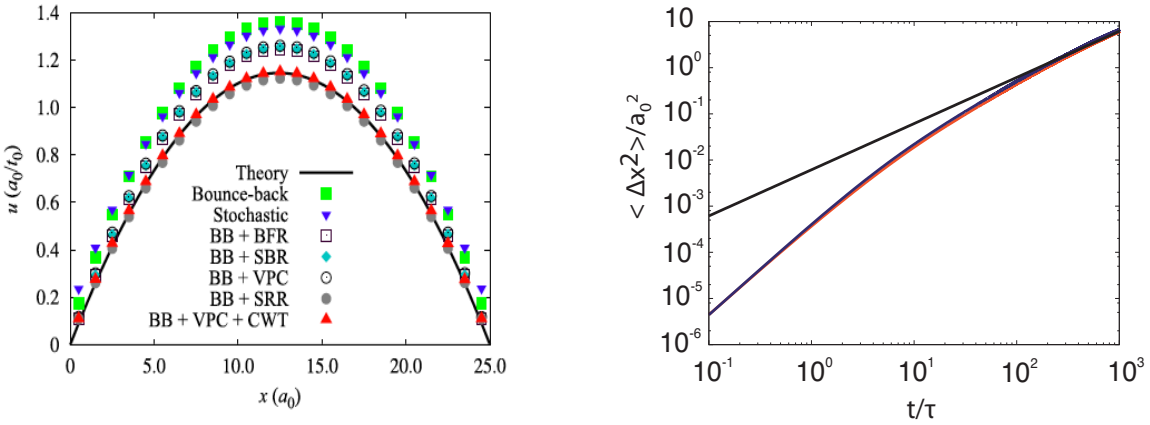

(a) (b)

Figure 3.11: **(a)** A Poiseuille flow in a channel with geometry $25a_0 \times 25a_0 \times 50a_0$ is simulated with a SRD−a algorithm using a rotation angle $\alpha = \pi/2$, a density $n = 32$ and a mean free path $\lambda = 0.2a_0$. Different boundary conditions are compared, which are described in detail in the text. Even though the phenomenological flow profile is received with all approaches, significant differences can be observed in the absolute values of the profile. From: [180]. **(b)** The mean square displacement of a colloid of radius $R = 3$ with (blue) and without (red) virtual particles, was simulated with a MPC+a algorithm. The fluid had a mean free path of $\lambda = 0.29$, given in units of the grid constant a_0, and a particle density $n = 5$. Both simulations approach the analytical result (black).

Gaussian distributed, instead of drawing the velocity of each virtual particle one random vector **a** can be added to the mean velocity. This random vector has a distribution with an average of zero and variance $n_{\mathrm{VP}}\, k_B\, T$. If, however, angular momentum should be conserved more care has to be taken, as will be discussed in the subsequent.

Poiseuille Flow

After the first simulation of Lamura [143], the Poiseuille flow has been investigated in detail for SRD/MPC fluids with Stochastic Reflection Conditions as describes in [182] as well as Bounce Back conditions [180]. In general, it has been shown that, similar to the results of the colloid, Stochastic Reflection Boundary conditions are not able to recapture no slip boundary neither with or without virtual particles [182]. However, even for Bounce Back Boundary conditions special care has to be taken to a detailed implementation of the virtual particles. Here, the results of Whitmer and Luijten will be recaptured as they are the basis of the simulation performed in the rest of this work.

Four different implantations of the virtual particles can be distinguished

- Bulk Filling Rule (BFR)
  This is the original implementation of virtual particles introduced by Lamura and Gompper [143]. If the number of particles in cell overlapping with a cell is smaller than the average particle density, the boundary cell is filled with virtual particles. This, however leads to an increase in the particle density at the boundary as the number of particles

in the bulk cells fluctuates but in the boundary only fluctuations to a density above the average are allowed.

- Symmetrized Bulk Filling Rule (SBR)
  In order to avoid the higher density of the particles induced by the (BFR), a symmetrized version has been proposed, where, if the particle number is higher than the average density, the contribution of the virtual particles is subtracted from the mean velocity.

- Simple Rescaling Rule (SRR)
  Instead of inducing virtual particles, the mean velocity is rescaled by $n_{\text{fluid}}/n_{\text{av}}$.

- Virtual Particle Conditions (VPC)
  This approach has been introduced together with an angular conservation in SRD/MPC algorithms [138]. Instead of applying the virtual particles to each cell, only the total number of virtual particles in an object is fixed. Their position is drawn randomly. This leads to a distribution of particles which fluctuates on the cell level. However, for complex geometries it is difficult to obtain the correct particle distribution.

In figure 3.11(a) the different implementation of the virtual particles are compared. It is obvious that the VPC-SRD nicely agrees with the analytic result. The SRR-SRD algorithm seems to fit the analytic curve also quite well, but this is only obtained for a certain parameter set, while the other results are quite robust.

Colloid

For an algorithm without angular conservation the position of the particles must not be determined. As has been discussed above, only the local density of the virtual particles matters. However, if angular momentum is important, as e.g. for a rotating object like a colloid, the detailed position of each particle is significant. Different possibilities have been discussed of placing the particles [138]. In this work, according to [138, 180], the particles are placed randomly inside the object a distance $\sqrt{3}\,a_0$ from the boundary with a global density equally to the bulk. This is similar to the VPC rules discussed above. The velocity of the virtual particles is drawn form a Maxwell-Boltzmann distribution but the local velocity of the boundary is added afterwards.

After the collision step, the momentum and angular momentum change of the virtual particles is ascribed to the immersed object. In the case a colloid that means the respective momenta are changed as follows

$$\Delta P = \sum_{i \in \text{VP}} m\,(\mathbf{v}_i^{\text{old}} - \mathbf{v}_i^{\text{new}}), \tag{3.85}$$

$$\Delta L = \sum_{i \in \text{VP}} m\,(\mathbf{r}_i^{\text{old}} - \mathbf{R}_{\text{coll}}) \times (\mathbf{v}_i^{\text{old}} - \mathbf{v}_i^{\text{new}}). \tag{3.86}$$

It has to be stressed that the angular momentum is obtained with respect to the center of the colloid. If it is calculated with respect to the center of mass of the local collision box this leads to a wrong decay of the orientation correlation function which is essential for the investigation of a Janus particle.

Finally, it has been shown that if virtual particles are neglected the friction of the colloid is significantly underestimated if analytical results are compared to simulations [182]. However, as can be seen in figure 3.11(b), for the mean square displacement no significant deviation between simulations with and without virtual particles can be observed.

3.6 Binary Fluid

There have been two distinct approaches to simulate binary SRD/MPC fluids. The first algorithm introduces a velocity dependent second collision step which leads to a non-ideal equation of state and will be called Multiphase Multiparticle Collision Dynamics (MMPC) in the subsequent. The second one generalizes the Multiparticle Collision Step towards different particle types A and B. This algorithm inherits the ideal gas equation of the state from the original algorithm and will be called Reactive Multiparticle Collision Dynamics (RMPC) in the rest of the work. In this section, both approaches will be explained and their applications will be discussed.

3.6.1 Multiphase Multiparticle Collision Dynamics (MMPC)

If a binary mixture consists of two immiscible components quenching the system can lead to domains of the either of these. This is known as spinodal decomposition [91]. Depending on the temperature there is metastable state in which the densities of the two phases module through the system or a stable one in which droplet formation occurs. Here, the latter one will be considered. The droplet formation arises due to a nucleation process which is driven by the surface tension between the two phases. For a surface tension to exist there must be an attractive force between particles of the same type and a repulsive force between particles of different types. This would lead to an equation of state which is not ideal and, hence, not straight forwardly introduced in a SRD/MPC fluid. In order to introduce surface tension, a first approach was given by Hashimoto and coworkers [183]. They incorporated a further collision step in the scheme which orientated the mean particle flow of one type in the direction of density gradient of this type. The approach leads to the formation of droplets with a surface curvature described by Laplace Law $\Delta p \sim 1/R$. This states that the curvature is proportional to the pressure difference between the two phases. The approach has been further extended to a more general collision rule [184] and to amphiphilic fluids, consisting of a binary fluid and objects with a hydrophilic and hydrophobic part [185]. Although the extension of the MPC approach described so far conserves energy and momentum, it has not yet been proven that it leads to thermodynamically consistent results.

In order to derive a thermodynamically consistent version of the multiphase SRD/MPC fluid, Tüzel and coworkers extend the SRD/MPC approach with a non-ideal equation of state described in section 3.3.3 to a binary mixture [186]. The collision imposed between the particles in the larger grid is not applied to all particles in the cells but to different particle types in each of the cells. This leads to a momentum flux between the two particles types and to a net attraction between particles of the same type and a repulsion of particles of opposite type. They could show that this approach also leads to the Laplace Law. However, it can be

shown that this approach leads to a thermodynamically consistent non ideal contribution to the pressure which can be related to parameter of the simulation. Further the algorithm leads to the correct fluctuation dissipation theorem at the boundary of the two phases. Like in the non-ideal SRD/MPC approach, in 3.3.3, the diffusion constants [187] and the viscosity [160] can be obtained.

3.6.2 Reactive Multiparticle Collision Dynamics (RMPC)

In the case of miscible binary fluids like the ones relevant for the reaction diffusion system, it can be assumed that the system obeys an ideal gas equation of state and therefore the SRD/MPC algorithm can be extended straight forwardly. Each type α of particles is first rotated with respect to the particle specific mean velocity

$$\mathbf{V}_\zeta^\alpha = \frac{\sum_{i=1}^{N_\zeta} \Theta^\alpha \mathbf{v}_i}{N_\zeta^\alpha}. \tag{3.87}$$

Here, N_ζ is the total particle number. The function Θ_i^α is one if a particle is of type α and zero otherwise. Afterwards, a rotation is applied to all particles types together. This leads to the new velocity [188]

$$\mathbf{v}_i^{\text{new}} = \mathbf{V}_\zeta + \omega_\zeta(\Theta_i^\alpha \mathbf{V}_\zeta^\alpha - \mathbf{V}_\zeta) + \sum_\alpha (\omega_\zeta^\alpha \omega_\zeta(\mathbf{v}_i - \mathbf{V}_\zeta^\alpha)). \tag{3.88}$$

As this approach shares the basic structure with the classical SRD/MPC approach it is straight forward to extend the Liouville equation of the phase space density towards different particle types [188]

$$\frac{\partial}{\partial t} P(\mathbf{V}^{(N)}, \mathbf{X}^{(N)}) = (-\mathrm{L}_0 + \mathcal{C} - 1) P(\mathbf{V}^{(N)}, \mathbf{X}^{(N)}), \tag{3.89}$$

where the streaming operator is given by the Liouville operator for each type

$$\mathrm{L}_0 = \sum_\alpha \sum_{i=1}^{N} \theta_i^\alpha (\mathbf{v}_i \cdot \nabla_i). \tag{3.90}$$

The collision is similar to the SRD/MPC collision but contains a further contribution including all particle types

$$\begin{aligned} \mathcal{C}P(\mathbf{V}^{(N)}, \mathbf{X}^{(N)}) = \frac{1}{|\Omega|^L} \sum_{\Omega^L} \sum_{m=0}^{\infty} \delta(t - m\,\tau) \int d\mathbf{V}'^{(N)} P(\mathbf{V}'^{(N)}, \mathbf{X}^{(N)}, t) \\ \prod_\alpha \prod_{i=1}^{N} \Theta_i^\alpha \delta(\mathbf{v}_i - \mathbf{V}'_\zeta - \omega_\zeta(\mathbf{V}'^\alpha_\zeta - \mathbf{V}'_\zeta)) \\ \omega_\zeta^\alpha \omega_\zeta(\mathbf{v}'_i - \mathbf{V}'_{zeta}). \end{aligned} \tag{3.91}$$

As the algorithm conserves momentum and velocity as the original approach, it clearly is described by a microcanonical distribution at equilibrium

$$P_0(\mathbf{V}^{(N)}, \mathbf{X}^{(N)}) = \mathcal{N}\delta\left(\frac{1}{2N}\sum_{i=1}^{N}\sum_{\alpha}\theta_i^\alpha m^\alpha |\mathbf{v}_i|^2 - \frac{d}{2\beta}\right) \times \left(\sum_{i=1}^{N}\sum_{\alpha}\theta_i^\alpha m^\alpha(\mathbf{v}_i - \mathbf{v}_{\text{equi}})\right), \tag{3.92}$$

where $\mathcal{N}$ is just a normalization constant. In the limit of large N this converges to a Boltzmann distribution which has been observed numerically [188]. A formal H-Theorem has not been given in literature yet but as this approach inherits the structure of the classical approach and a Boltzmann distribution has been obtained in the stationary state it can be assumed that the algorithm leads to the correct equilibration behavior. The transport coefficients can be derived using Green-Kubo relations where the only difference is that the viscosity must be considered for the total fluid while the diffusion constant of each component depends only on the density of this particle type. The diffusion of each of the particles can be further controlled by only considering a fraction γ of the particles of one type for the collision step with the other components [189].

The next step is to allow reactions between different species in the algorithm. Reactions are treated as birth-death stochastic processes where particles can be deleted or created with a certain probability. This approach does not conserve momentum and energy in general, which has to be incorporated separately. Here, first of all the theoretical foundation of this extension will be described. Afterwards, it will be discussed how to implement this approach practically.

In order to introduce arbitrary reactions between the different components a further reaction step has to be incorporated in the Liouville equation of the system

$$\frac{\partial}{\partial t}P(\mathbf{V}^{(N)}, \mathbf{X}^{(N)}) = (-\mathrm{L}_0 + \mathcal{R}(\mathcal{C} - 1))P(\mathbf{V}^{(N)}, \mathbf{X}^{(N)}), \tag{3.93}$$

with the operator $\mathcal{R}$ including the reactions in the Liouville equation. A particular reaction is given by

$$R_\mu : \sum_{l=1}^{s}\nu_l^\mu\, X_l \xrightarrow{k_\mu} \sum_{l=1}^{s}\bar{\nu}_l^\mu\, X_l, \tag{3.94}$$

where $X_l \in \{1..s\}$ is one of the s species and ν_l^μ and $\bar{\nu}_l^\mu$ are the stoichiometric coefficients [190]. It can be constructed as following:

- Assume that $P^C(\mathbf{V}^{(N)}, \mathbf{X}^{(N)}, t)$ is the probability distribution after the collision step.
- The probability that a certain reaction occurs in a given cell and leads to particles with a given velocity is

$$P(\mathbf{V}^{N_\zeta}, \mathbf{X}^{N_\zeta}, t)_{\mu,\zeta} = p_\mu^\zeta(N'^\zeta)\prod_{l=1}^{s}\delta_{N_l^\zeta, N'^\zeta_l + \Delta_l^\mu}\prod_{k=1}^{-\Delta_l^\mu}\int d\mathbf{x}_{N_{l+k}^\zeta}\int d\mathbf{v}_{N_{l+k}^\zeta} \prod_{j=1}^{\Delta_l^\mu}\frac{1}{V_C}\phi_0(\mathbf{v}_{N'^\zeta_{l+j}})P^C(\mathbf{V}^{(N)}, \mathbf{X}^{(N)}, t). \tag{3.95}$$

Here, $p_\mu^\zeta(N'^\zeta)$ is the probability that the reaction takes place, which will be discussed in detail below. The probability ϕ_0 for a given velocity is a Boltzmann distribution and $\Delta_l^\mu = \bar{\nu}_l^\mu - \nu_l^\mu$ is the change in the number of particles of a given type l.

- Finally, the reaction operator is given by

$$\mathcal{R}P^C(\mathbf{V}^{(N)}, \mathbf{X}^{(N)}) = \underbrace{\sum_{N'} \underbrace{\underbrace{\prod_{\zeta=1}^{N_c} \underbrace{\sum_{\mu=0}^{r} P(\mathbf{V}^{N_\zeta}, \mathbf{X}^{N_\zeta}, t)_{\mu,\zeta}}_{\text{any reaction r occurs in a cell } \zeta}}_{\text{the reaction occurs in any cell}}}_{\text{the total number of particles in the system is } N'} . \tag{3.96}$$

Even though this operator looks very complicated, it is just the probability that the state of the system is altered due to a reaction. The only thing still missing is an expression for the probability $p_\mu^\zeta(N'^\zeta)$, which states if a certain reaction occurs or not. As it is assumed that the reactions are birth-death processes it is straight forward to show that

$$p_\mu^\zeta(N'^\zeta, \tau)) = \frac{a_\mu^\zeta}{a_0^\zeta}(1 - e^{-a_0^\zeta \tau}), \tag{3.97}$$

with τ being the collision time and the factor

$$a_\mu^\zeta = k_\mu \prod_{l=1}^{s} \frac{N_l^\zeta!}{(N_l^\zeta - \nu_l^\mu)!}, \tag{3.98}$$

containing the reaction constant and the combinatorial factor which counts the number of possible reactions in a cell. For this extension of the SRD/MPC approach, even though the Liouville equation can be derived as has been discussed, a H-Theorem has not been derived. This is supposed to be not as easily possible as in the classical as due to the birth-death structure of the reaction phase space is not conserved as momentum and energy fluctuate due to a Boltzmann distribution. However, for various reactions, extensions have been proposed that are capable of conservating both [190]. For the Janus swimmer treated in this work, the reaction operator significantly simplifies as a conversion of particles always occurs in a certain region.

In the application of the algorithm, in order to decide if a certain reaction should take place in a cell of the grid, a Gillespie algorithm is applied. This is a very effective way to solve a master equation for a stochastic process [191] .

3.6.3 Application of the RMPC Algorithm

The algorithm described here has successfully been applied to various systems like motile and no motile enzymes [188, 192] as well as to the Selkov model. The latter is a simple model of the phosphofructokinase, part of the glycolytic cycle, and consists of six separate reactions [190]. Here, a cubic autocatalytic reaction is used as a benchmark for the code developed for

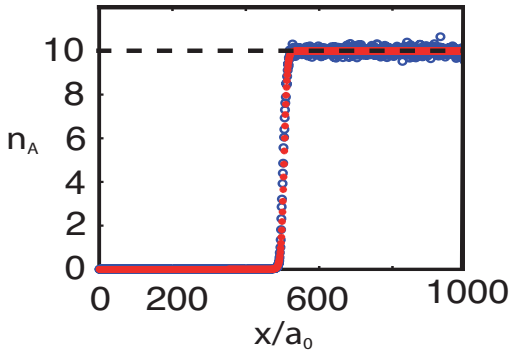

Figure 3.12: A binary MPC fluid with an autocatalytic reaction $A + 2B \rightarrow 3B$ shows propagating waves. The initial conditions were $n_{A/B} = 0, 10$ for $x < L/2$ and $n_{A/B} = 10, 0$ for $x > L/2$ with a temperature $k_B T = 1/3$ and $L = 1000\, a_0$. For small simulation times, the simulation (blue) fits the analytic results (red) very well. For lager times, deviations occur as reflecting boundaries have been used.

this work, which has previously been reported in literature [189]. Two types of particles are restricted to separated halves of the simulation box. If they meet within one box a Gillespie algorithm with the reaction rate k is applied to the following reaction

$$A + 2B \rightarrow 3B. \tag{3.99}$$

The continuum equation for the density of this system

$$\frac{\partial}{\partial t} n_A(\mathbf{r}, t) = -k\, n_A\, n_B^2 + D\nabla^2 n_A, \tag{3.100}$$

can be solved in the frame moving with the boundary between the two compartments $\xi = x - ct$. This leads to the solution

$$n_A(\xi) = n_0(1 + e - c\xi/D)^{-1}, \tag{3.101}$$

with the front speed $c = \sqrt{D\, k\, n_0^2/2}$. In this model there is no fit parameter as the diffusion constant can be calculated, as has been described in section 3.4.2, and the density as well as the reaction constant are free parameters. It is expected that at the boundary between particle of type A and B, due to the autocatalytic reaction, a propagating wave can be observed. As can bee seen in figure 3.12, the code satisfactorily reproduces the front propagation within the error bars. In contrast to the literature [189], instead of open boundary conditions periodic ones have been used. It can be seen that for a small system finite size effects occur at short time scales while for larger systems it takes the system significantly longer until it shows effects of the finite size.

In this section, two extensions of the classical SRD/MPC approach have been described for multiphase systems. While the first can be used to simulate immiscible fluids and leads to a non-ideal equation of state, the second one gives a miscible fluid with an ideal equation of state. The latter one can be straight forwardly extended to reactive fluids which will be used in the rest of this work.

3.7 Units in SRD/MPC

The basic units to describe a physical system neglecting electric currents are length, time, mass, particle number and thermodynamic temperature. As has nicely been discussed by Padding and Louis [144], this is not the case for a SRD/MPC fluid as well as for other simulation techniques like Lattice Boltzmann. Special care has to be taken if a simulated system is compared to a real physical system investigated in an experiment.

Further, as the SRD/MPC algorithm was developed to mediate between the microscopic and macroscopic time scales that can occur in soft matter systems, it has to be assured that during the mapping the time ordering of the system is conserved, as given in table 3.13, even though the time scales in the simulation are closer together than in a real physical system.

3.7.1 Units

In order to distinguish between basic units and derived units, the length can be measured in terms of the cell length a_0, the energy as a thermal energy $k_B\,T$ and the mass as the one of the fluid particle m. As there is no interaction between the fluid particles besides the collisions, the fluid, as has been discussed previously 3.4.3, only contains kinetic energy. Therefore, the following relation, derived from the kinetic energy,

$$m_0 \left(\frac{a_0}{t_0}\right)^2 = k_B\,T, \tag{3.102}$$

describes the relation between the units. This makes the time in contrast to every intuition a derived unit that has to be rescaled if for example the temperature of the simulation is altered.

3.7.2 Mapping into the Real World

As has been discussed above, the units of a simulation do not correspond to the units of a real world system but have to be mapped onto each other. Further, the hydrodynamic numbers are not related to the absolute values of transport coefficient but only to their ratio. This

Basic Units	Derived Units	Transport coefficients
Length: a_0	Time: $t_0 = a_0\sqrt{\frac{m}{k_BT}}$	Diffusion constant: $D_0 = \frac{a_0^2}{t_0} = a_0\sqrt{\frac{k_BT}{m}}$
Energy: k_BT	particle density: $n = \frac{n_0}{a_0^3}$	Kinematik viscosty: $\nu_0 = \frac{a_0^2}{t_0} = a_0\sqrt{\frac{k_BT}{m}}$
Mass: m		Viscosity: $\eta = \frac{m}{a_0 t_0} = \frac{\sqrt{m\,k_BT}}{a_0^2}$

Figure 3.13: In the MPC approach, the basic units are length, mass and energy. In contrast to the Si units, here, time and density become derived units. Therefore, also the transport coefficients have to be given in terms of the simulation units.

Solvent time scales		Brownian time scales	
Solvent collision time	τ_{col}	Fokker Planck time	τ_{FP}
Solvent relaxation time	τ_f	Enskog relaxation time	$\tau_E = \frac{M_C}{\zeta_E}$
Hydrodynamic time scales		Browninan relaxation time	$\tau_B = \frac{M_C}{\zeta_B}$
Sonic time	$\tau_{cs} = \frac{R}{c_S}$	Colloid diffusion time	$\tau_D = \frac{R^2}{D_{col}}$
Kinematic time	$\tau_\nu = \frac{R^2}{\nu}$		
Stokes time	$\tau_S = \frac{R}{v_S}$		

Time ordering
$\tau_{col} < \tau_f, \tau_{FP} < \tau_E, \tau_{cs} < \tau_B < \tau_\nu < \tau_D, \tau_s$

Figure 3.14: The relevant time scales in a fluid and their relations. A simulation approach will not be able to give the correct numbers of the time scales but should sustain their relations.

means, if the hydrodynamic numbers are the same, e.g. in a lava or honey flow, even though the absolute values of their material properties differs significantly, their physical properties are similar. The following rescaling scheme should be kept in mind to map simulation results onto real physical problems.

$$\text{Simulation} \overset{Re,Pe,a_0,t_0}{\longleftrightarrow} \text{Dimensionless System} \overset{Re,Pe,a_{P_i},t_{P_i}}{\longleftrightarrow} \text{Physical System } (P_i)$$

Here, P_i can be a different physical system that is obtained by different scaling factors a_{P_i}, t_{P_i} but has the same hydrodynamic numbers.

Consider an example originally given in the work of Padding and Louis [144] to clarify this condition. The diffusive behavior of a colloid with diffusion time $t_D = 5s$ should be investigated. In the simulation, a colloid with radius $R = 2a_0$ is used which leads to a size of the real world sphere of diameter $a_{P_i} = 0.5\mu$m and to a time scale $t_{P_i} = 0.02$s. The time scale as has been described above can no longer be chosen freely as it is a derived unit. The simulation parameters now do not have to be chosen to lead to the correct other time scale but only to capture the basic relation like for example for the kinematic time $\tau_\nu < \tau_D$.

3.8 Alternative Simulation Techniques

Beside the Multiparticle Collision approach, two further techniques are used to simulate low Reynolds number hydrodynamics which are Lattice Boltzmann Simulations (LB) [193] and Dissipative Particle Dynamics (DPD) [194]. The LB fluid model solves the discrete Boltzmann

equation on a lattice while the DPD approach is an off-lattice technique solving Netwon's equation of motion with a particular set of forces. Here both techniques are outlined shortly and compared to MPC.

3.8.1 Lattice Boltzmann Simulations

One of the classical techniques for simulating hydrodynamics is the Lattice Boltzmann method (LB) which evolved from Lattice Gas Automata (LGA). The latter are particle based lattice simulations in which a lattice node can be occupied by a particle or being empty. Each particle move in a streaming step with its velocity and if two or more particles approach a node at the same instance, they collide with a prescribed collision rule. As these kinds of simulations are stochastic because of the finite number of particles a lot of averaging has to be done to arrive at the description level of Navier-Stokes hydrodynamics. Nevertheless, it has been proven that LGAs are capable of reproducing Navier-Stokes like behavior.

In order to avoid this amount of averaging Lattice Boltzmann Simulations are working on the level of the discrete one-particle distribution function $f_i(\mathbf{x})$ with $i \in \{1, \ldots, \beta\}$ giving the lattice direction. The distribution on each node evolves according to a discrete Boltzmann equation

$$\underbrace{f_i(\mathbf{x} + \mathbf{c}_i, t + \Delta t) = f_i(\mathbf{x}, t)}_{\text{streaming}} + \underbrace{\mathcal{L}_{ij}(f_j(\mathbf{x}, t) - f^{eq}(\mathbf{x}, t))}_{\text{collision}}. \tag{3.103}$$

From the distribution function, the hydrodynamic fields can be obtained straight forwardly by summing over the discretized velocity e.g. $\rho(\mathbf{x}) = \sum_{i=1}^{\beta} f(\mathbf{x})_i$ and $\mathbf{p}(\mathbf{x}) = \sum_{i=1}^{\beta} \mathbf{c}_i f(\mathbf{x})_i$. The form of the equilibrium distribution $f^{eq}(\mathbf{x}, t)$ can be obtained analytically. As the simplest version of the Collision operator L_{ij} the Bhatnagar, Gross and Krook (BGK) matrix $L_{ij} = \delta_{ij}/\tau$ can be used where τ is the collision parameter.

However, Lattice Boltzmann suffers from the lack of Galilean invariance as it is lattice based. This drawback can be diminished by certain lattice types which are also relevant for the hydrodynamic limit as this depends significantly on the chosen lattice type.

Hydrodynamic and Thermodynamic Properties

As the LB approach uses a discrete Boltzmann equation it is straight forward to prove that the technique reproduces Navier-Stokes like behavior in the long time limit and it obeys an H-Theorem. The simplest version, similar to the MPC approach, has an ideal gas equation of state and is, hence, a compressible fluid. However, for small Mach numbers $\mathrm{Ma} < 0.2$ this effect can be neglected.

Fluctuations in LBM

The classical Lattice Boltzmann approach does not contain thermal fluctuations. Stochasticity only arises through the initial conditions of the simulations. As fluctuations can not be

neglected at mesoscopic scales relevant for many soft matter systems they can be incorporated into LBM in the spirit of fluctuating hydrodynamics.

The first approach by Ladd [195] added a Gaussian random variable to the discretized Boltzmann equation (3.8.1). This leads to a correct behavior in the limes of small wavelengths, but for other modes can lead to spurious effects. Further, it is known that under certain conditions the algorithm does not relax towards equilibrium. Therefore, for each simulation using this algorithm an extensive testing is necessary. In order to ensure this relaxation process Adhikari et. al. [196] proposed a fluctuating Lattice Boltzmann approach which is similar to Ladd's but whose stochastic variable ξ_i is linked by its Fluctuation Dissipation Theorem (FDT) to all dissipative processes in the simulation. It must further be ensured that the fluctuation in ξ_i exactly conserves density and momentum.

Boundary Conditions

In order to simulate e.g. colloids, the lattice based approach has to be coupled to boundaries which can be freely orientated in space. Various approximations have been proposed to mimic the local interaction with the fluid model [197] and to incorporate local Brownian forces. Nevertheless, these interactions are only correct to the first order.

Even though the MPC approach shares hydrodynamic as well as thermodynamic properties with the LB technique, its advantage is that it naturally contains thermal fluctuations and boundaries can be implemented straight forwardly without applying approximation schemes.

3.8.2 Dissipative Particle Dynamics

One of the widely used off-lattice simulations for hydrodynamics which naturally contain thermal fluctuations is Dissipative Particle Dynamics (DPD). Here, the fluid is modeled by discrete particles which are not considered to be an atomistic representation of the fluid but mesoscopic clumps of the liquid. Their dynamic is governed by Newtons equations of motion

$$\frac{d\,\mathbf{r}_i}{d\,t} = \mathbf{v}_i, \quad \frac{d\,\mathbf{v}_i}{d\,t} = \mathbf{f}_i. \tag{3.104}$$

The difference towards Brownian Dynamic Simulations (BD) or Molecular Dynamic Simulations (MD) lies in the choice of the force $\mathbf{f}_i$ which is chosen such that it guaranties momentum conservation

$$\mathbf{f}_i = \sum_{j \neq i} (\underbrace{\mathbf{F}^C_{ij}}_{\text{Conservative Force}} + \underbrace{\mathbf{F}^D_{ij}}_{\text{Dissipative Force}} + \underbrace{\mathbf{F}^R_{ij}}_{\text{Random Force}}). \tag{3.105}$$

The conservative force is derived from a soft potential leading to a repulsion between the fluid particles. A commonly used form is

$$\mathbf{F}^C_{ij} = \begin{cases} a_{ij}(1 - r_{ij})\,\hat{r}_{ij}, & \text{if } (r_{ij} < 1), \\ 0 & \text{if } (r_{ij} \geq 1). \end{cases} \tag{3.106}$$

As a friction or drag force

$$\mathbf{F}^D_{ij} = -\gamma\, w^d(r_{ij})\,(\hat{\mathbf{r}}_{\mathbf{ij}} \cdot \mathbf{v}_{ij})\,\hat{\mathbf{r}}_{\mathbf{ij}}, \tag{3.107}$$

is used. Finally, a Random Force

$$\mathbf{F}_{ij}^{R} = \sigma\, w^{R}(r_{ij})\, \theta_{ij}(t)\, \hat{\mathbf{r}}_{\mathbf{ij}}, \tag{3.108}$$

is applied. The Gaussian variable θ_{ij} is defined via

$$\langle \theta_{ij}(t) \rangle = 0, \quad \langle \theta_{ij}(t)\, \theta_{kl}(t') \rangle = (\delta_{ik}\, \delta_{jl} + \delta_{il}\, \delta_{jk})\, \delta(t - t'). \tag{3.109}$$

As the forces are antisymmetric momentum is conserved in the standard algorithm. Energy conservation, however, is not guaranteed which does not matter as long as the system is isothermal.

Thermodynamic and Hydrodynamic Properties

It has been proven that on long length and time scales DPD resembles Navier-Stokes behavior for the density and the velocity fields [198]. That does not necessarily show that also the thermodynamic properties of a fluid can be expected. As there is no energy conservation it is obvious that heat conduction is not captured by the DPD model. However, in 1995 Español [199] formulated a Fokker-Planck equation for a N-particle distribution function of the DPD algorithm

$$\frac{\partial \rho}{\partial t} = \mathcal{L}^{C} \rho + \mathcal{L}^{D} \rho. \tag{3.110}$$

Here, $\mathcal{L}^{C}$ is the classical Liouville operator of an Hamiltonian system and $\mathcal{L}^{D}$ contains the dissipative as well as stochastic contributions of the dynamic. It has been shown that in order obtain a Gibbs-Boltzmann distribution in the stationary state a sufficient condition is $\mathcal{L}^{D} \rho = 0$. That leads naturally to a condition for the weight functions of the dissipative and random forces as well as a Fluctuation Dissipation theorem

$$w^{D}(r) = w^{R}(r)^{2} \quad \text{and} \quad \sigma^{2} = 2\, k_{B} T\, \gamma. \tag{3.111}$$

The detailed expression for the weight functions can, however, be chosen freely. A commonly used form is

$$w^{D} r = \begin{cases} (1 - r)^{2}\ , & \text{if } (r < 1), \\ 0 & \text{if } (r \geq 1). \end{cases} \tag{3.112}$$

Further, under the assumption of continuous time, a Boltzmann equation for the DPD schema has been derived [152] and a H-Theorem been proven. This shows that the technique provides the correct evolution towards equilibrium and that thermodynamic relations can be used to derive for example transport coefficients. Therefore, similar to the MPC approach, different hydrodynamic regime, characterized through their set of hydrodynamic numbers, can be investigated. However, care has to be taken for the Schmidt number which in the classical DPD approach is rather small. Even though techniques have been proposed to reach higher Schmidt numbers this is still a crucial point in DPD [200].

Boundary Coniditions

The investigation of composed systems like colloids or polymers [194, 201] is straight forward in DPD. Boundaries can be implemented in the same way as for a MPC code [202]. In order to compare the possibility to implement multi component systems see [203].

As MPC as well as DPD are both off-lattice simulations concerning the streaming step many methods, like the implementation of boundaries, can be interchanged between both. However, DPD has the major drawback that the effect of the Schmidt number has be investigated carefully as it does not necessarily lead to the correct behavior.

3.9 Conclusion

Simulating low Reynolds number hydrodynamics is a challenging task. Even though it is a topic which has been addressed by physicists for many years, there is still no "one for all solution". Especially in biological as well as soft matter systems, there is an urgent need for techniques which can further incorporate thermal fluctuations, ubiquitous in these systems. In this chapter, the MPC technique has been introduced, which is a particle based Navier-Stokes solver, containing thermal fluctuations naturally. It is a combination of a lattice and an off-lattice approach, as it solves the Newton equations of the fluid particles in free space. The interaction between the particles is, however, mimicked by a lattice collision step. This step can be chosen freely and canonical as well as microcanonical approaches exist. In the rest of this work, the canonical approach is used. Even though it is slightly slower than the microcanonical one, it has been shown that it is straight forward to implement and no special care has to be taken concerning the correlation functions. Further, it naturally conserves temperature locally even if an interaction between the colloid and the fluid takes place.

The basic MPC algorithm is neither Galilean invariant nor does it conserve angular momentum. Both effects can be incorporated into the code. The former can be received by a grid shifting procedure during the collision and the latter by an extension of the collision step itself. Their effect on the algorithm can be observed in the transport coefficients like e.g. the diffusion constant or the viscosity of the fluid. In general, the transport coefficients of the various versions of the technique can be obtained analytically. It is shown that in the simulations done for this work, the simulation results nicely fit the analytical results. The analytical results of the transport coefficients should not be confused with properties of a real fluid. In order to map an MPC fluid onto a system investigated by an experiment care has to be taken. As the approach aims to close the gap between the various time scales of a hydrodynamic problem just certain properties can be mapped and others have to be treated only qualitatively. It is shown that especially the Reynolds number is of an order of magnitude larger than in a real fluid. Further, the approach is only capable of simulating systems with sufficiently small velocities as the Mach number is not obtained correctly because the MPC approach only simulates a compressible fluid. Therefore, care has to be taken if a system dealing with sound propagation should be investigated.

In order to implement complex objects in a MPC fluid special care has to be taken which boundary conditions should be applied. It is shown that the Bounce Back Boundary Conditions lead to the correct long time as well as short time behavior of the velocity and angular

velocity autocorrelation function. Even the power law of both long time behaviors can be resolved correctly. If a boundary is immersed in the fluid spurious effects can arise because of the grid shifting procedure. It leads on average to only partially filled cells in the region close to the boundary. Therefore, virtual particles have to be introduced in the region where the grid overlaps with the boundary. This can especially be seen by a Poiseuille flow in a channel driven by an external force.

Finally, the MPC algorithm can be extended to more complex objects like e.g. fluids constituted of different particle types. Here, it has to be distinguished between immiscible and miscible components. While for the former it is important to obtain the correct surface tension between the fluid phases, for the latter the constituents can mix. In order to simulate the motion of a selfdiffusiophoretic swimmer an miscible approach has to be used, in which the constituents are also able to interact with each other. This approach is called Reactive Multiparticle Collision Dynamics (RMPC). It can also be used to investigate e.g. wave propagation in binary mixtures.

It has been shown that the MPC approach is a valuable tool to investigate systems at low Reynolds numbers. As it is straight forward to implement even complex objects as well as different particle types, it is an ideal technique to consider the selfdiffusiophoretic swimmer discussed in section 2.

4 Selfdiffusiophoretic Swimmer

The controlled motion of objects at small length scales is an active field of research. Inspired by the motion of bacteria, many systems have been suggested which can propel themselves through a fluid at low Reynolds numbers. As most of the proposed approaches are based on a mechanically driven propulsion it is, due to their size, experimentally very difficult to control them. Alternatively, gradient driven systems can be used which move along external or self-produced gradients. In chapter 2 such systems have been described extensively, recapturing the experimental as well as theoretical literature. In the latter, mainly the propulsion of swimmers which rely on steady-state arguments has been addressed. In order to understand the motion of a swimmer in a broader context, simulations have to be performed which can investigate the swimmer from its initial phase to its long time limit. Here, simulations based on the Multiparticle Collision approach are performed which are able to investigate, especially, a Janus colloid in a self-produced particle gradient.

This chapter is organized as follows. In the first section, the basic model is described. Afterwards, its relevant parameters are discussed and related to the relevant hydrodynamic numbers, described previously in section 3.2. The principles of the propulsion mechanism are explained and the role of the gradient is discussed. Finally, the long time limit is investigated. It will be shown that the simulations performed are the first which are able to reproduce the experimentally observed results.

4.1 Model

In the simulations of objects based on the MPC technique, two approaches have been used. The first one builds up complex objects with Lennard-Jones spheres as described section 3.5.1. Such simulations have e.g. been used to investigate the collective behavior of self-propelled rods and flagella [204]. The details of the hydrodynamic flow field around such an object, however, cannot be resolved due to the coarse graining. As it is assumed that the collective effects of such objects arise mainly due to excluded volume, such an approach seems to be justified. In order to describe the interaction around an object a hard sphere object has to be considered as has e.g. been done in studies of the squirmer model [147]. In such an approach, the surface interaction of the swimmer with the fluid can be modeled correctly, first of all to distinguish between a slip and a non slip boundary condition and further to ensure the correct angular momentum transition from the fluid to the object an vice versa. The model is set up as follows

- Colloid with excluded volume and Bounce Back Boundaries, as described in section 3.5.1
- Binary fluid composed of two components A and B with equal physical properties, as described in section 3.6.2

- In a region $L < R$ smaller than the colloid radius $R = 3a_0$ the two particle types are converted according to $A \to B$ with a probability p_C
- The particles of type B interact with the colloid through a potential ϕ, given by

$$\phi = \epsilon\, e^{-r/L}, \tag{4.1}$$

  which is a short range potential used previously in analytical treatment [89]. The A particles only interact via a hardcore potential.
- For the system of size $24a_0 \times 24a_0 \times 24a_0$, periodic boundaries are applied. If particles of type B are crossing the outer boundary they are reconverted in particles of type A

Most of the analytic investigations of Janus colloids whose motion is based on self-produced gradients rely on the implementation of a slip velocity at the surface between a colloid and the fluid. In simulations, such an approach can only be used if the slip velocity is independent of the interaction with the fluid, as for example in the squirmer model [141]. In the literature, two possibilities have been introduced to address a selfphoretic Janus colloid analytically. The first one uses an explicit form of the slip velocity while the second is based on a matching procedure. The former one uses the explicit expression

$$\mathbf{v}_S(\mathbf{x}) = -\kappa \frac{\partial C_{||}(\mathbf{x})}{\partial \mathbf{x}}. \tag{4.2}$$

Such an approach is not feasible for a simulation approach as it is not clear how to define a particle gradient in such a coarse grained description, while it is straight forward in a field equation approach as described in chapter 2. Therefore, the latter approach has to be used and the interaction between the fluid and the solid body has to be modeled explicitly, as is done here.

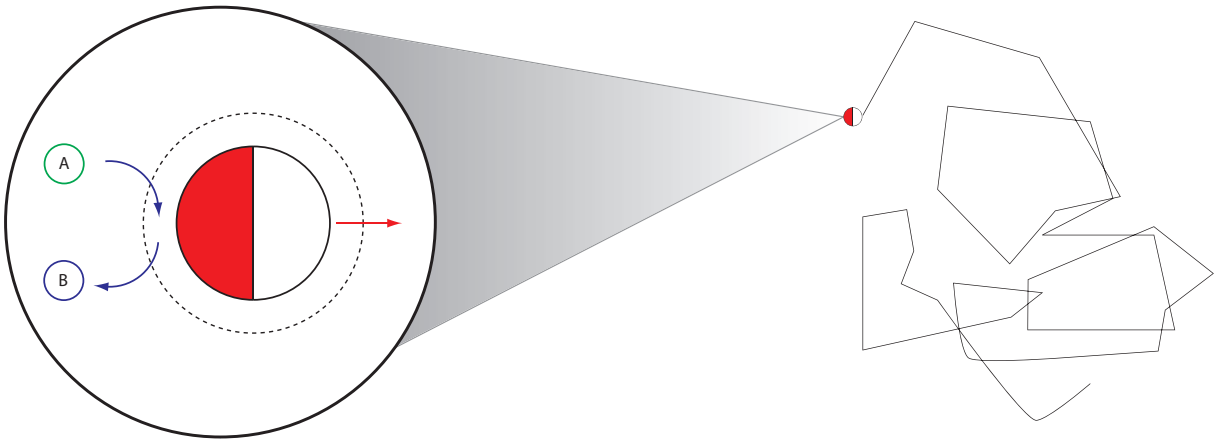

Figure 4.1: On the left, the swimmer is depicted schematically. On the coated hemisphere (red) of the Janus colloid the particles of type A are converted into particles of type B. Inside the dashed circle a potential of mean force ϕ acts on the particles of type B leading to a net propulsion. As shown on the right-hand side, on length scales accessible in experiments mainly the path of the swimmer is observable, which shows diffusive behavior but with a significantly increased diffusion constant.

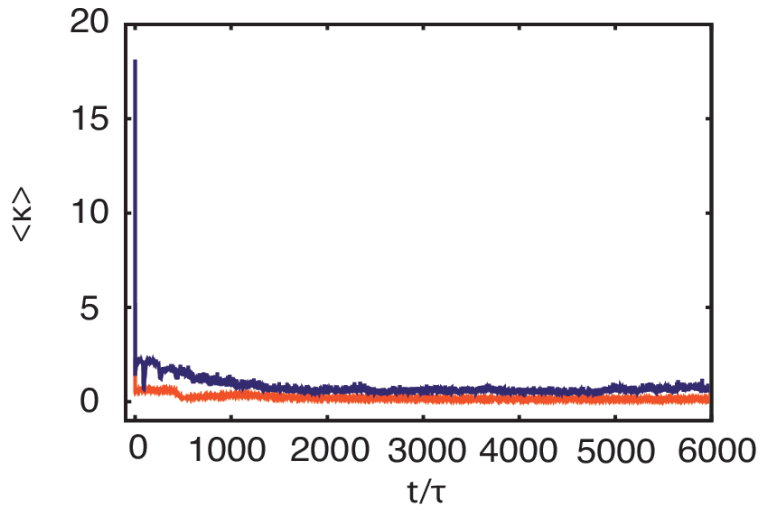

Figure 4.2: Time evolution of the averaged surface production rate κ of a Janus colloid with the interaction length L = 2 a_0 (blue) and L = 0.5 a_0 (red). At the initial phase, the production rate increases significantly due to the predominance of A particles. Afterwards, it decays to a continuous production rate for both interaction lengths.

4.2 Hydrodynamic Numbers in the Simulation

As has been described in section 3.2, the regime of a hydrodynamic system can be defined by a set of hydrodynamic numbers. In the simulation for this work they can be estimated as

- *Knudsen Number* $Kn = \frac{\lambda}{R} \approx 0.01$
  The discrete nature of the fluid leads to fluctuation effects not present in a continuums description
- *Schmidt Number* $Sc = \frac{\nu}{D} \approx 32$
  The MPC algorithm is clearly in a fluid like regime
- *Reynolds Number* $Re = \frac{UR}{\nu} \approx 0.05 \ldots 0.4$
  It can be assumed that the fluid around the swimmer can be described by low Reynolds hydrodynamics
- *Peclet Number* $Pe = \frac{UR}{D} \approx 1.7 \ldots 11.4$
  While for small velocities of the swimmer it can be assumed that diffusion contributes to the relaxation of the fluid, for larger velocities this cannot be ensured

The hydrodynamic numbers are all in the regime expected for a MPC algorithm describing low Reynolds number hydrodynamics. Care has only to be taken in the case of the Peclet number which can become high for a swimmer with a large mean velocity.

4.3 Propulsion

As the simulations are performed at low Reynolds numbers it cannot be assumed that the interaction between the B particles and the Janus colloid is sufficient to propel the swimmer.

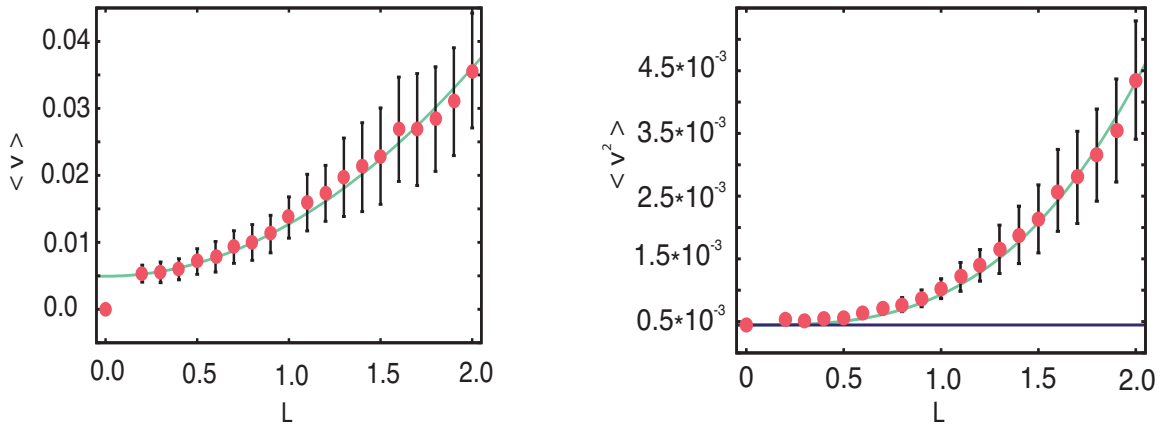

(a) **(b)**

Figure 4.3: **(a)** The mean propulsion velocity $< \mathbf{v} >$ of a Janus colloid depending on the interaction length L. The red dots are simulation results while the green curve is a quadratic fit. Initially, at $L = 0$ the mean propulsion velocity of a Brownian colloid is shown, which is zero as would be expected.
(b) The mean square propulsion $< \mathbf{v}^2 >$ depending on the interaction length L. Again, the red dots correspond to simulation data, the green curve depicts L^3. The blue line is the analytic result for a Brownian particle. For small values of L the error bars are smaller than the symbol size.

It could be guessed that the motion of the swimmer is immediately damped. Further, it is not assured a priori that the swimmer reaches a steady-state. Therefore, it has to be ensured that the swimmer can build up a net propulsion and reaches a steady-state before looking into the details of averaged quantities necessary to understand the long time limit.

Initial Phase

As the initial configuration of the fluid consists of a homogenous concentration of A particles with $n_A = 5$, the simulation has to relax into a steady-state. As an observable to control this process the surface production rate κ can be used. It is the number of particles converted from A to B during one time step τ normalized to the surface of the swimmer. Its time evolution, given in figure 4.2, is averaged of many realizations of a single moving Janus colloid. After an initial phase of 1000 to 2000 time steps the rate has on average decayed to a constant rate. The initial burst of the production rate can be attributed to the initial configuration of the system.

Velocity of the Swimmer

The mean velocity of a Brownian colloid has to be zero $< \mathbf{v} >= 0$. The particle has no intrinsic velocity at all and it moves only due to diffusion. A straight forward extension of a classical Brownian colloid would be a particle with a velocity v_0 along a predefined axis which only changes its direction due to rotational diffusion. It is a well known result that this leads to an increase in the diffusion constant of the swimmer as well as a short time ballistic

regime of its mean square displacement [119]. In the case of the Janus colloid considered here, the intrinsic velocity itself becomes a fluctuating observable as it depends on the particle gradient surrounding the colloid. Its direction is given by the normal of the surface separating the active and non-active hemisphere of the swimmer. For convention, it is assumed that it points in the non-active half-sphere such that it describes the direction away form the cloud of produced particles.

In figure 4.3(a), the mean velocity of a Janus colloid is plotted against the interaction length L in which the solute particles are converted. Obviously, the velocity depends significantly on this quantity. A quadratic dependence can be fitted as has previously been proposed in literature [8] and discussed in chapter 2. Further, it can be found that the absolute values of the velocity of the simulation are significantly lower than the analytical results. This was expected as the simulation aims to give a coarse grained description of the system. It conserves the order of the relevant time scales but not their absolute values as has been discussed in section 3.7. One necessary condition to obtain the analytical results is that the diffusion time of the solute molecules is much smaller than the rotation diffusion time of the colloid $\tau_D \ll \tau_R$. It has been shown in section 2.4.4 that this is equivalent to $a/R \ll 1$, here a is the radius of the solute molecules and R the radius of the colloid. For a colloid with the size in the μm range these time scales are separated by three orders of magnitude $\tau_D/\tau_R \approx 10^{-3}$ [120]. In the simulations of Janus colloid investigated with the MPC technique both time scales are of the same order. This means that the local solute concentration cannot fully equilibrate until the colloid has already started to reorientate itself such that it disturbs the solute cloud. There are two ways to avoid this. The first would be an increased radius of the colloid which leads to an increase of the rotation diffusion time. However, this is computational extremely costly, as also the system size has to be increased to avoid finite size effects. Alternatively, the hydrodynamic radius of the solute molecules could be reduced. As this scales as $a \sim n^{-1}$ [144], inverse with the particle density, in order to derive a substantial decrease of the ratio of the diffusion and rotational diffusion time the particle density must be increased by a factor of 10. This would lead to a tremendously longer computational time. Therefore, the mean velocity of the Janus colloid as well as its local behavior should be treated with care if investigated with a MPC approach. However, the long time limit as discussed in the next section is not effected by this problem as the details of the interaction of the swimmer with the fluid are not relevant and only the fluctuating behavior of it is of interest.

As the MPC fluid only contains kinetic energy, the temperature of the system is proportional to the mean square velocity of an immersed Brownian colloid due to the equipartition theorem $3\,k_B\,T = M < \mathbf{v}^2 >$, with M being the mass of the colloid. For active systems, it has been shown that an effective temperature of the colloid can be defined [77, 205] as a non-equilibrium counterpart of the equilibrium temperature, which scales as $k_B\,T_{\text{eff}} \sim \text{Pe}^2$. As in the system described here, the only constitute of the Peclect number which alters is the mean velocity and this is proportional to the square of the interaction length, it can be assumed that it scales with L^4. However, as is shown in figure 4.3(b), only a scaling with L^3 is observed. It can be assumed that this is due to the non-constant magnitude of the intrinsic velocity. In previous approaches [205], it has always been assumed to be constant.

For both quantities discussed here, the MPC approach is only sufficient to reproduce the scaling behavior while a fit to analytical results is not possible due to the shrinked time ordering. However, the details of this microscopic behavior are not relevant for the long time

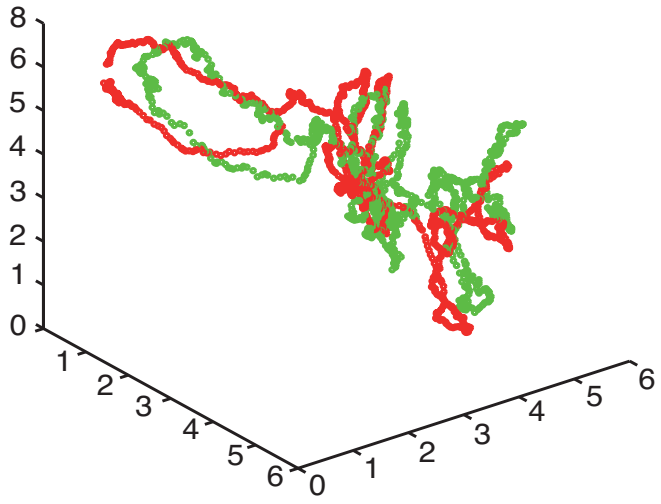

Figure 4.4: The red line shows the path of the center of a Janus colloid. The green curve gives the corresponding path of the center of mass of the solute particles cloud produced by the colloid. It clearly follows the motion of the Janus particle as it also moves down its own particle gradient.

limit of the swimmer if it is compared to experimental results.

4.4 The Particle Gradient

It is important to understand that the gradient driven swimmer described in this work is surrounded by a low Reynolds number fluid. Its motion should not be confused with the one of a rocket which moves through momentum it obtains by throwing mass in the opposite direction of its motion. In low Reynolds number hydrodynamics, such a motion is damped immediately. Therefore, the motion along the gradient is based on the gradient of the chemical potential along the swimmer. This difference becomes clear if the motion of the product cloud is considered. In a rocket, the center of mass of the vast products moves opposite to the rocket. In the gradient driven motion described here, it moves in the same direction as the swimmer. This can be understood as the relaxation of the gradient is diffusive and occurs on a time scale shorter than the one of the motion of the colloid. If it is assumed that the colloid is at rest during the relaxation of the product particles, it is obvious that it is entropically favorable that the product particles diffuse around the colloid leading to a homogenous distribution around the colloid. As, however, the colloid moves, the gradient cannot relax completely around it. Therefore, the center of mass of the product follows the motion of the swimmer as can be seen in figure 4.4. This is a necessary condition to ensure that the swimmer shows the correct long time behavior. If the cloud is not moving in the same direction as the swimmer it has to be assumed that the motion is based on a pressure gradient which arises due to artifacts of the

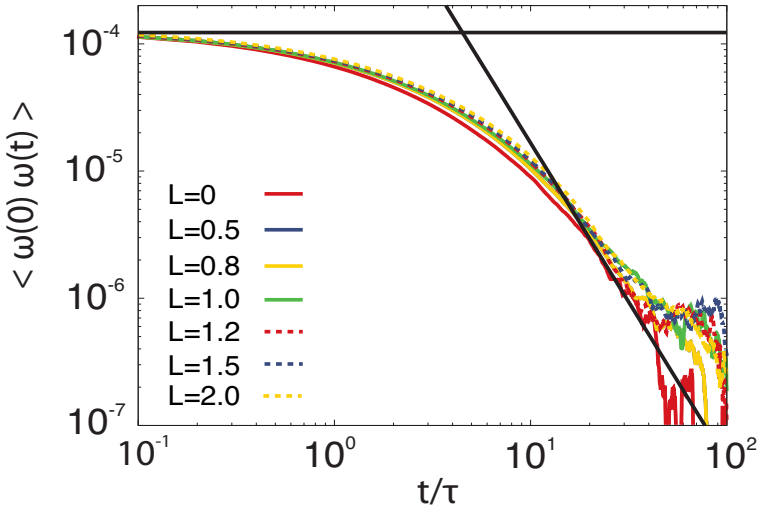

Figure 4.5: The angular correlation function $\langle \omega(0)\,\omega(t) \rangle$ of a Brownian particle can be characterized by its value for $t \to 0$ and a long time tail $t^{-5/3}$, both shown here in black. They are also seen in the correlation functions of the Janus colloid as its angular diffusion is not affected by the catalytic reaction of the fluid particles. The interaction length L has no significant effect on the correlation function. Here, $L = 0$ denotes a Brownian colloid which only interacts with the fluid through a hardcore potential.

simulation technique used, as most approaches are not able to produce a correct incompressible fluid.

4.5 Short Time Limit

The short time limit of a non-active colloid can be investigated by the velocity and angular velocity autocorrelation function. It has been shown by analytical as well as simulation approaches that both correlation functions show a similar behavior [181]. On short time scales, both correlation functions decay exponentially as the velocities are altered by stochastic interactions with the solvent as predicted by the Enskog theory for dense gases. In the long time limit, a power law decay with $t^{-3/2}$ for the velocity autocorrelation function and for the angular velocity autocorrelation function $t^{-5/2}$ is predicted by mode coupling theory due to the momentum conservation in the fluid. In section 3.5.1 it has been shown that the MPC approach is able to reproduce these correlation functions correctly in the long time as well as short time limit.

Angular Correlation Function of the Swimmer

For the swimmer with different interactions lengths L the propulsion has only minor effects on the angular velocity autocorrelation function, as can be seen in figure 4.5. There is a slightly slower decrease in the exponential decay as for the Brownian colloid which increases with the length L. This effect, however, is extremely small and can be as well an artifact of the discrete nature of the simulation technique which has previously been reported in literature for other

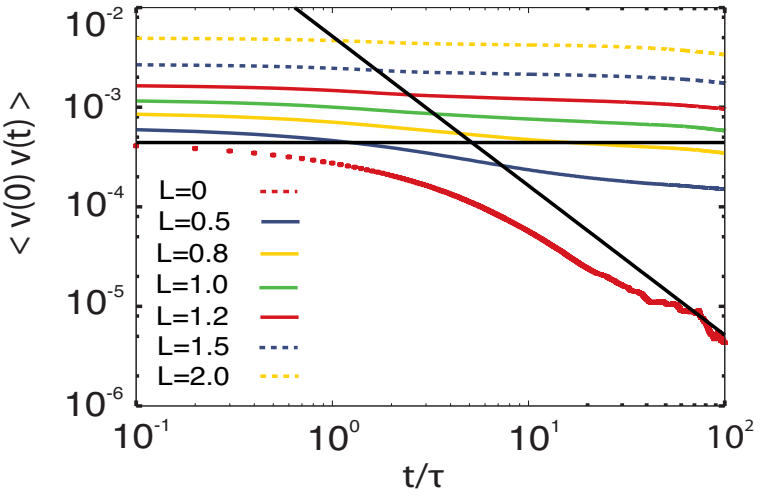

Figure 4.6: The velocity correlation $\langle v(0)\, v(t)\rangle$ of a Brownian particle, here denoted by $L = 0$, can also be described by the limit $t \to 0$ and a power law decay as $t^{-3/2}$ which is reproduced by the MPC algorithm. However, for a Janus colloid the long time limit cannot be observed due to the increase of the velocity correlations produced by the propulsion mechanism, leading to an increased ballistic behavior at short length scales.

correlation functions [141]. The long time tail shows slightly higher correlation than would be expected for a non-driven colloid. This effect is rather small and does not lead to a significant effect which would be sustained in the long time behavior of the swimmer. This proves that the propulsion mechanism only slightly effects the rotational behavior of the swimmer and on length scales reachable in experiments such effects should not be visible.

Velocity Correlation Function of the Swimmer

The velocity correlation function shows significant deviations from the behavior known for a Brownian colloid in a fluid, as shown in figure 4.6. The short time relaxation of the non-driven colloid vanishes in the propelled case and the correlation of the velocity sustains over very long time scales. In the regime where for a non-driven colloid already the long time tail can be observed, the driven particle shows very strong velocity correlations. This proves that in the ballistic regime the velocity of the swimmer is significantly increased for the self-driven swimmer. The fluid surrounding the swimmer needs highly increased time scales to alter the velocity of the swimmer. As can be further seen, the thermal energy associated with the initial value of the swimmer $< \mathbf{v}(0) \cdot \mathbf{v}(0) >$ increases with the interaction length L due to the activity of the swimmer. This behavior can also be observed in the behavior of the mean square displacement described in the next section.

Orientation Correlation Function

The orientation correlation function confirms the conclusion drawn from the angular velocity correlation function. The propulsion mechanism leads to a faster decay of the orientation correlation function, shown in figure 4.7(a). This effect is very weak and does not influence the

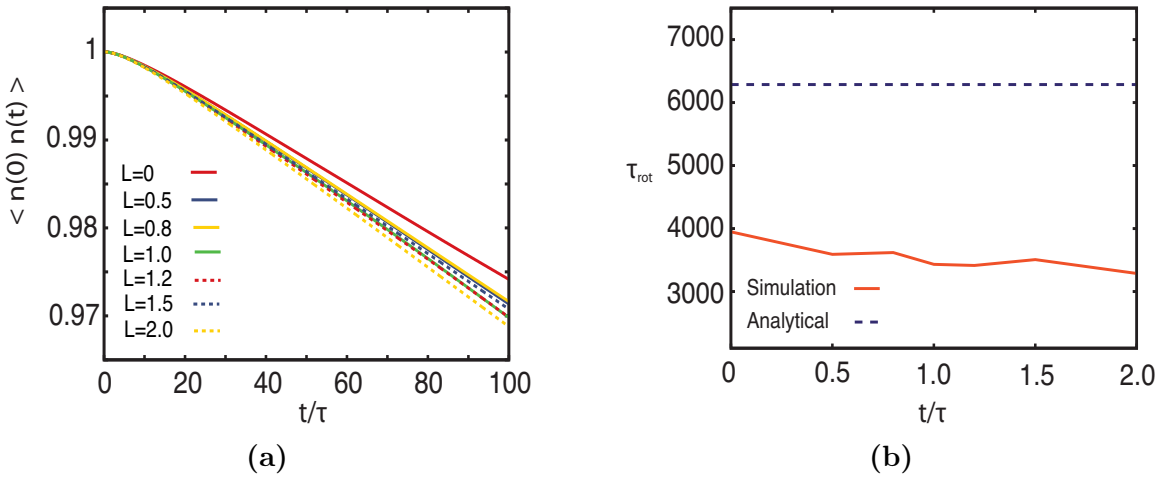

Figure 4.7: **(a)** The orientation correlation $\langle n(0)\, n(t)\rangle$ of the Janus colloid shows the same exponential decay as the one of a Brownian particle, denoted by $L = 0$. There are deviations in the long run which are beyond the error bars, not depicted here.
(b) The rotation diffusion time does not show any dependence on the interaction length L. The deviation from the Brownian analytical result has been reported previously in literature and is based on discretization effects.

long time behavior of the swimmer. From the decay of the orientation correlation function, the rotation diffusion time can be obtained by an exponential fit. The value deviates significantly from the result obtained from the Brownian theory, see figure 4.7(b). However, it has previously been reported that this can arise from discretization effects of the algorithm [141]. Further, is has been proposed that the short time decay of the algorithm should be analyzed with the Enskog theory for dense gases [182, 206] which differs slightly from the Brownian theory [181]. Nevertheless, there is no significant effect of the propulsion mechanism on the orientation correlation function. This confirms the theory of selfdiffusiophoresis, described in [105].

4.6 Long Time Limit

So far, it has been shown that the Janus colloid simulated with an MPC approach is able to reproduce the qualitative behavior which would be expected from a theoretical point of view. In order to use it as a model to learn more about the real world, it should match the known experimental results. The short time behavior is difficult to address in an experiment due to the resolution of the applied techniques. The main conclusions drawn from the experiments described in section 2.2 have been derived from the long time limit of the mean square displacement. For this regime it is possible to show that the Janus particle moves due an enhanced diffusion, described by the diffusion constant

$$D_{eff} = 2\, D_0 + V^2\, \tau_r. \tag{4.3}$$

As has been shown above, the rotation diffusion time is not affected by the selfduffusiophoretic propulsion mechanism. Using the velocities derived from the simulation it is possible to find

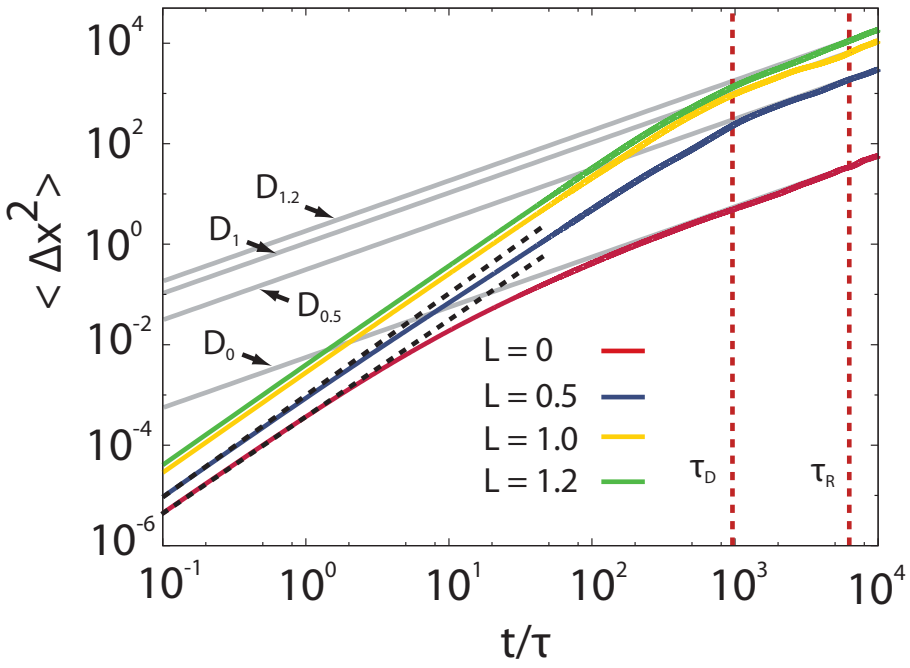

Figure 4.8: The mean square displacement $\langle \Delta x^2 \rangle$ of a Brownian particle (red curve, $L = 0$) compared to the ones of Janus colloids with different interaction lengths L. Even for a very short interaction length L a significant increase of the diffusion constant can be observed. The diffusion constants for all colloids match the analytically expected values for time scales larger than the rotation diffusion time τ_R. The second depicted time τ_D is the diffusion time of the fluid elements, which describes the time it needs to diffusive a length of the radius of the colloid. The black dashed line shows the initial ballistic regime which is not significantly extended due to the propulsion. The crossover between both regimes seems to be significantly reduced.

the enhanced diffusion constants, as can be seen in figure 4.8. Even for the smallest interaction zone, the diffusion constant is enhanced by a factor of the order of 10^2. This is comparable to the increase observed in experiments of Janus colloids [6, 7]. The diffusion time of the colloids as well as the rotation diffusion time are not altered by the propulsion. However, the swimmer shows a sharper transition from the short time ballistic regime to the diffusion regime than the Brownian particle.

For length scales of the interaction zone up to $L = 1.2$ the simulation reproduces the expected diffusion behavior. The velocity of the particle is strongly increased and the diffusive regime in the mean square displacement cannot be resolved accurately. This might result from the necessity of better statistics or due to a significantly increased Peclet number and the need to consider convective effects.

This shows that the simulations, shown so far, completely describe the long time limit of a selfdiffusiophoretic Janus colloid. It describes the increase of the diffusion constant correctly also observed in experiments which have so far not been explained by other approaches. As it seems to be difficult to extend the analytical results even further, this might be a good starting point for further investigations. Also, it clarifies the necessary assumptions which have to be made in analytic approaches.

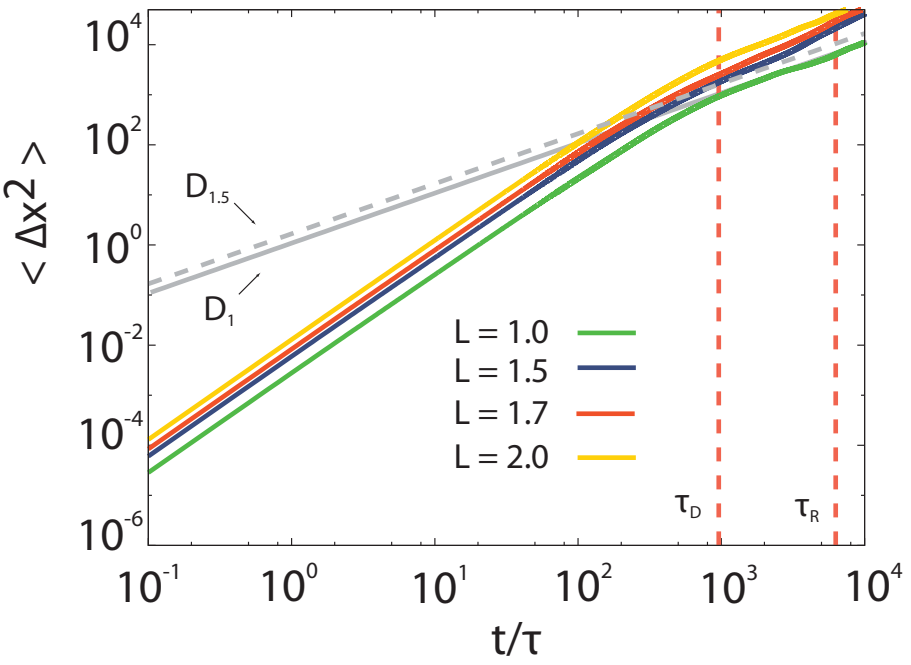

Figure 4.9: The mean square displacement $\langle \Delta x^2 \rangle$ for $L = 1$ (green), $L = 1.5$ (blue), $L = 1.7$ (red) and $L = 2.0$ (yellow). For interaction lengths larger than $L = 1$ it is not possible to observe the long time diffusion limit accurately.

4.7 Conclusion

The simulations of the MPC fluid and a selfdiffusiophoretic Janus colloid show that the approach is capable of explaining the phenomenological behavior of this kind of swimmers. Most analytical results for such a system consider the mean propulsion velocity of the colloid. The main result is that the velocity of a selfdiffusiophoretic swimmer is proportional to the square of its interaction length [8, 89]. This behavior can also be observed in the simulations performed for this work. However, quantitative deviations can be observed. This was to be expected as the analytical approaches are based on a time and length scale separation between the interaction zone around the swimmer and the overall evolution of the flow field as well as the product particle density around the swimmer. The MPC technique as a coarse graining approach aims to reduce the time scale separation in a hydrodynamic system in order to make them treatable with a simulation. Therefore, it has to be decided which length and time scale should be resolved accurately and which has to be implemented rather phenomenologically. In order to ensure the qualitatively correct behavior on small length scales it has to be ensured that the mechanism of propulsion leads to the expected results.

It is shown that the colloid indeed behaves like a low Reynolds number swimmer. This becomes obvious if the motion of the cloud of product particles is considered. In contrast to the expected behavior in a gaseous environment, its center of mass moves in the same direction as the Janus colloid. This can be understood as also the particle cloud moves under low Reynolds number conditions, and it is not pushed away form the swimmer but moves along the self-produced gradient. The colloid itself shows a reduced decay of the velocity correlation

function which shows that the propulsion mechanism leads to an increased persistence of the intrinsic velocity. As has been discussed previously, the rotation diffusion of the object is not effected by the propulsion mechanism. On the one hand, the angular velocity autocorrelation function shows the power law decay expected from Enskog theory [181]. On the other hand, the rotation diffusion time is not affected.

In experiments concerning Janus swimmers, mostly the long time limit is investigated [6, 7]. Therefore in this work, the focus is on the diffusive behavior of the colloid. In experiments it was observed that even though the rotation diffusion time is not altered by the propulsion the diffusion constant is significantly increased, as it scales with the square of the intrinsic velocity. The observed increase of the diffusion constant was up to an order of $\mathcal{O}(10^2)$. In this work, similar results have for the first time also been observed in simulations.

It shows that diffusiophoresis is a fascinating topic, which has not yet been fully understood. Due to the coupling of hydrodynamics with the motion of a particle gradient, it is a complex phenomenom at the foundation of soft matter physics. It could be a model system not only to build highly controllable swimmers at low Reynolds numbers, but also to investigate the applicability of field theoretical approaches in statistical mechanics.

5 Outlook

As has been shown in this work, the MPC approach is an ideal tool to investigate even complex soft matter systems like selfdiffusiophoretic Janus colloids. However, care has to be taken with the implementation of the approach. As has been described in chapter 3, it has to be ensured that the correct hydrodynamic regime is considered, described by the relevant hydrodynamic numbers. Even though the algorithm can simulate systems with low Reynolds as well as Peclet numbers, both are never as low as would be found in experiments. Further, only slow hydrodynamic flows can be investigated, as the MPC fluid is compressible and, hence, cannot resolve the sound propagation in a medium correctly. This is a problem it shares with competing approaches like Lattice Boltzmann. First approaches are trying to overcome this drawback. Further investigation is needed to develop more universal fluid models.

In this work, it has been shown that the MPC approach is able to reproduce qualitatively the expected behavior of a Janus colloid, especially the scaling behavior of the mean propulsion $\mathbf{v}$ with the interaction length L. It has been proven that the swimmer model is a low Reynolds swimmer, as the motion is based on the interaction of the colloid with the produced particle cloud and not on inertia effects. The center of mass of the solute cloud moves in the same direction as the swimmer and not opposite to it. Further, the swimmer interacts with the cloud only via a short range surface potential as has been assumed in the analytical work investigating such a system [89]. As it is an interfacial effect, careful separation of the time scales of the fluid and the colloid is needed. In order to go one step beyond the long time limit described in this work, simulations have to be developed which are able to reproduce the correct solute cloud around the swimmer, especially if collective effects should be addressed. This has not been achieved with the approaches used so far and any result given in literature should be considered carefully. In general, as the MPC particles are only a coarse grained description of the fluid with a typical density between $n = 5-20$, the concentration of different particle types is of the same order. In most analytical approaches, however, it is assumed that the solute concentration is much lower than the solvent concentration. In the simulation performed for this work, the diffusive time scale of the fluid and the rotational diffusion time scale of the swimmer are of the same order where in experiment they are separated by a order of $\mathcal{O}(10^2)$. The discrepancy arises as in the simulations the ratio of the radius of the fluid particles and the colloid is not as small as assumed in analytical as well as experimental results known so far. Therefore, the simulations done in this work can be considered as a first step towards a more general treatment of selfdiffusiphoresis in which the constraint of small solute particles can be disregarded.

For the long time limit the details of the simulations are less relevant. It has been shown that the diffusion constant of a Janus colloid significantly increases due to the propulsion gained from the interaction with the solute particles. The effect is of the same order of magnitude as has been previously observed in experiments [6, 7]. It would be elucidate for further work to compare the results obtained by simulations in detail with the experimental data.

A Transport Coefficients

Transport coefficients of the SRD as well as the MPC algorithm can be derived analytically by various approaches like Green-Kubo relations or kinetic theory. As these are the fundamental quantities to control the quantitative results of a new algorithm, here, the two most important ones are recaptured. Taking the forms from literature, care has to be taken as there are some misprints which would lead to slight deviations. In the following, δt_c is the collision time and a_0 is the cell size. The parameter d is the dimension in which the algorithm is applied. The expressions c_m, f_m and s_m depend on the algorithm applied and are functions of the particle density n.

The prefactors of the functions are

Algorithm	A	B
SRD−a	$\frac{2}{d}(1-\cos(\theta))$	$1-\cos(2\,\theta)$
SRD+a		$\frac{2}{5}(2-\cos(\theta)-\cos(2\,\theta))$
MPC−a	1	1
MPC+a		

A.1 Viscosity

The general form of the viscosity can be given as

$$\eta = \eta_{\text{kin}} + \eta_{\text{col}}, \tag{A.1}$$

$$= \frac{n\,k_B\,T\delta t_c}{a_0^d}\left(\frac{1}{\mathbf{c_m}} - \frac{1}{2}\right) + \frac{m}{a_0^d\,\delta t_c}\,\mathbf{f_m}. \tag{A.2}$$

The algorithm specific functions c_m and f_m are given by

Algorithm	c_m	f_m
SRD−a MPC−a	$\frac{B\,(n-1+e^{-n})}{n}$	$\frac{A\,a_0\,(n-1+e^{-n})}{12}$
SRD+a	$B(-e^{-n}(1+n))$ $+\left(Ad-\frac{B(3d+2)}{2}\right)\frac{1-e^{-n}(1+n+n^2/2)}{2n}$	$\frac{A\,a_0^2}{24}\left(n-\frac{7}{5}+e^{-n}\left(\frac{7}{5}+\frac{2n}{5}-\frac{3n^2}{10}\right)\right)$
MPC+a	$B(1-e^{-n}(1+n))+\left(A+\frac{B}{d}\right)\frac{n\,e^{-n}}{d+2}$ $+\left(Ad-\frac{B(3d+2)}{2}\right)\frac{1-e^{-n}(1+n+n^2/2)}{2n}$	$\frac{A\,a_0^2}{24}\left(n-\frac{7}{5}+e^{-n}\left(\frac{7}{5}+\frac{2n}{5}+\left(\frac{1}{d}-\frac{3}{10}\right)n^2\right)\right)$

A.2 Diffusion Constant

The general form of the diffusion is given by

$$D=\frac{k_bT\,\delta t_c}{m}\left(\frac{1}{\mathbf{s_m}}-\frac{1}{2}\right). \tag{A.3}$$

The algorithm specific function s_m is given by

Algorithm	s_m
SRD−a	$\frac{A\,(n-1+e^{-n})}{d\,n}-1$
SRD+a	$A\left(1-\frac{d+1}{2n}+\frac{e^{-n}}{2}\left(\frac{(d-3)n}{2}+d-1+\frac{d+1}{n}\right)\right)$
MPC−a	$\frac{A\,(n-1+e^{-n})}{n}$
MPC+a	$A\left(1-\frac{d+1}{2n}+\frac{e^{-n}}{2}\left(\frac{(d-1)(d-2)n}{2}+d-1+\frac{d+1}{n}\right)\right)$

B Solving Hydrodynamic Problems

The MPC and SRD approaches are constructed to investigate fluctuating hydrodynamics. However, in certain regimes they should recapture the results from classical low Reynolds number hydrodynamics. Hence, in order to test the validity of an algorithm, classical problems of hydrodynamics can be used as a benchmark. Here, three typical approaches are described shortly to solve problems in low Reynolds number hydrodynamics. Other approaches exist as well but these are the mostly used ones.

B.1 Streaming Function

In analogue to electrodynamics, for an incompressible fluid with $\nabla \cdot \mathbf{v} = 0$, a vector potential can be defined as [13]

$$\mathbf{v} = \nabla \times \psi. \tag{B.1}$$

In the case of a three dimensional problem there is no ease by expressing one vector potential by another. If the problem can be reduced, due to symmetry, to two dimensions, the velocity field can be deduced by one component of the vector field $\psi_z = \psi$. In the case of a spherical problem the velocity field becomes [66]

$$v_r = -\frac{1}{r^2 \sin(\theta)} \frac{\partial \psi}{\partial \theta}, \tag{B.2}$$

$$v_\theta = -\frac{1}{r \sin(\theta)} \frac{\partial \psi}{\partial r}. \tag{B.3}$$

The function ψ is called streaming function as it is constant along streamlines of the fluid. Solutions of the streaming function can for example be obtained by the Ansatz

$$\psi = \sin^2(\theta)\left(A_1 r^4 + A_2 r^2 + A_3 r + \frac{A_4}{r4}\right), \tag{B.4}$$

where the set of parameters $\{A_1, \ldots, A_4\}$ can be deduced from boundary conditions. Even though the applicability of the approach is only restricted to two dimensional problems, it is an easy way to find the flow field of simple problems and compare their decay with the momentum expansion of a hydrodynamic flow field [207, 208].

B.2 Faxen Theorem

In order to iterate the hydrodynamic interaction between objects in fluid, different approximation schemes have been proposed. As the fluid mediates the interaction between immersed

objects, hydrodynamic problems become retarded problems as the effect of one object onto the flow field can be reflected by other objects. Therefore, most schemes investigating hydrodynamics only contain the interaction up to a certain order, while the MPC algorithm, as it explicitly models the fluid, captures all hydrodynamic interactions.

In order to obtain the velocity of a sphere in a fluid the Faxen Theorem can be used [209]

$$\mathbf{v}_p = -\frac{1}{6\,\pi\,\eta\,R}\mathbf{F}_p^h + \mathbf{u}_0(\mathbf{r}_p) + \frac{1}{6}R^2\nabla_p^2\mathbf{u}_0(\mathbf{r}_p). \tag{B.5}$$

Here, $\mathbf{u}_0$ is the hydrodynamic flow field at the position of the sphere and $\mathbf{F}_p^h$ is the force onto the object. In the case $\mathbf{u}_0 = 0$, this resembles Stokes law of a sphere and can, hence, be considered as a first order extension of it. In the case of more complex objects the pre-factor of the force has to be substituted by the respective motility coefficient. The Faxen theorem can be used as the basis of iterative schemes like the method of reflection which incorporates higher order hydrodynamics.

B.3 Rodne-Prager Tensor

In the introduction, the Oseen tensor, as the fundamental solution of a delta force, has been given. Due to the linearity of the Stokes equation, complex objects, like polymers, can be composed from the superposition of such point forces [15]. These approaches are only considering the first order hydrodynamics. In order to go one step further, the Rode-Prager motility matrix can be used which contains already the effect of the first reflexion of the hydrodynamic interaction. The velocity can, similar to the Oseen, tensor be written as

$$\mathbf{v} = M(\mathbf{r}) \cdot \mathbf{F}, \tag{B.6}$$

with the Rodne-Prager Tensor

$$M(\mathbf{r}) = \frac{3}{4}\frac{R}{r}\left(\mathbf{1} + \frac{\mathbf{rr}}{r^2}\right) + \frac{1}{4}\left(\frac{R}{r}\right)^3\left(\mathbf{1} + 3\frac{\mathbf{rr}}{r^2}\right), \tag{B.7}$$

with R being the radius of the sphere.

All the approaches described here are iterative schemes to tackle the effect of hydrodynamics at low order. There are situations where this is sufficient as the higher order contributions decay considerably fast and the exact local hydrodynamic interaction is not relevant for the problem considered. However, most of these schemes are computationally demanding in complex situations. Therefore, simulations directly introducing a fluid model like DPD or MPC are more efficient to implement and automatically contain the complete hydrodynamics.

Bibliography

[1] E. Purcell, Life at low reynolds number, American Journal of Physics **45**, 3 (1977).

[2] H. C. Berg, *E. Coli in Motion*, Springer-Verlag New York, 2004.

[3] R. Dreyfus, J. Baudry, M. Roper, M. Fermigier, H. Stone, and J. Bibette, Microscopic artificial swimmers, Nature **437**, 862 (2005).

[4] S. Bleil, D. Marr, and C. Bechinger, Field-mediated self-assembly and actuation of highly parallel microfluidic device, Appl. Phys. Lett. **88**, 1 (2006).

[5] J. Anderson, Colloidal transport by interfacial forces, Ann.Rev.Fluid.Mech. **21**, 61 (1989).

[6] J. Howse, R. Jones, A. Ryan, T. Gough, R. Vafabaksh, and R. Golestanian, Self-motile colloidal particles: From directed propulsion to random walks, Phys. Rev. Lett. **99**, 48102 (2007).

[7] G. Volpe, I. Buttinoni, D. Vogt, H.-J. Kümmerer, and C. Bechinger, Microswimmers in patterened environments, Soft Matter **7**, 8810 (2011).

[8] R. Golestanian, T. Liverpool, and A. Ajdari, Propulsion of a molecular machine by asymmetric distribution of reaction products, Phys. Rev. Lett. **94**, 220801 (2005).

[9] M. Popescu, S. Dietrich, and G. Oshanin, Confinement effects on diffusiophoretic self-propellers, J. Chem. Phys. **130**, 1 (2009).

[10] J. F. Brady and G. Bossis, Stokesian dynamics, Annual Review of Fluid Mechanics **20**, 111 (1988).

[11] R. Chelakkot, R. G. . Winkler, and G. Gompper, Flow - induced helical coiling of semiflexible polymers in structured microchannels, Phys. Rev. Lett. **109**, 178101 (2012).

[12] C. Pooley, G. Alexander, and J. Yeomans, Hydrodynamic interaction between two swimmers at low reynolds number, Phys. Rev. Lett. **99**, 1 (2007).

[13] G. Batechlor, *An Introduction to Fluid Dynamics*, Cambridge Mathematical Library, Cambridge University Press, Cambridge, 2007.

[14] P. Nelson, *Biological Physics*, W.H. Freeman and Company, 2004.

[15] E. Lauga and T. Powers, The hydrodynamics of swimming microorganisms, Rep. Prog. Phys. **72**, 1 (2009).

[16] A. Najafi and R. Golestanian, Simple swimmer at low reynolds number: Three linked spheres, Phys. Rev. E **69**, 1 (2004).

[17] L. Becker, S. Koehler, and H. Stone, On the self-propulsion of micro-machines at low reynolds number: Purcell's three-link swimmer, Journal of Fluid Mechanics **490**, 15 (2003).

[18] D. Tam and A. Hosoi, Optimal stroke pattern for purcell's three-link swimmer, Phys. Rev. Lett. **98**, 1 (2007).

[19] G. Alexander, C. Pooley, and J. Yeomans, Scattering of low-reynolds-number swimmer, Phys. Rev. E **78**, 1 (2008).

[20] R. Zargar, A. Najafi, and M. Miri, Three-sphere low-reynolds-number swimmer near a wall, Phys. Rev. E **80**, 1 (2009).

[21] M. Leoni, J. Kotar, B. Bassetti, P. Cicuta, and M. Lagomarsino, A basic swimmer at low reynolds number, Soft Matter **5**, 472 (2009).

[22] P. Tierno, R. Golestanian, I. Pagonabarraga, and F. Sagues, Controlled swimming in confined fluids of magnetically actuated colloidal rotors, Phys. Rev. Lett. **101**, 218304 (2008).

[23] S. Jung, K. Mareck, L. Fauci, and M. Shelly, Rotational dynamics of a superhelix towed in a stokes fluid, Physics of Fluid **19**, 1 (2007).

[24] J. Shaevitz, J. Lee, and D. Fletcher, Spiroplasma swim by a processive change in body helicity, Cell **122**, 941 (2005).

[25] I. Llopis and I. Pagonabarraga, Hydrodynamic regimes of active rotators at fluid interfaces, Eur. Phys. J. E **26**, 103 (2008).

[26] I. Götze and G. Gompper, Flow generation by rotating colloids in planar microchannels, EPL **92**, 1 (2010).

[27] I. Götze and G. Gompper, Dynamic self-assembly and directed flow of rotating colloids in microchannels, Phys. Rev. E **84**, 31404 (2011).

[28] B. Grzybowski, H. Stone, and G. Whitesides, Dynamic self-assembly of magnetized, millimetre-sized objects rotating at a liquid-air interface, Nature **405**, 1033 (2000).

[29] I. Tuval, L. Cisnero, C. Dombrowski, C. Wolgemuth, J. Kessler, and R. Goldstein, Bacterial swimming and oxygen transport near contact lines, PNAS **102**, 2277 (2005).

[30] K. Drescher, R. Goldstein, N. Michel, M. Polin, and I. Tuval, Direct measurement of the flow field around swimming microorganisms, Phys. Rev. Lett. **105**, 168101 (2010).

[31] V. McKelvey-Martin, M. Green, P. Schmezer, B. Pool-Zobel, M. D. Mao, and A. Collins, The single cell gel electrophoresis assay (comet assay): A european review, Mutation Research/Fundamental and Molecular Mechanisms of Mutagenesis **288**, 47 (1993).

[32] P. Lammert, J. Prost, and R. Bruinsma, Ion drive for vesicles and cells, J. Theor. Biol. **178**, 387 (1996).

[33] H.-R. Jiang, N. Yoshinaga, and M. Sano, Active motion of a janus particle by self-thermophoresis in a defocused laser beam, Phys. Rev. Lett. **105** (2010).

[34] F. Weinert, M. Wühr, and D. Braun, Light driven microflow in ice **94**, 113901 (2009).

[35] J. Nardi, R. Bruinsma, and E. Sackmann, Vesicle as osmotic motors, Phys. Rev. Lett. **82**, 5168 (1999).

[36] S. Thutupalli, R. Seeman, and S. Herminghaus, Swarming behavior of simple model squirmers, N.J. Phys. **13**, 1367 (2011).

[37] J. Howse, Autonomous propulsion, Nature Chem. **4** (2012).

[38] D. Wilson, R. Nolte, and C. van Hest, Autonomous movement of plytinum-loaded stomatocytes, Nature Chem. **4**, 268 (2012).

[39] G. Rückner and R. Kapral, Chemically propelled nanodimer, Phys. Rev. Lett. **98**, 150603 (2007).

[40] S. Ebbens, R. Jones, J. Ryan, R. Golestanian, and J. Howse, Self-assembled autonomous runners and tumblers, Phys. Rev. Lett. **82**, 15304 (2010).

[41] L. Valadares, Y.-G. Tao, N. Zacharia, V. Kitaev, F. Galembeck, R. Kapral, and G. Ozin, Catalytic nanomotors: Self-propelled sphere dimers, small **6**, 565 (2010).

[42] S. Thakur and R. Kapral, Self-propelled nanodimer bound state pairs, J. Chem. Phys. **133**, 204505 (2010).

[43] S. Thakur and R. Kapral, Collective dynamics of self-propelled sphere-dimer motor, Phys. Rev. Lett. **85**, 26121 (2012).

[44] F. Drube, K. Alim, G. Witz, G. Dietler, and E. Frey, Excluded volume effects on semiflexible ring polymers, Nano Letters **10**, 1445 (2010).

[45] F. Thüroff, F. Wagner, and E. Frey, The effect of internal and global modes on the radial distribution function of confined semiflexible polymers, EPL (Europhysics Letters) **91**, 38004 (2010).

[46] K.-C. Lee and A. Liu, Force-velocity relation for actin-polymerization-driven motility from brownian dynamics simulations, Biophysical Journal **97**, 1792 (2009).

[47] A. Gholami, J. Wilhelm, and E. Frey, Entropic forces generated by grafted semiflexible polymers, Phys. Rev. E **74**, 041803 (2006).

[48] H. Hinsch, J. Wilhelm, and E. Frey, Quantitative tube model for semiflexible polymer solutions, The European Physical Journal E: Soft Matter and Biological Physics **24**, 35 (2007).

[49] J. Wilhelm and E. Frey, Radial distribution function of semiflexible polymers, Phys. Rev. Lett. **77**, 2581 (1996).

[50] T. Ando and J. Skolnick, Crowding and hydrodynamic interactions likely dominate in vivo macromolecules motion, PNAS **104**, 18457 (2010).

[51] R. Golestanian, J. Yeomans, and N. Uchida, Hydrodynamic synchronization at low reynolds number, Soft Matter **7**, 3074 (2011).

[52] D. L. Ermak and J. A. McCammon, Brownian dynamics with hydrodynamic interactions, The Journal of Chemical Physics **69**, 1352 (1978).

[53] Y. Kim and R. Netz, Pumbing fluids with periodically beating grafted elastic filaments, Phys. Rev. Lett. **96**, 158101 (2006).

[54] Y. von Hansen, M. Hinczewski, and R. R. Netz, Hydrodynamic screening near planar boundaries: Effects on semiflexible polymer dynamics, The Journal of Chemical Physics **134**, 235102 (2011).

[55] R. Golestanian, Collective thermotaxis of thermally active colloids, Phys. Rev. Lett. **108**, 38303 (2012).

[56] J. Munoz-Garcia and Z. Neufeld, Aggregation of chemotactic organisms in a differential flow, Phys. Rev. E **80**, 61902 (2009).

[57] A. Celani and M. Vergassola, Bacterial strategies for chemotaxis response, PNAS **107**, 1391 (2010).

[58] Y. Hong, N. Blackman, N. Knopp, A. Sen, and D. Velegol, Chemotaxis of nonbiological colloidal rods, Phys. Rev. Lett. **99**, 178103 (2007).

[59] M. Manjare, B. Yang, and Y.-P. Zhao, Bubble driven quasioscillatory translation motion of catalytic micromotors, Phys. Rev. Lett. **109**, 128305 (2012).

[60] N. Suematsu, Y. Ikura, M. Nagayama, H. Kitahata, N. Kawagishi, M. Murakami, and S. Nakata, Mode-switching of the self-motion of a camphor boat depending on the diffusion distance of camphor molecules, J. Phys. Chem. C **114**, 9876 (2010).

[61] I. Buttinoni, F. Kümmel, and C. Bechinger, Active brownian motion tunable by light, J. Phys.: Condens Matter **24**, 284129 (2012).

[62] R. Piazza and A. Parola, Thermophoresis in colloidal suspensions, J. Phys.: Condens Matter **20**, 153102 (2008).

[63] R. Ebersole and R. McCormik, Separation and isolation of viable bacteria by capillary zone electrophoresis, Nature Biotechnology **11**, 1278 (1993).

[64] U. Cordova-Figueroa and J. Brady, Osmotic propulsion: The osmotic motor, Phys. Rev. Lett. **100**, 158303 (2008).

[65] J. Brady, Particle motion driven by solute gradients with application to autonomous motion: continuum and colloidal perspective, J. Fluid Mech. **667**, 216 (2011).

[66] F. Jülicher and J. Prost, Generic theory of colloidal transport, Eur. Phys. J. E **29**, 27 (2009).

[67] N. Suematsu, S. Nakata, A. Awazu, and H. Nishimori, Collective behavior of inanimate boats, Phys. Rev. Lett. **81**, 56210 (2010).

[68] M. Kohira, Y. Hayashima, M. Nagayama, and S. Nakata, Synchronized self-motion of two camphor boats, Langmuir **17**, 7124 (2001).

[69] N. Mano and A. Heller, Bioeletrochemical propulsion, JACS **127**, 11574 (2005).

[70] B. Derjaguin, G. Sidorenkov, E. Zubashchenkov, and E. Kiseleva, Kinetic phenomena in boundary films of liquids, Kolloidn. Zh. **9** (1947).

[71] B. Derjaguin, S. Dukhin, and A. Korotkova, Kolloidn. Zh. **23** (1961).

[72] M.-J. Lin and D. Prieve, Electromigration of latex induced by a salt gradient, J. Colloid Int. Sci. **95**, 327 (1983).

[73] W. Lechnick and J. Shaeiwitz, Measurement of diffusiophoresis in liquids, J. Colloid Int. Sci. **102**, 71 (1984).

[74] P. Staffeld and J. Quinn, Diffusion-induced banding of colloid paricles via diffusiophoresis 1. electrolytes, J. Colloid Int. Sci. **130** (1989).

[75] J. Ebel, J. Anderson, and D. Prieve, Diffusiophoresis of latex particles in electrolyte gradients, Langmuir **4**, 396 (1988).

[76] J. Palacci, C. Cottin-Bizonne, C. Ybert, and L. Bocquet, Osmotic traps for colloids and macromolocules based on logharitmic sensing in salt taxis, Soft Matter **8**, 90 (2012).

[77] B. Abecassis, C. Cottin-Bizonne, C. Ybert, and L. Bocquet, Colloidal motility and pattern formation under rectified diffusiophoresis, Phys. Rev. Lett. **104**, 138302 (2010).

[78] C. Cottin-Bizonne and C. Y. and, Boosting migration of large particles by solute contrasts, Nature Materials **7**, 785 (2008).

[79] H. Keh and Y. Wan, Diffusiophoresis of a colloidal sphere in nonelectrolyte gradients perpendicular to two plane walls, Chem. Eng. Sci. **63**, 1612 (2008).

[80] S. Joo, S. Lee, J. Liu, and S. Qian, Diffusiophoresis of an elongated cylindrical nanoparticle along the axis of a nanopore, Chem. Phys. Chem. **11**, 3281 (2010).

[81] J. Lou and E. Lee, Diffusiophoresis of a spherical particle normal to a plane, J. Phys. Chem. C **112**, 2584 (2008).

[82] P. Staffeld and J. Quinn, Diffusion-induced banding of colloid paricles via diffusiophoresis 2. non-electrolytes, J. Colloid Int. Sci. **130**, 88 (1989).

[83] D. Prieve, J. Anderson, J. Ebel, and M. Lowell, Motion of a particle generated by chemical gradients. part.2 electrolyte, J. Fluid Mech. **148**, 247 (1984).

[84] J. Anderson and D. Prieve, Diffusiophoresis caused by gradients of strongly adsorbing solutes, Langmuir **7**, 403 (1991).

[85] W. Paxton, K. Kistler, C. Olmeda, A. Sen, S. S. Angelo, Y. Cao, T. Mallouk, P. Lammert, and V. Crespi, Catalytic nanorods: Autonomous movement of striped nanorods, J. Am. Chem. Soc. **126**, 13424 (2004).

[86] S. Fournier-Bidoz, A. Arsenault, I. Manners, and G. Ozin, Synthetic self-propelled nanorotors, Chem. Comm. , 441 (2005).

[87] T. Mallouk, A. Sen, and W. Paxton, Motility of catalytic nanoparticles through self-generated forces, Chem. Eur. J. **11**, 6462 (2005).

[88] W. Paxton, S. Sundararajan, T. Mallouk, and A. Sen, Chemical locomotion, Angew. Chem. Int. Ed. **45**, 5420 (2006).

[89] B. Sabass and U. Seifert, Nonlinear, electrocatalytic swimming in the presence of salt, J. Chem. Phys. **136**, 214507 (2012).

[90] I. Therkauff, C. Cottin-Bizonne, J. Palacci, C. Ybert, and L. Bocquet, Dynamic clustering in active colloidal suspension with chemical signaling, Phys. Rev. Lett. **108** (2012).

[91] P. Chaikin and T. Lubensly, *Principles of condensed matter physics*, Cambridge University Press, 1997.

[92] J. Anderson and D. Prieve, Diffusiophoresis: Migration of colloidal particles in gradients of solute concentration, Separation and Purification Methods **13**, 67 (1984).

[93] E. Shchukin, A. Pertsov, A. Amelina, and E. Zelenev, *Colloid and Surface Chemistry*, Elsvier Science and Technology, 2001.

[94] J. R. Strubinger and J. F. Parcher, Surface excess (gibbs) adsorption isotherms of supercritical carbon dioxide on octadecyl-bonded silica stationary phases, Analytical Chemistry **61**, 951 (1989).

[95] M. K. Chaudhury and G. M. Whitesides, How to make water run uphill, Science **256**, 1539 (1992).

[96] F. Brochard, Motions of droplets on solid surfaces induced by chemical or thermal gradients, Langmuir **5**, 432 (1989).

[97] L. Scriven and C. Sternling, Marangoni effects, Nature **187**, 186 (1960).

[98] E. Lauga, Enhanced diffusion by reciprocal swimming, Phys. Rev. Lett. **106**, 178101 (2011).

[99] J. W. Bush and D. L. Hu, Walking on water: Biolocomotion at the interface, Annu. Rev. Fluid Mech **38**, 339 (2006).

[100] A. Ajdari and L. Bocquet, Giant amplification of interfacially driven transport by hydrodynamic slip: Diffusio-osmosis and beyond, Phys. Rev. Lett. **96**, 186102 (2006).

[101] J. Anderson, M. Lowell, and D. Prieve, Motion of a particle generated by chemical gradients. part 1. non-electrolyte, J. Fluid Mech. **117**, 107 (1982).

[102] S. Ebbens, M.-H. Tu, J. Howse, and R. Golestanian, Size dependence of the propulsion velocity for catalytic janus-sphere swimmer, Phys. Rev. Lett. **85**, 20401 (2012).

[103] D. Huang, C. Cottin-Bizonne, C. Ybert, and L. Bocquet, Massive amplification of surface-induced transport at superhydrophobic surfaces, Phys. Rev. Lett. **101**, 64503 (2008).

[104] A. Hammack, Y.-L. Chen, and J. K. Pearce, Role of dissolved salts in thermophoresis of dna: Lattice-boltzmann-based-simulations, Phys. Rev. E **83**, 31915 (2011).

[105] R. Golestanian, T. Liverpool, and A. Ajdari, Designing phoretic micro- and nanoswimmer, N.J. Phys. **9**, 126 (2007).

[106] J. Happel and H. Brenner, *Low Reynolds Number Hydrodynamics*, Prentice-Hall, 1965.

[107] M. Teubner, The motion of chaged colloidal particles in electric fields, J. Chem. Phys. **76**, 5564 (1982).

[108] H. Stone and A. Samuel, Propulsion of microorganisms by surface distortion, Phys. Rev. Lett. **77**, 4102 (1996).

[109] S. Spagnoli and E. Lauga, Jet propulsion without inertia, Phys. Fluid **22**, 21902 (2010).

[110] E. Lauga and A. Davis, Viscous maragoni propulsion, J. Fluid Mech. **705**, 120 (2012).

[111] S. Duhr and D. Braun, Thermophoretic depletion follows boltzmann distribution, Phys. Rev. Lett. **96**, 168301 (2006).

[112] A. Würger, Thermophoresis in colloidal suspension driven by marangoni forces, Phys. Rev. Lett. **98**, 138301 (2007).

[113] M. Braibanti, D. Vigolo, and R. Piazza, Does thermophoretic mobility depend on particle size?, Phys. Rev. Lett. **100**, 108303 (2008).

[114] M. K. Phibbs and P. A. Giguère, Hydrogen peroxide and its analogues: Iii. absorption spectrum of hydrogen and deuterium peroxides in the near ultraviolet, Canadian Journal of Chemistry **29**, 490 (1951).

[115] M. Popescu, M. Tasinkevych, and S. Dietrich, Pulling and pushing a cargo with a catalytically active carrier, EPL **95**, 1 (2011).

[116] L. Baraban, M. Tasinkevych, M. Popescu, S. Sanchez, S. Dietrich, and O. Schmidt, Transport of cargo by catalytic janus micromotors, Soft Matter **8**, 48 (2012).

[117] Y.-G. Tao and R. Kapral, Design of chemically propelled nanodimer motors, J. Chem. Phys. **128**, 164518 (2008).

[118] D. Lüsenbrink, M. Yang, and M. Ripoll, Thermophoresis of colloids by mesoscale simulations, J. Phys.: Condens Matter **24**, 284132 (2012).

[119] B. ten Hagen, S. van Teeffelen, and H. Löwen, Brownian motion of a self-propelled particle, J. Phys.: Condens Matter **23**, 194119 (2011).

[120] R. Golestanian, Anomalous diffusion of symmetric and asymmetric active colloids, Phys. Rev. Lett.; Physical Review Letters **102** (2009).

[121] D. Saintillan and M. Shelly, Instabilities, pattern formation, and mixing in active suspensions, Phys. Fluid **20**, 123304 (2008).

[122] D. Saintillan and M. Shelly, Orientational order and instabilities in suspensions of self-locomotion rods, Phys. Rev. Lett. **99**, 58102 (2007).

[123] C. Valeriani, R. Allen, and D. Marenduzzo, Non-equilibrium dynamics of an active colloidal "chucker", J. Chem. Phys. **132**, 1 (2010).

[124] M. Enculescu and H. Stark, Active colloidal suspensions exhibit polar order under gravity, Phys. Rev. Lett. **84**, 41924 (2011).

[125] J. Taktikos, V. Zaburdaev, and H. Stark, Collective dynamics of model microorganism with chemotactic signaling, Phys. Rev. E **58**, 51901 (2012).

[126] J. Taktikos, V. Zaburdaev, and H. Stark, Modeling a self-propelled autochemotatic walker, Phys. Rev. E **84**, 41924 (2011).

[127] A. Einstein, Investigation on the theory of the brownian movement, Annalen der Physik (1905).

[128] G. Bird, Recent advances and current challenges for dsmc, Comp. Math. Apll. **35**, 1 (1998).

[129] P. D. Gennes, *Scaling Concepts in Polymer Physics*, Cornell University Press, 1979.

[130] A. Malevantes and R. Kapral, Mesoscopic model for solvent dynamics, J. Chem. Phys. **110**, 8605 (1999).

[131] A. Malevantes and J. Yeomans, Dynamics of short polymer chains in solution, Eurphys. Lett. **52**, 231 (2000).

[132] E. Tützel, M. Strauss, T. Ihle, and D. Kroll, Transport coefficients for stochastic rotation dynamics in three dimensions, Phys. Rev. E **68**, 36701 (2003).

[133] C. Huang, A. Chatterji, G. Sutmann, G. Gompper, and R. Winkler, Cell-level canonical sampling by velocity scaling for multiparticle collision dynamics simulations, J. Comp. Phys. **229**, 168 (2010).

[134] E. Allahyarov and G. Gompper, Mesoscale solvent simulations: Multiparticle-collision dynamics of three dimensional flows, Phys. Rev. E **66**, 36702 (2002).

[135] H. Noguchi, N. Kikuchi, and G. Gompper, Particle-based mesoscale hydrodynamic techniques, Eurphys. Lett. **78**, 10005 (2007).

[136] G. Gompper, T. Ihle, D. Kroll, and R. Winkler, Multi-particle collision dynamics: A particle-based mesoscale simulation approach to the hydrodynamics of complex fluids, Adv. Polym. Sci. (2009).

[137] H. Noguchi and G. Gompper, Transport coefficients of off-lattice mesoscale-hydrodynamics simulations techniques, Phys. Rev. E **78**, 16706 (2008).

[138] I. Götze, H. Noguchi, and G. Gompper, Relevance of angular momentum conservation in mesoscale hydrodynamics simulations, Phys. Rev. E **76**, 46705 (2007).

[139] I. Pagonabarraga, M. H. J. Hagen, and D. Frenkel, Self-consistent dissipative particle dynamics algorithm, Eurphys. Lett. **42**, 377 (1998).

[140] S. Meßlinger, B. Schmidt, H. Noguchi, and G. Gompper, Dynamical regimes and hydrodynamic lift of viscous vesicles under shear, Phys. Rev. E **80**, 011901 (2009).

[141] I. Götze and G. Gompper, Mesoscale simulations of hydrodynamic squirmer interactions, Phys. Rev. E **82**, 1 (2010).

[142] T. Ihle and D. Kroll, Stoachstic rotation dynamics: A galilean-invariant mesoscopic model for fluid flow, Phys. Rev. E **63**, 20201 (2001).

[143] A. Lamura, G. Gompper, T. Ihle, and D. Kroll, Multi-particle collision dynamics: Flow around a circular and a square cylinder, Eurphys. Lett. **56**, 319 (2001).

[144] J. Padding and A. Louis, Hydrodynamic interations and brownian forces in colloidal suspensions: Coarse-graining over time and length scales, Phys. Rev. E **74**, 31402 (2006).

[145] E. Guyon, J.-P. Hulin, L. Petit, and C. Mitescu, *Physical Hydrodynamics*, Oxford University Press, 2001.

[146] M. Yang and M. Ripoll, Simulation of thermophoretic nanoswimmer, Phys. Rev. Lett. **84**, 61401 (2011).

[147] M. Downton and H. Stark, Simulation of a model microswimmer, J. Phys.: Condens Matter **21**, 1 (2009).

[148] S. D. Groot and P. Mazur, *Non-Equilibrium Thermodynamics*, Dover Publications, 1984.

[149] T. Ihle, Chapman-enskog expansion for multi-particle collision model, Phys. Chem. Chem. Phys. **11**, 9667 (2009).

[150] H. Chen, H-theorem and generalized semi-detailed balance condition for lattice gas systems, Journal of Statistical Physics **81**, 347 (1995).

[151] B. Dubrulle, U. Frisch, M. Hénon, and J.-P. Rivet, Low-viscosity lattice gases, Journal of Statistical Physics **59**, 1187 (1990).

[152] C. A. Marsh, G. Backx, and M. H. Ernst, Fokker-planck-boltzmann equation for dissipative particle dynamics, EPL (Europhysics Letters) **38**, 411 (1997).

[153] C. A. Marsh and P. V. Coveney, Detailed balance and h -theorems for dissipative particle dynamics, Journal of Physics A: Mathematical and General **31**, 6561 (1998).

[154] T. Ihle and D. Kroll, Stochastic rotation dynamics i. formalism, galilean invariance, and green-kubo relation, Phys. Rev. E **67**, 66705 (2003).

[155] S. Chapman and T. Cowling, *The Mathematical Theory of Non-Uniform Gases*, Cambridge Mathematical Library, Cambridge University Press, 1970.

[156] C. Pooley and Y. Yeomans, Kinetic theory derivation of the transport coefficients of stochastic rotation dynamics, J. Phys. Chem. B **109**, 6505 (2005).

[157] T. Ihle, E. Tüzel, and D. Kroll, Equilibrium calculations of transport coefficients for a fluid-particle model, Phys. Rev. E **72**, 46707 (2005).

[158] F. Schwabl, *Statistische Mechanik*, Springer Berlin / Heidelberg, 2006.

[159] T. Ihle, E. Tüzel, and D. Kroll, Consistent particle-based algorithm with a non-ideal equation of state, Eurphys. Lett. **73**, 664 (2006).

[160] T. Ihle and E. Tüzel, Static and dynamic properties of a particle-based algorithm for non-ideal fluids and binary mixtures, Prog. Com. Fluid. Dyn. **8**, 1 (2008).

[161] M. L. Bellac, F. Mortessagne, and G. Batrouni, *Equilibrium and Non-Equilibrium Statistical Thermodynamics*, Cambridge University Press, 2010.

[162] T. Ihle, E. Tützel, and D. Kroll, Resummed green-kubo relation for fluctuating fluid-particle model, Phys. Rev. E **70**, 35701 (2004).

[163] N. Kikuchi, C. Pooley, J. Ryder, and J. Yeomans, Transport coefficients of a mesoscopic fluid dynamics model, J. Chem. Phys. **119**, 6388 (2003).

[164] T. Ihle and D. Kroll, Stochastic rotation dynamics ii. transport coefficients, numerics, and long-time tails, Phys. Rev. E **67**, 66706 (2003).

[165] M. Ripoll, M. Mussawisade, R. Winkler, and G. Gompper, Dynamic regimes of fluids simulated by multiparticle-collision dynamics, Phys. Rev. E **72**, 16701 (2005).

[166] H. Hijar and G. Sutmann, Hydrodynamic fluctuations in thermostatted multiparticle collision dynamics, Phys. Rev. E **83**, 46708 (2011).

[167] D. Lüsenbrink and M. Ripoll, Temoperature inhomogenities simulated with multiparticle-collision dynamics, J. Chem. Phys. **136**, 84106 (2012).

[168] E. Tüzel, T. Ihle, and D. Kroll, Dynamic correlations in stochastic rotation dynamics, Phys. Rev. E **74**, 56702 (2006).

[169] L. Landau and E. Lifschitz, *Fluid Mechanics*, Perfamon, 1959.

[170] J. Elgeti and G. Gompper, Self-propelled rods near surfaces, EPL **85**, 38002 (2009).

[171] T. Ishikawa and T. Pedley, Coherent structures in monolayer of swimming particles, Phys. Rev. Lett. **100**, 1 (2008).

[172] E. Falck, J. Lahtinen, I. Vattulainen, and T. Ala-Nissila, Influence of hydrodynamics on many-particle diffusion in 2d colloidal suspensions, Eurphys. Lett. **13**, 267 (2004).

[173] J. Sane, J. Padding, and A. Louis, Coarse-graining dynamics for convection-diffusion of colloids: Taylor dispersion, Arxiv **0903.3493v1** (2009).

[174] M. Ripoll, P. Holmqvist, R. Winkler, G. Gompper, J. Dhont, and M. Lettinga, Attractive colloidal rods in shear flow, Phys. Rev. Lett. **101**, 168302 (2008).

[175] Y. Yang, J. Elgeti, and G. Gompper, Cooperation of sperm in two dimensions: Synchronization, attraction, and aggregation through hydrodynamic interaction, Phys. Rev. E **78**, 61903 (2008).

[176] S. Y. Reigh, R. G. Winkler, and G. Gompper, Synchronization and bundling of anchored bacterial flagella, Soft Matter **8**, 4363 (2012).

[177] M.-J. Huang, R. Kapral, A. Mikhailov, and H.-Y. Chen, Coarse-grain model for lipid bilayers self-assembly and dynamics: Multiparticle collision description of the solvent, Arxiv **1204.6103v1** (2012).

[178] J. Padding and A. Louis, Hydodynamic and brownian fluctuations in sedimenting suspensions, Phys. Rev. Lett. **93**, 220601 (2004).

[179] M. Hecht, J. Harting, T. Ihle, and H. Hermann, Simulation of claylike colloids, Phys. Rev. E **74**, 21403 (2005).

[180] J. Whitner and E. Luijten, Fluid-solid boundary conditions for multiparticle collision dynamics, J. Phys.: Condens Matter **22**, 104106 (2010).

[181] J. Padding, A. Wysocki, H. Löwen, and A. Louis, Stick boundary conditions and rotational velocity auto-correaltion functions for colloidal particles in a coarse grained representation of the solvent, J. Phys.: Condens Matter **17**, 3393 (2005).

[182] A. Imperio, J. Padding, and A. Louis, Force calculation on walls and embedded particles in multiparticle-collision-dynamics simulations, Phys. Rev. E **83**, 46704 (2011).

[183] Y. Hashimoto, Y. Chen, and H. Ohashi, Immiscible real-coded lattice gas, Comp. Phys. Comm. **129**, 56 (2000).

[184] Y. Inoue, Y. Chen, and H. Ohashi, A mesoscopic simulation model for immiscible multiphase fluids, Journal of Computational Physics **201**, 191 (2004).

[185] T. Sakai, Y. Chen, and H. Ohashi, Real-coded lattice gas model for ternary amphiphilic fluids, Phys. Rev. E **65**, 031503 (2002).

[186] E. Tüzel, G. Pan, T. Ihle, and D. M. Kroll, Mesoscopic model for the fluctuating hydrodynamics of binary and ternary mixtures, EPL (Europhysics Letters) **80**, 40010 (2007).

[187] T. Ihle, Transport coefficients of multi-particle collision algorithms with velocity-dependent collision rules, Journal of Physics: Condensed Matter **20**, 235224 (2008).

[188] K. Tucci and R. Kapral, Mesoscopic model for diffusion-influenced reaction dynamics, J. Chem. Phys. **120**, 8262 (2004).

[189] K. Tucci and R. Kapral, Mesoscopic multiparticle collision dynamcis of reaction-diffusion fronts, J. Phys. Chem. B **109**, 21300 (2005).

[190] K. Rohlf, S. Fraser, and R. Kapral, Reactive multiparticle collision dynamics, Comp. Phys. Comm. **179**, 132 (2008).

[191] D. Gillespie, Exact stochastic simulation of coupled chemical reactions, J. Chem. Phys. **81**, 2340 (1977).

[192] J.-X. Chen and R. Kapral, Mesoscopic dynamics of diffusion-influenced enzyme kinetics, J. Chem. Phys. **134**, 44503 (2011).

[193] A. Succi, *The Lattice Bolzmann Equation for Fluid Dynamics and Beyond*, Oxford University Press, Oxford, 2001.

[194] R. D. Groot and P. B. Warren, Dissipative particle dynamics: Bridging the gap between atomistic and mesoscopic simulation, The Journal of Chemical Physics **107**, 4423 (1997).

[195] A. Ladd, Numerical simulations of particulate suspensions via a discretized boltzmann equation. part1. theoretical foundation, J. Fluid Mech. **271**, 285 (1994).

[196] R. Adhikari, K. Stratford, M. Cates, and A. Wagner, Fluctuating lattice boltzmann, Eurphys. Lett. **71**, 473 (2005).

[197] A. Ladd and R. Verberg, Lattice boltzmann simulations of particle-fluid suspensions, J. Stat. Phys. **104**, 1191 (2001).

[198] P. Español, Hydrodynamics from dissipative particle dynamics, Phys. Rev. E **52**, 1734 (1995).

[199] P. Español and P. Warren, Statistical mechanics of dissipative particle dynamics, EPL (Europhysics Letters) **30**, 191 (1995).

[200] V. Symeonidis, G. E. Karniadakis, and B. Caswell, Schmidt number effects in dissipative particle dynamic simulations of polymers, J. Chem. Phys. **125**, 184902 (2006).

[201] J. Huang, Y. Wang, and M. Laradji, Flow control by smart nanofluidic channels:âĂĽ a dissipative particle dynamics simulation, Macromolecules **39**, 5546 (2006).

[202] S. . Haber, N. . Filipovic, M. . Kojic, and A. . Tsuda, Dissipative particle dynamics simulation of flow generated by two rotating concentric cylinders : Boundary conditions, Phys . Rev . E **74**, 046701 (2006).

[203] A. Tiwari and J. Abraham, Dissipative - particle - dynamics model for two - phase flows, Phys . Rev . E **74**, 056701 (2006).

[204] Y. Yang, V. Marceau, and G. Gompper, Swarming behavior of self-propelled rods and swimming flagella, Phys. Rev. E **82**, 31904 (2010).

[205] D. Loi, S. Mossa, and L. Cugliandolo, Effective temperature of active complex matter, Soft Matter **7**, 3726 (2011).

[206] A. Imperio, J. Padding, and A. Louis, Diffusion of spherical particles in microcavities, J. Chem. Phys. **134**, 154904 (2011).

[207] J. Blake and A. Chwang, Fundamental singularities of viscous flow, J. Eng. Math. **8**, 23 (1974).

[208] A. Chwang and T. Y.-T. Wu, Hydrodynamics of low-reynolds-number flow. part.2. singularity method for stokes flows, J. Fluid Mech. **67**, 787 (1975).

[209] J. Dhont, *An Introduction to Dynamics of Colloids*, Elsvier, 1996.

Danksagung

Als erstes möchte ich Prof. Frey für seine Unterstützung in den letzten Jahren und die Möglichkeit, diese Arbeit anzufertigen, danken. Mit seiner Begeisterung für die Wissenschaft konnte er mich auch in den zähen Phasen immer wieder anspornen.

Daniela Aschenbrenner möchte ich für all die Geduld, Wärme und Zuversicht in den letzten Jahren danken. Ich hoffe, ich kann Dir das Alles in den nächsten Jahren wieder zurückgeben.

Ich möchte meinen Eltern für ihre Unterstützung nicht nur während der Promotion danken, vor allem für das Gefühl, dass egal was ich mache, Ihr immer hinter mir steht.

An dieser Stelle möchte ich all den Freunden danken, die mich die letzten Jahre manchmal ertragen, immer aber unterstützt haben.

Steffen Rulands möchte ich für seine Kollegialität während langer Abschnitte der Arbeit und für interessante gemeinsame Erfahrungen darüber hinaus danken.

"Universität Bayern e.V." möchte ich für die Untestützung durch mein Forschungsstipendium danken.

Abschließend möchte ich dem ganzen LS Frey für ein paar sehr abwechslungsreiche Jahre danken.

Ich versichere, die Arbeit selbstständig angefertigt und dazu nur die im Literaturverzeichnis angegebenen Quellen benutzt zu haben.

München, den 13. Mai 2013